DSEC 2025 DRIVETRAIN AND SYSTEMS ENGINEERING CONFERENCE

Eurogress, Aachen — March 11 - 12, 2025

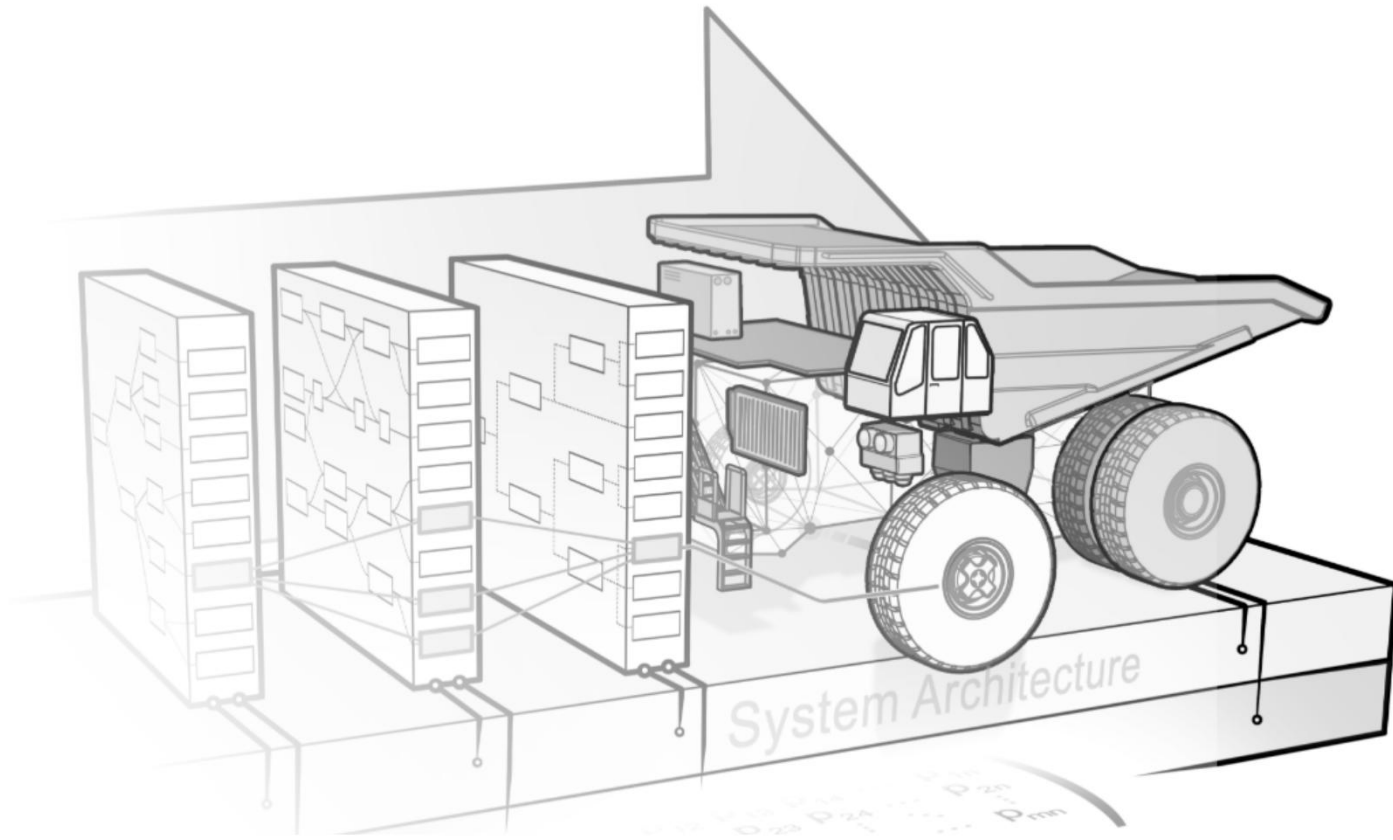

CONFERENCE PROCEEDINGS

sponsored by

hosted & organized by

Please note:

This is the collection of the conference proceedings.

If you are interested in the peer-reviewed journal publications, follow this link:

https://link.springer.com/collections/ebaaidfffi

Table of Contents

Drivetrain Technology:
Performance and Efficiency

Cost Reduction of Four-Point Bending Tests by using an innovative electrohydraulic Drive Concept

Luis Böhm (M.Sc.)[1], Lorenz Kade (M.Eng.)[1], Dr. Kai Ehrich[2], Dr. Timo Jungblut[2].

[1]IABG mbH, Ottobrunn, Germany

[2]Nordex Energy SE, Rostock, Germany

Keywords: *electrohydraulic, cost reduction, four-point bending, electrification*

Abstract: One aim of sustainable wind turbine development is a rapid and efficient design of optimized, cost-effective and durable rotor blades. In this context, model-based design is common practice. However, suitable material models and parameters are required for an operationally reliable design. This demands experimentally determined data. For this purpose, a suitable testbench for material characterization and quality assurance tests by means of up to 13 m long carbon fibre reinforced polymer (CFRP) or carbonfibre reinforced plastic (CRP)-beams was developed. These beams are qualified in a dynamic force range of ±200 kN and in a static force range of ±400 kN. The electrification of the hydraulic drivetrain enables the recuperation of compression work during endurance testing. The resulting reduction in operating costs of up to €48,000.- per year compared to testbenches using conventional servo-hydraulic drives is demonstrated by numerical simulations and experimental data.

1 Introduction

The wind energy industry is characterized by a rapid pace of innovation, with new turbine generations being introduced at short intervals. This fast-paced innovation is driven by a dual focus on increasing Annual Energy Production (AEP) as well as improving turbine reliability and efficiency. As manufacturers compete to produce turbines with higher AEP, they are also investing heavily in research and development to improve the performance and durability of their products.

The development of rotor blades is a key focus in the wind energy industry, as they play a critical role in driving Annual Energy Production (AEP) and achieving the desired levels of reliability and efficiency. As the primary component responsible for capturing wind energy, rotor blades must be designed to maximize energy output while also meeting strict performance standards.

In the past, Nordex Energy SE developed efficient rotor blades with a slender design and a general approach applicable to multiple target markets. However, as demand for renewable wind energy continues to grow worldwide, the target markets are becoming more diverse and demand more specialized products to meet their unique requirements. This has led to an increased need for development, while still maintaining an application-specific development, as was previously achieved with a more general development approach.

To address these new requirements, Nordex Energy SE now aims to simplify and de-risk the development of new blades by increasing component testing for both new and existing blade types. This approach will reduce the need for expensive and time-consuming full blade tests and ensure that new products meet the necessary performance standards.

The wind energy industry has long been familiar with the approach of using component testing to streamline the development process. However, this approach was often unaffordably expensive due to the high development costs associated with creating specialized tests. Additionally, rising energy costs have made this approach even more challenging.

To address these issues, IABG has developed a new test rig (see figure 1) for the Nordex Energy SE that will allow for fast in-house testing and development of products by testing components at a whole new level. This innovative new approach will help to reduce costs and streamline the development process, ultimately enabling Nordex Energy SE to bring new and improved products to market faster and efficiently. Furthermore, the reliability of turbines can be improved through a deeper understanding of design details and their testing. In addition, an innovative electro-hydraulic drive concept reduces the energy costs of these time-consuming tests. By investing in such a cutting-edge technology, Nordex Energy SE is helping to drive the growth and evolution of the wind energy industry.

2 Description of the Testbench and the Drive Concept

The following section describes a test bench, which was developed for testing beams composed of a wooden core laminated with Carbon Fiber Reinforced Polymer (CFRP) or Carbonfibre Reinforced Plastic (CRP) material specimens. The test bench essentially has two objectives. Firstly, it is used to generate data for the parameterization and alignment of numerical models for the design of the rotor blades. Secondly, it is used to analyze and validate design variants at component level. The test bench is designed for both static and dynamic testing scenarios. Static tests are performed with maximum forces of up to ± 400 kN, amplitudes up to ± 500 mm and slow actuator speeds, enabling precise characterization of the material's response under high loads. Dynamic fatigue tests are conducted to capture Wöhler curves, applying cyclic loads with a maximum force of ± 200 kN, amplitudes up to ± 500mm and frequencies up to 2 Hz.

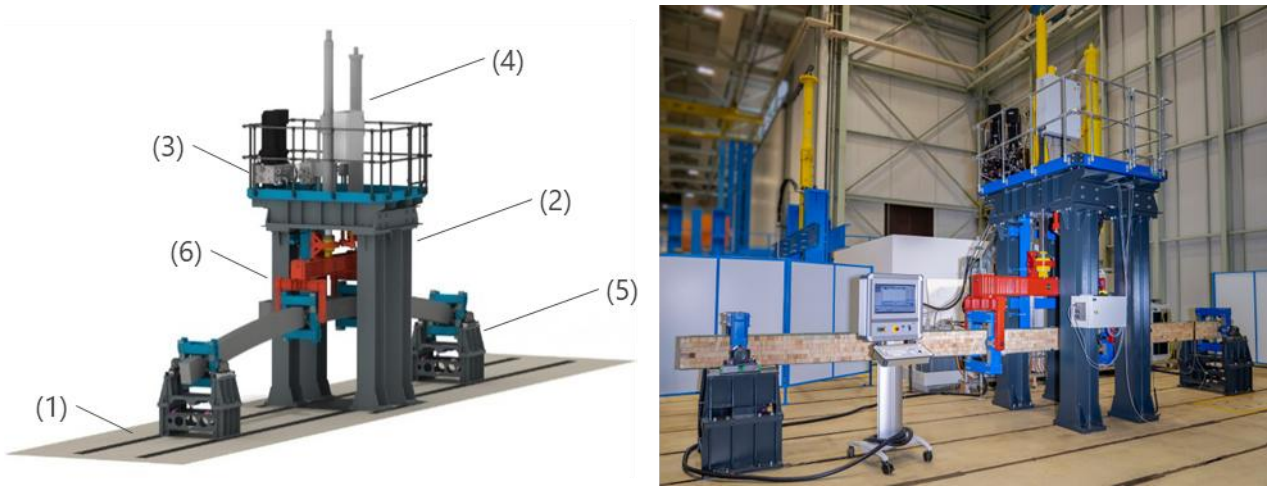

Figure 1: Beam Test Bench. (1) foundation, (2) portal structure, (3) hydraulic drive system, (4) hydraulic cylinders, (5) movable bearings, (6) loading frame.

Hydraulic cylinders are employed to apply the required static and dynamic loads to the test specimens. The volume flow of pressurized oil to be generated by the pump is the product of the piston area of the hydraulic cylinder and the speed of the piston rod. The piston area in turn results from the system pressure and the required maximum force. The dynamic tests are carried out at significantly higher speeds than the static tests. At the same time, only lower forces are required. To fulfil

all requirements with the smallest possible pumps, the test bench therefore comprises two cylinders: a cylinder with a maximum force of 400 kN for the static tests and a cylinder with a smaller piston area for the dynamic tests (200 kN).

As shown in figure 1 the test bench consists of a foundation (1) and a portal structure (2) which consists of a hydraulic drive system (3) and two hydraulic cylinders (4). The CFRP- and CRP-beams are connected to the test bench at four points. At the outer points, the beam is supported on two movable bearings (5) mounted to the foundation. The two inner points serve as force application, which is facilitated by a loading frame (6). This loading frame can be connected to either the cylinder designed for static tests or the cylinder for endurance testing. The cylinders are mounted on the portal.

A special feature of the test stand is its innovative and energy-efficient drive concept. Instead of a conventional servo-hydraulic approach, an electro-hydraulic drive concept was implemented. In this case, the oil flow is not controlled by servo valves but directly generated by a pump which is driven by a servo motor, ensuring efficient and reliable operation for both static and dynamic testing conditions.

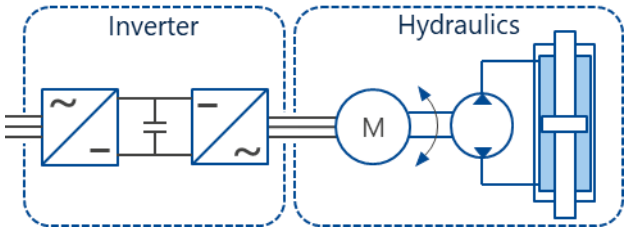

Figure 2: Principle of an electrohydraulic drive.

The electrohydraulic system is based on a radial piston pump driven by a servomotor, which is controlled by a frequency converter. The cylinder motion is achieved by pumping oil between the two chambers of the cylinder. By regulating the pump speed, different cylinder velocities can be achieved. To compensate leakage, the closed hydraulic circuit between the pump and the cylinder is preloaded using an auxiliary unit. The principle is shown in Figure 2. The drive concept offers significant advantages over a conventional servo-hydraulic implementation. The following chapter highlights these advantages.

3 Comparison of Electro- and Servo hydraulics

In a servo-hydraulic system, an electric motor (typically an asynchronous machine) generates a flow of pressurized oil. The movement of the hydraulic cylinder is controlled with a servo valve, which can be simplified as an adjustable throttle. The valve restricts the flow of oil, allowing only the amount required for the desired cylinder movement to pass through. The energy of the pressurized oil that is not utilized for the process is dissipated as heat at the servo valve. These high energy losses result in a significant temperature rise of the oil, requiring an additional cooling system, which consumes further energy. Moreover, any kinetic or potential energy stored in the test specimen cannot be recuperated and is therefore lost.

In contrast, electrohydraulic systems directly generate the required oil flow rates through speed-controlled, highly dynamic motor-pump units. This approach provides two major advantages in terms of energy efficiency.

On the one hand, the elimination of energy-dissipating servo valves avoids the energy losses typically associated with throttling. On the other hand, the ability of the motors to operate in generator mode allows energy to be recuperated. During the unloading phase of the test specimen, deformation energy introduced during the loading phase can be recovered, temporarily stored electrically, and reused for subsequent loading cycles. Figure 3 gives an overview of the energy flows for both drive concepts. [HOF22]

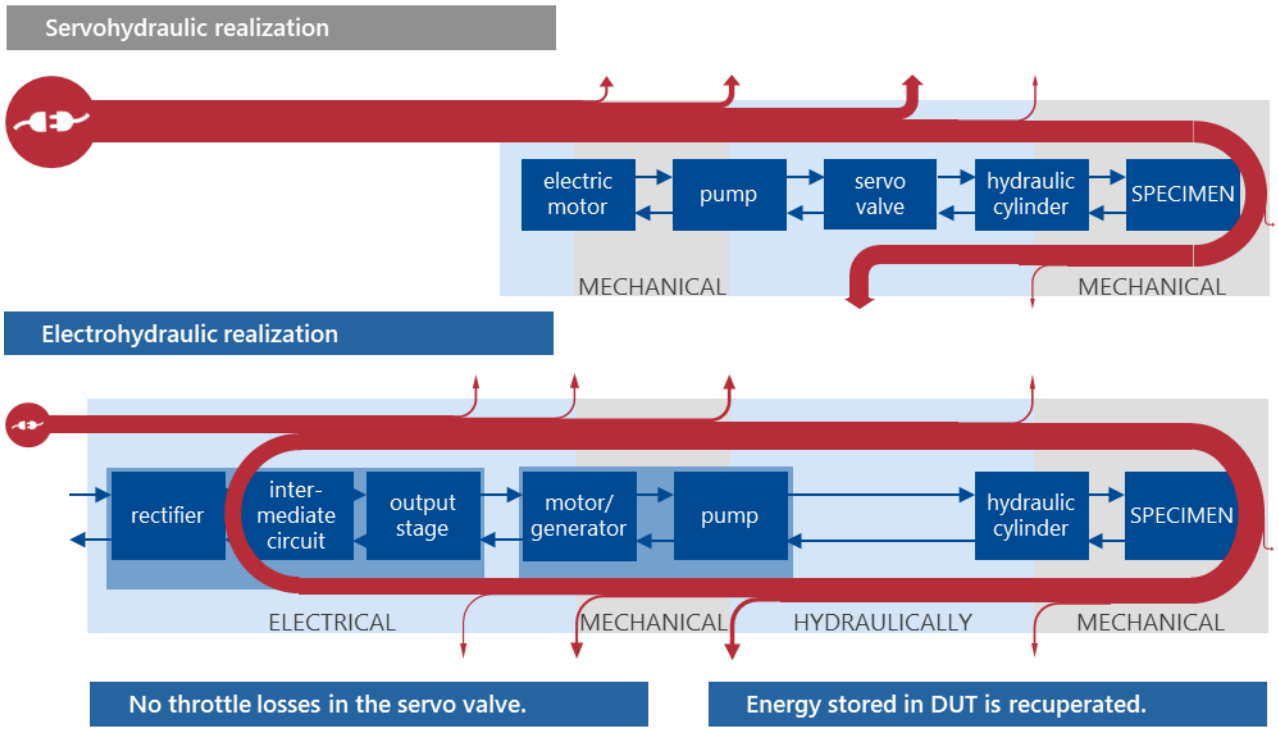

Figure 3: Energy flow of an electrohydraulic compared to a servo hydraulic drive.

The mentioned advantages have been investigated through simulations and experiments. The following section presents the results.

3.1 Experimental Investigation

As outlined above, the results from beam tests are crucial for the development of wind turbine blades. Thus, experimental data was already needed during the development and realization time of the test bench. For this purpose, tests were carried out by IABG for Nordex using as many existing components as possible in a preliminary test setup. As oil supply, different sized cylinders, various servo valves and a modular mechanical system were available on site at IABG, the test setup was realized servo-hydraulically. The test setup is illustrated in Figure 4 and described in detail in the following.

The beam's position was recorded using a cable pull encoder, while the applied force was measured with a load cell. Hydraulic pressure and flow were monitored at key points including the supply, the return lines, and the hydraulic cylinder chambers.

The data obtained from this preliminary test setup enables an experimental comparison of both drive concepts. However, this comparison is limited due to the following two points:

1. For the servo-hydraulic tests at IABG, cylinders of different sizes were available for the dynamic tests. Thus, to minimize the required pressurized oil flow rate, the cylinder sizes were matched to the forces required for each test. This approach ensured that the costs for carrying out the test were kept as low as possible. In contrast, the electrohydraulic test bench has only one cylinder, which is used for all dynamic tests.
2. The electrohydraulic test stand is dimensioned for the required maximum speed. The servo-hydraulic tests were carried out at slightly higher speeds to reduce the test times.

To compare the two approaches, the focus is therefore not on power consumption but rather on energy consumption per load cycle, measured in kWs. Two test series were conducted. The first test used an amplitude of 88 mm at a frequency of 2 resp. 1.3 Hz. The second test reduced the amplitude to 71 mm at 2 Hz resp. 1.6 Hz. As already mentioned, the servo-hydraulic system (cylinder piston area of 1909 mm²) was optimized for this single load case, whereas the test bench was designed to cover a broader operating range (cylinder piston area of 8796 mm²). The results are shown in table 1.

Test	Servohydraulic	Electrohydraulic
72.0 mm @ 2.0/1.6 Hz	30.0 kWs	8.3 kWs
88.0 mm @ 2.0/1.3 Hz	34.3 kWs	10.2 kWs

Table 1: Experimental results.

In the first test, the servo-hydraulic test bench consumed approximately 3.7 times more energy than the electrohydraulic test bench, while in the second test, the demanded energy was 3.4 times higher. By utilizing an electrohydraulic drive, the energy costs for a test campaign of 1 million cycles could be reduced from €2,000.- to €550.- assuming an electricity price of €0.22 per kWh.

This significant difference highlights the potential energy savings achievable with the more efficient electrohydraulic system. Furthermore, if the servo-hydraulic test setup had the same cylinder dimensions as the electrohydraulic driven test bench, its energy consumption would be even higher. This underlines the substantial energy savings and cost reductions offered by adopting an electrohydraulic test bench.

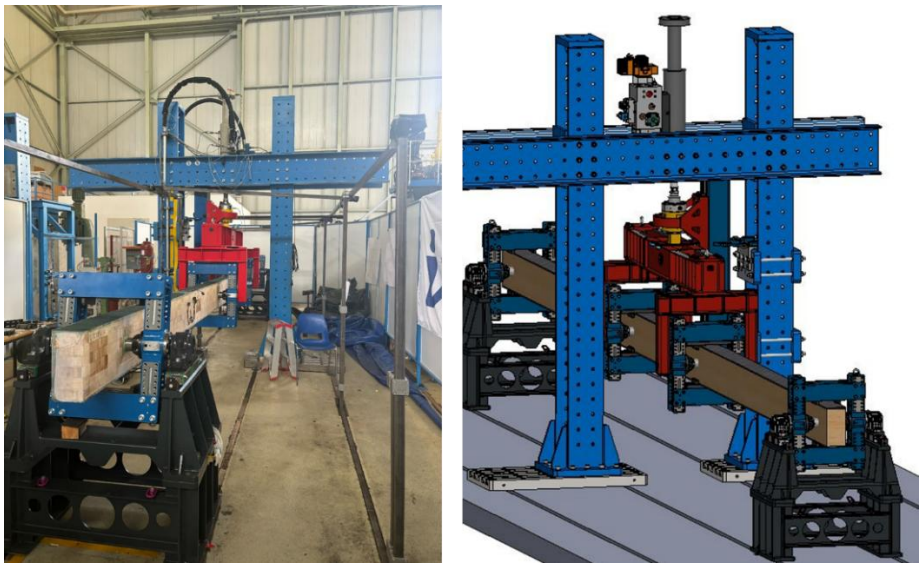

Figure 4: Servo hydraulic test setup.

3.2 Numerical Investigation

As the experimental data are not fully comparable, an additional numerical comparison was carried out. For this purpose, models of a servo-hydraulic and an electrohydraulic test bench were developed and calibrated by experimental data.

The servo-hydraulic model was created in MATLAB Simulink (see figure 5). A significant advantage of this model is its parameterized with component data. It can therefore be realistically scaled. The model was calibrated with measurement data from the IABG beam testing campaign. The error in the simulated power consumption ranged between 5.1% and 7.7% below the measured power.

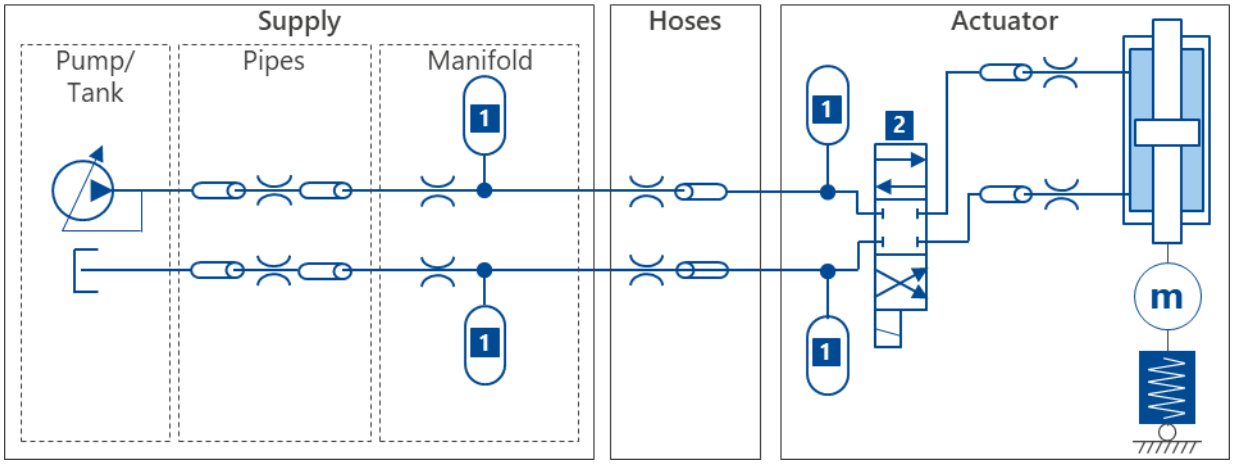

Figure 5: : Structure of the servo hydraulic model. (1) hydraulic accumulators, (2) servo valve.

The energy consumption of the electrohydraulic system was simulated using a model combining a MATLAB-based hydraulic system model and a manufacturer-provided model for the electrical components. This simulation was confirmed using measurement data from the beam test bench. The simulated power consumption was found to be 30% to 35% lower than the measured values. This discrepancy can be explained by inaccuracies in the modelling of the pump and the energy management system.

Figure 6 and Figure 7 show a comparison between the energy consumption of the two drive concepts as a function of frequency and amplitude for two test scenarios, a test specimen with high stiffness (800 kN/m, Figure 6) and a test specimen with low stiffness (40 kN/m, Figure 7). The figures illustrate the energy requirement of the servo-hydraulics in relation to the energy requirement of the electro-hydraulic solution as a percentage, whereby a modal damping of 10% was assumed in both cases.

Across both scenarios, the electrohydraulic system demonstrates similar trends in energy savings compared to the servo-hydraulic system. The electrohydraulic system achieves its highest efficiency at low frequencies and high amplitudes. Here, the servo hydraulics require up to 13 times more energy. Conversely, for high frequencies and low amplitudes, the servo-hydraulic system requires less electrical energy to achieve the test load. Further energy required for cooling the oil is not considered here. Taking this energy into consideration would lead to a further improvement in the achievable energy savings.

With the softer beam, slightly higher energy savings are observed at high amplitudes, which shows that the energy-saving characteristics of the system are relatively constant over the entire operating range of the test bench.

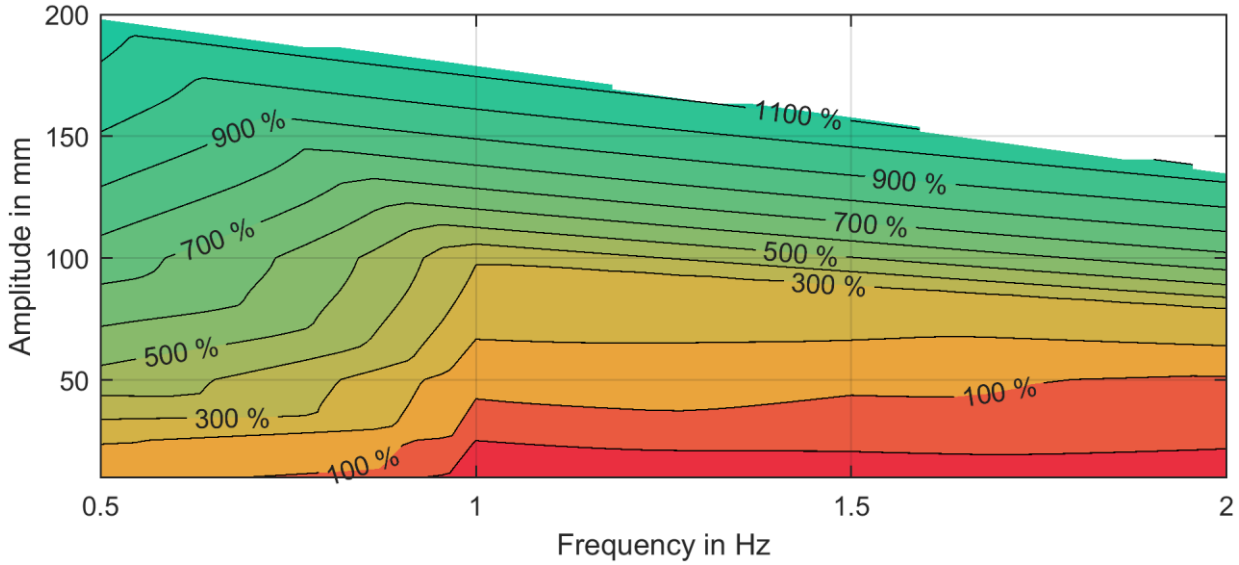

Figure 6: Relative energy consumption of a servohydraulic drive compared to an electrohydraulic drive in a test scenario with a high stiffness (800 kN/m).

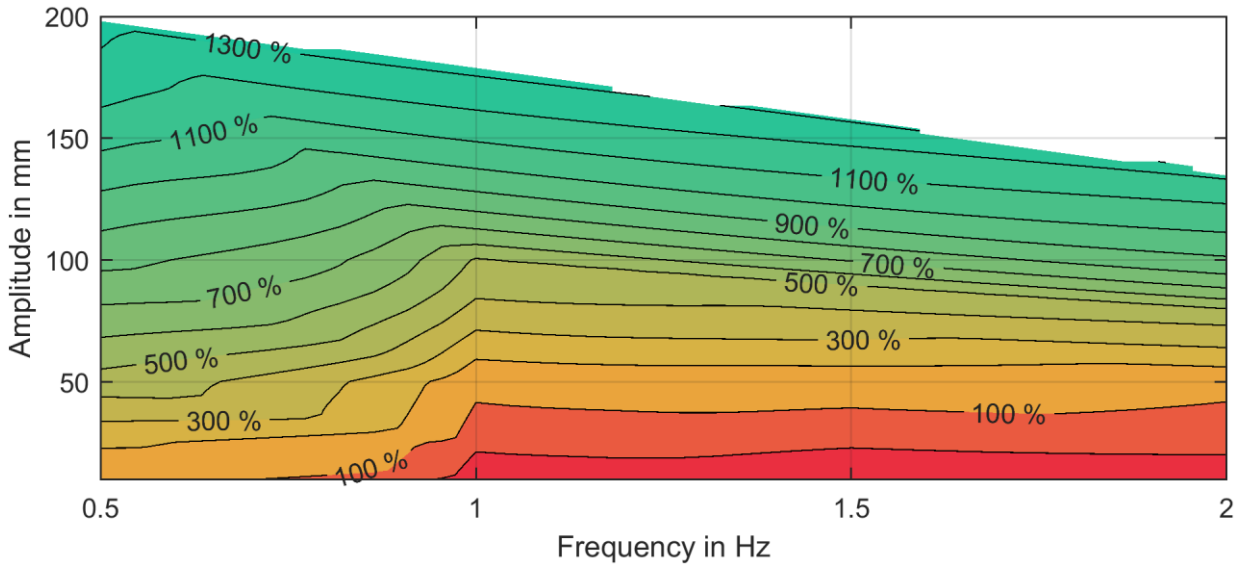

Figure 7: Relative energy consumption of a servohydraulic drive compared to an electrohydraulic drive in a test scenario with a low stiffness (40 kN/m).

Both beam characteristics were further analyzed through a representative Wöhler test with a duration of two weeks (see Table 2). The results highlight significant energy savings: the electrohydraulic system reduces energy consumption by an average of 89% for the soft and 87% for the stiff beam.

Converting the energy savings into operational costs reveals significant cost benefits. With an electricity price of €0.22 per kWh and a testing campaign involving nine specimens (six weeks of test duration), the energy costs decrease significantly from €6,963.- to €1.855.- and respectively from €7,591.- to €1,481.- in case of the soft beam.

Based on these results, a theoretical annual energy cost saving of up to €48,000 is achieved. This highlights the significant economic potential of electrohydraulic drive systems in extended fatigue testing scenarios.

Amp.	Freq.	Load Cycles	Low Stiffness (40 kN/m)			High Stiffness (800 kN/m)		
			Peak Force	Servo hyd.	Electro hyd.	Peak Force	Servo hyd.	Electro hyd.
[mm]	[Hz]	[mio]	[kN]	[kWh]	[kWh]	[kN]	[kWh]	[kWh]
100.00	1.00	1.00	4.00	31.46	6.99	80.00	27.67	8.98
130.00	0.75	0.10	5.20	85.50	9.70	104.00	88.21	11.59
160.00	0.50	0.01	6.40	139.73	12.43	128.00	149.45	14.49
			Total:	**256.70**	**29.12**	**Total:**	**265.00**	**35.05**

Table 2: Representative Wöhler Beam Test. Both simulations were carried out with beams whose stiffness covered the operating range of the test rig well.

4 Discussion and Conclusion

A test bench was developed for the qualification of CFRP- and CRP materials in the wind energy industry. Since the material samples cannot be arbitrarily miniaturized, they are laminated onto up to 13-meter-long balsa wood beams and qualified using a four-point bending test. Due to this requirement, the test bench must handle dynamic alternating loads of up to 200 kN and static loads of up to 400 kN. To reduce operational costs, the test bench is equipped with an energy efficient electrohydraulic drive system capable of recuperating energy stored in the specimen and minimizing hydraulic losses compared to conventional servo-hydraulic systems.

Experiments demonstrated that this system could reduce energy costs in comparison to a servo hydraulic drive by approximately 70%. Through simulations comparing various cylinder sizes, it was shown that energy savings of up to 91% are possible. Applying these findings to a typical testing campaign with two different beam stiffnesses could result in annual energy cost savings of up to €48,000. These results highlight that the system is particularly advantageous for applications involving low frequencies and high amplitudes, making it especially suitable for such use cases.

Moreover, the drive concept has potential for application in other testing scenarios where energy can be recuperated from motion. This includes tests with specimens that exhibit stiffness and undergo significant deformations while testing. The concept could also be applied to testing scenarios where large masses are moved using sinusoidal excitations.

Overall, this drive system provides a tool that can shorten development cycles in the wind energy sector by enabling development-oriented testing of components and materials. Additionally, the reduction in energy costs makes long-term durability tests economically viable.

5 Bibliography

[HOF22] Hoffmann, Sebastian; Glauer, Stefan; Dany, Sasha; Schmidt, Holger: Flexible und energieeffiziente Prüfsysteme für Dauerlaufprüfungen. Prüfmethodik für Betriebsfestigkeitsversuche in der Fahrzeug-industrie. DVM, Sindelfingen, 2022

Drivetrain Technology:

Noise, Vibration, Harshness

An efficient simulation chain for predicting the vibro-acoustic behavior of industrial gear units

Dr.-Ing. Prateek Chavan[1], Dipl.-Ing. Markus Lutz[1]

[1]SEW-EURODRIVE GmbH & Co KG

Keywords: *airborne sound, multibody simulation, gear unit, vibro-acoustics*

Abstract

Predicting the vibro-acoustic behavior of gear units typically involves a two-stage process: First, the assembly is modelled in a flexible Multibody Simulation (MBS) at a specific operating point. Second, based on the resulting structure-borne sound, a simulation of the airborne sound is calculated to get the far-field results. This simulation of far-field airborne sound is often time consuming, computationally expensive and generates large amount of data. Moreover, if different software are utilized, the same assembly model must be duplicated in both the MBS software and the airborne sound simulation software, leading to redundant modeling effort.

This paper introduces an efficient simulation chain for predicting the vibro-acoustic behavior of industrial gear units. Here, the focus lies on the efficient design of the airborne sound simulation. We present approaches for reducing computational effort and data generation, without significantly compromising on accuracy. Furthermore, potential methods for the improved transfer of interface forces between the structure-borne and airborne simulation software are discussed. Subsequently, the proposed simulation chain is implemented for an exemplary industrial gear unit and compared with corresponding experimental measurements.

1 Introduction

Industrial gear units provide high driving torques in a variety of applications such as material handling, hoisting, mixers, agitators, etc. The acoustic behavior of such gear units is an important property, which must be calculated in early design stages for potential optimization. For the accurate simulation of the gear units operating point in the time domain, system non-linearities such as mesh stiffness, bearing stiffness and excitation must be modelled as well. Flexible Multiple Body Dynamics Simulation (MBS) offers a suitable environment for simulating the dynamic behavior at different operation points and loading conditions. Here, the shafts, housing, and covers are modeled as linear elastic bodies, while the gear mesh, bearing behavior and certain joints are represented by non-linear force elements. The non-linear and time dependent contact between gear teeth and the behavior of the bearings are represented using analytical formulations.

Such a flexible MBS can be utilized not only for analyzing the dynamic behavior but also for simulating the acoustic behavior of the gear unit. The vibration of the radiating structure (gearbox-cover assembly) from the MBS can be exported to a subsequent external sound propagation simulation. Depending on which data are transferred between the MBS and acoustic analysis, different vibro-acoustic simulation chains are possible which correspond to different modelling and computation effort. For example, the reaction forces and torques acting at the bearings can be used for the acoustic analysis or the surface velocity at the gearbox-cover node can directly be exported [WER22].

The aim of this paper is to implement and evaluate two different vibro-acoustic simulation chains and demonstrate the advantages of the 'Modal Participation Factor'-based vibro-acoustic simulation chain.

For implementing the vibro-acoustic simulation chains, a three-stage industrial gear unit 'X3KS100' manufactured by SEW EURODRIVE GmbH & Co KG is selected as the test object. The gear unit with 6450 Nm nominal torque and transmission ratio of i = 13.47 represents the smallest unit in the X-range portfolio.

2 Simulation chains for vibro-acoustic prediction

Independent of the simulation chain, the starting point for the acoustic analysis is the CAD-Model of the gear unit assembly. The FEM-models of relevant component CAD models are then prepared. This involves de-featuring, meshing, defining the interface nodes and subsequently exporting the Craig-Bampton reduced model. The reduced models of the components are then assembled in the MBS by defining joints, bearings and gear pairs. The component as well as assembly models of the test gear unit were systematically validated and documented in [CHA23].

Once the validated MBS-model is available, the required constant operating point is simulated in the MBS by applying the loads and rotational speeds. The time domain results of such a simulation can then be utilized for the sound propagation simulation. Two possible approaches for using the MBS result data are discussed here (Figure 1).

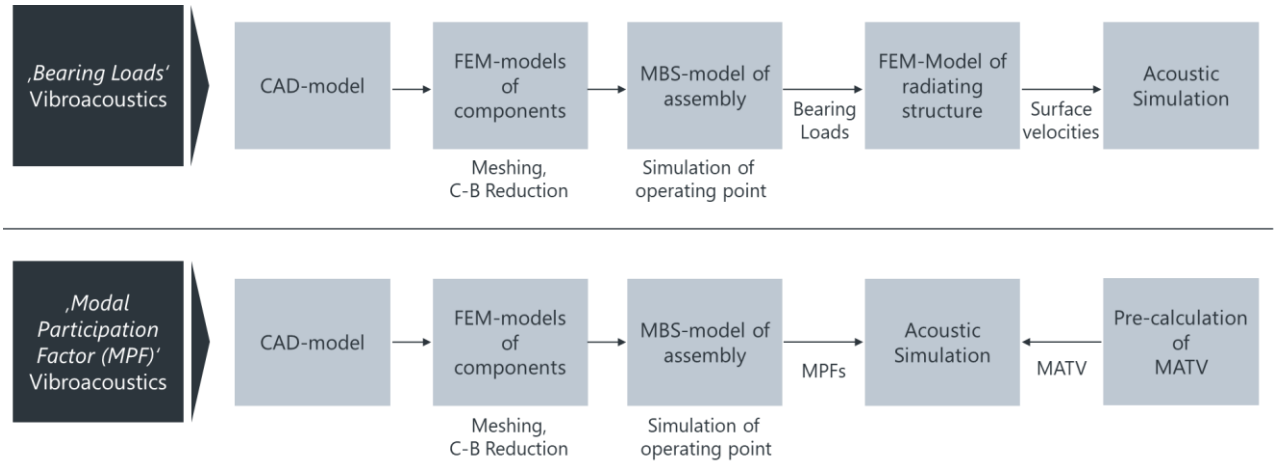

Figure 8: Two considered approaches for vibro-acoustic simulation

2.1 Bearing loads vibro-acoustics

In this approach, the time domain bearing reaction forces and torques occurring during the simulated operation point are extracted from the MBS. These reaction forces and torques are then applied to an identical model of the sound radiating structure (housing, bearing cover and inspection cover assembly) in the acoustic simulation software. Figure 2 illustrates the implementation of this simulation chain with Simpack and ANSYS Workbench.

The bearing reaction loads between the inner and outer races of all gear unit bearings are first split into static and dynamic components. The static components are applied as bearing preloads at the bearing seats of the housing-cover assembly model in the acoustic analysis software. The dynamic bearing load components are transformed to the frequency domain and applied at the bearing seats for the harmonic response calculation. The resulting frequency domain surface velocities are then

utilized in the harmonic acoustics step to calculate the external sound propagation from the housing-cover assembly. Using virutal far-field microphones, the acoustic response can be captured for comparison with microphone measurement from tests in hemi-anechoic chamber.

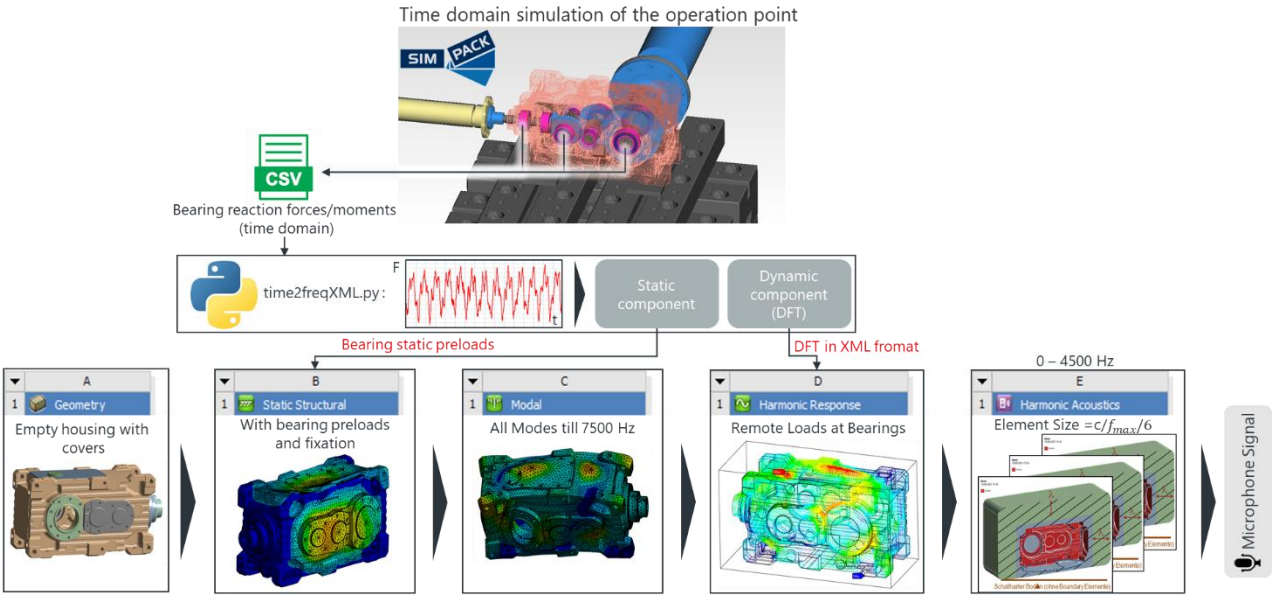

Figure 9: Implementation of bearing loads vibro-acoustics with Simpack and ANSYS Workbench

The main drawback of this approach is that the passive, sound radiating structure (housing-cover assembly) must be modelled not only in the MBS simulation but also in the acoustic analysis. Here, the boundary conditions should be identical to the MBS simulation. This results in double modelling effort and additional simulation time.

2.2 Modal Participation Factors (MPFs) Vibroacoustics

An alternative to using bearing reaction loads is to directly utilize the surface normal velocities at the external nodes of the housing-cover assembly from the MBS. In this way, the double modelling of the housing-cover assembly is avoided. If the frequency domain transfer function between the surface velocities and sound pressure at far-field microphone is pre-calculated, the following relation can be used to efficiently predict the response to arbitrary velocity excitation [GER01],

$$\{p(\omega)\} = [ATV(\omega)] \cdot \{\dot{x}(\omega)\}. \qquad \textbf{Eq. 1}$$

However, the extraction of surface normal velocities at all external nodes and their transformation to frequency domain leads to a large amount of data exchange and cumbersome data handling. A more elegant and efficient approach is to use modal transformation,

$$\{x\} = [\varphi] \cdot \{q\}. \qquad \textbf{Eq. 2}$$

Where φ is the modal matrix and q represents the modal coordinates or modal participation factors. Substituting Eq. 1 into 2,

$$\{p(\omega)\} = [ATV(\omega)] \cdot [\varphi] \cdot j\omega \cdot \{q\}. \qquad \textbf{Eq. 3}$$

Summarizing the frequency-dependent, constant terms in the Modal Acoustic Transfer Vector (MATV) [GER01], [HUA14],

$$[MATV(\omega)] = [ATV(\omega)] \cdot [\varphi] \cdot j\omega. \qquad \textbf{Eq. 4}$$

Where, MATV is the transfer function between the modal coordinates and the sound pressure at the microphones,

$$\{p(\omega)\} = [MATV(\omega)] \cdot \{q(\omega)\}. \qquad \textbf{Eq. 5}$$

Prerequisite for the application of this simulation chain is the ability to pre-calculate the frequency dependent acoustic transfer vector or the modal acoustic transfer vector. In the acoustic simulation software Wave6 from Dassault Systèmes, cached matrices containing the frequency based transfer functions can be created after the first simulation run. This functionality is used to implement the described MPF vibro-acoustic simulation chain (Figure 3).

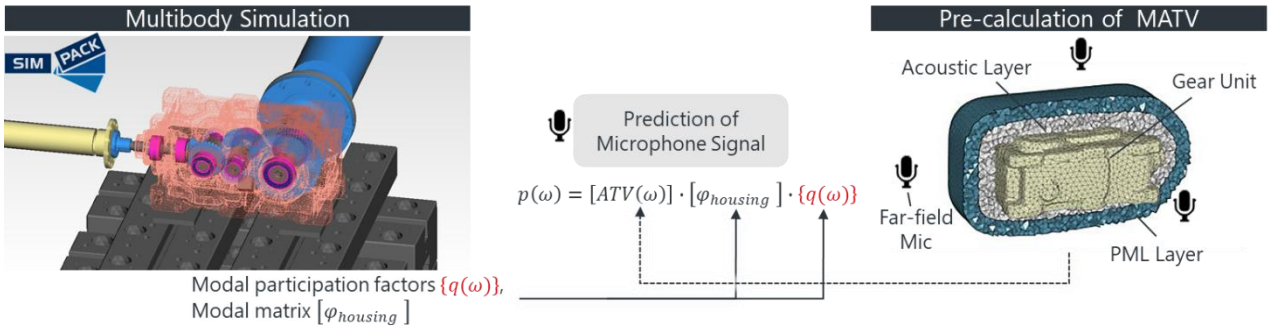

Figure 10: Implementation of MPF vibro-acoustics with Simpack and Wave6

3 Use Cases for MPF Vibro-acoustics

A key advantage of the MPF vibro-acoustics for gear units is that once the MATV is calculated for a housing-cover assembly, the same MATV can be utilized for acoustic predictions in case of excitation modifications or structural modifications. These modifications will (under certain conditions) only result in the modification of the MPFs, while the ATV and modal matrix remains unchanged. Thus, the Eq. 5 can be solved with the new MPFs obtained from the MBS to directly obtain the response at the far-field microphones without recalculating the sound propagation simulation.

Excitation modification in gear units can usually result from either a change in operating point (rotation speed, load torque, radial forces on output shaft) or when transmission ratio is changed. Modular gear units are designed such that a variety of transmission ratios and gear stages are possible while using the same gear housing-cover assembly. Thus, in both these cases of excitation modification, the same MATV can be utilized (Figure 4).

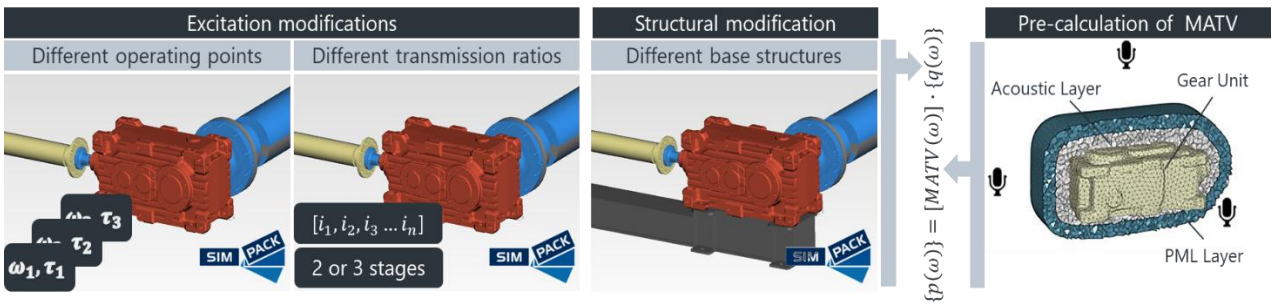

Figure 11: Use cases for predicting acoustic behaviour using MPF vibro-acoustics

The influence of structural modifications, which do not change the modal matrix of the sound radiating structure, can also be predicted efficiently with the same pre-calculated MATV. In case of gear units, the base structure (eg.: base frame) represents a variable structure which depends on the

application and does not affect the MATV of the housing-cover assembly. Thus, the influence of different foundations on the dynamic behavior can be considered in the MBS and resulting MPFs can be applied in Eq.5. In this case, the sound reflection and sound radiation from the base frame, drive and load shafts is ignored. If these effects are significant and need to be considered, the MATV must be calculated in a new acoustic simulation.

4 Summary

This paper demonstrates the utility of MPF based vibro-acoustic simulation chain for the efficient prediction of the acoustic behavior of industrial gear units. The implementation of the MPF vibro-acoustics for an industrial gear unit shows a reduction in modelling and compute time compared to bearing force vibro-acoustics. For modular gear units, the influence of certain modifications of excitation and base structure can be predicted without a recalculation of the sound propagation simulation.

5 Bibliography

[CHA23] Chavan, P. and Lutz, M.: *Validation of an industrial gearbox model for predicting vibro-acoustic behavior.* In: Proceedings of the International Conference on Gears, 13-15 September 2023, Garching/Munich, 2023.

[GER01] Gérard, F., Tournour, M., El Masri, N., Cremers, L., Felice, M. and Selmane A.: *Acoustic Transfer Vectors for Numerical Modeling of Engine Noise*. In: 2001 SAE Noise & Vibration Conference & Exposition, April/May, Traverse City, 2001.

[HUA14] Huang, Y. and Cui, Z.: *‚ATV and MATV Techniques for BEM Acoustics in LS-Dyna*'. In: 13th International LS-DYNA Users Conference, Detroit, 2014.

[WER22] Werner, D., Schneider, S., Neher, J., Graf, B. and Wender, B.: *Sound radiation of gearboxes - Reasons for deviations between calculated and measured sound power levels in NVH analyses.* In: Proceeding of ISMA2022 International Conference on Noise and Vibration Engineering, 12-14 September, Leuven, 2022.

Efficient Simulation of Rotordynamics and Acoustics of an Electric Drive Train with Electromagnetic Coupling

T. Dombrovskij[1], A. Boucke[1], Richard Schönen[1]

[1]Ingenieursgesellschaft für Strukturanalyse und Tribologie mbH, Germany, Schloss-Rahe-Str. 12, 52072 Aachen

Keywords: *electric drive train, electromechanical coupling, multi body simulation, roller bearings*

Abstract: In this paper a numerically efficient method for the calculation of electromagnetic forces and their integration into the simulation of elastic multibody systems is presented. The electromagnetic forces are calculated by solving the Maxwell equations and are stored as lookup tables based on rotational speed, torque, rotor position and eccentricity. A multi body simulation software is used for the calculation of the structure dynamics of the elastic bodies considering the electromagnetic forces based on the lookup tables of the previous step. The software package *FIRST* from IST is used here. The developed simulation model enables the analysis of dynamic and acoustic behavior (NVH) of electric drive trains under consideration of static and dynamic rotor eccentricities as well as bearing contacts. A test bench has been designed and a corresponding simulation model has been built to validate the simulation model by comparing measurements and simulations of multiple run-ups. Furthermore, parameter sensitivity studies have been carried out and the majority of the resulting workflow has been automated for a user-friendly application.

1 Introduction

In the current movement towards sustainable energy to reduce greenhouse gas emissions the electrification of driving systems rapidly gained relevance. The growing market share of electric motors in fields related to e.g. means of transportation, but also in fields like power generation, necessitate methods of analysis with appropriate model depth. This holds especially true for the analysis of NVH (Noise-Vibration-Harshness) behavior of electric motors and the prediction of the effect of vibrations on structural dynamics, bearing forces and therefore bearing life expectancy. Additionally, the noise of the motor is one of the purchase criteria for electric vehicles. Effects like an unbalanced magnetic pull caused by rotor eccentricity are particularly interesting for their contribution to NVH and their influence on the dynamic forces acting on the motor. Analyses of such effects can be used to e.g. suggest reasonable manufacturing tolerances. Simulating the interaction between the mechanical and the electromagnetic subsystems requires elastic multi-body simulation (eMBS) and can be computationally intensive, even with today's resources. Especially because the calculations have to be coupled with the excitation forces of the electromagnetic domain, which are time-dependent on the electric currents and the magnetic fields. The frequency of the excitation forces is determined from the control and power electronics as well as from the geometry and architecture of the electrical machine (e.g. rotor and stator poles).

Further nonlinear behavior, such as that of the rolling bearings, which is determined by bearing clearance and Hertzian contact stiffnesses, are mapped in the eMBS. The aim of this paper is to present an efficient simulation approach, which allows the consideration of static and dynamic eccentricity effects as well as present a comparison of different roller bearing calculation models and a user-friendly automation for sensitivity analysis.

2 Calculation of Electromagnetic Forces

The NVH analysis of electric drivetrains requires the simulation to be carried out in the time domain with subsequent transformation into the frequency domain. The symmetry of the Fourier transformation couples sampling rate and highest observable Eigenfrequency (Eq. 1). Consequently, the Eigenfrequencies of the reduced structure have to cover all modes up to at least $f_{\max}$.

$$f_{\text{sample}} = 2f_{\max} \qquad \textbf{Eq. 1}$$

The electromagnetic forces can be calculated using an external software package of choice. The requirement is that it is able to at least calculate the magnetic field density in the airgap on a discrete mesh. The radial and tangential force densities can be subsequently calculated using Eq. 2 and Eq. 3.

$$\sigma_{\text{Rad}} = \frac{\mathrm{B}_{\text{Rad}}^2 - B_{\text{Tan}}^2}{2\mu_0} \qquad \textbf{Eq. 2}$$

$$\sigma_{\text{Tan}} = \frac{\mathrm{B}_{\text{Rad}} \cdot B_{\text{Tan}}}{\mu_0} \qquad \textbf{Eq. 3}$$

These force densities can be integrated over each stator tooth and rotor pole to receive the electromagnetic force excitation. Some software packages e.g. MotorCAD [MOT25] already compute the integral force components. These electromagnetic forces are precomputed for multiple operating points with torque T, rotor eccentricity ε and rotor velocity v. The resulting lookup tables have the dimensions of $2(\Phi \times n_t \times s)$, where Φ is the number of discrete calculation points along one mechanical rotation, n_t is the number of stator teeth and s is the number of axial segments along the rotor axis. Figure 12 shows an example the integral radial and tangential forces of one axial segment for the case of static rotor eccentricity.

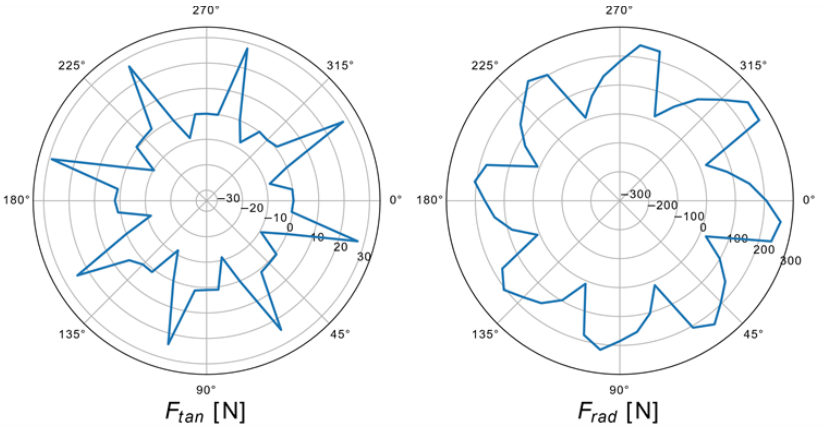

Figure 12: Polar plot of tangential and radial electromagnetic forces on the stator teeth with torque $T = 10$ Nm, rotational velocity $v = 3000$ and static eccentricity $\varepsilon \approx 28.5\%$ in the direction of $\phi = 0°$

For the different cases of eccentricity (concentric, static, dynamic) the forces are shown in the frequency domain in Figure 13. In the concentric case the multiples of stator teeth (48) and rotor poles (8) are seen in the space and time harmonics. In case of static eccentricity, the forces gain adjacent space harmonics. In case of dynamic eccentricity, the adjacent space harmonics are additionally shifted in the time harmonic direction, since the eccentricity changes over time and space.

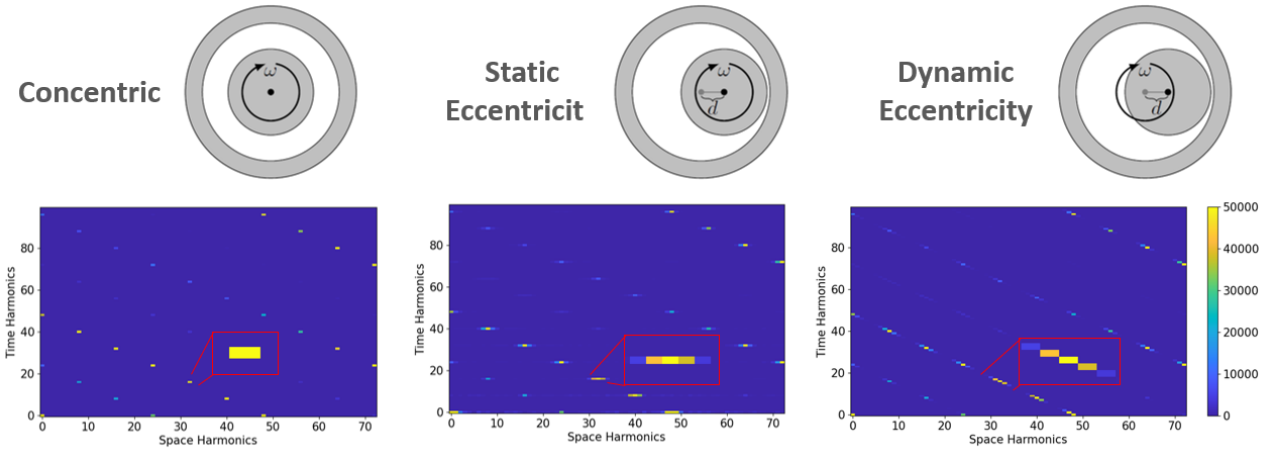

Figure 13: 2D FFT amplitudes of radial forces in [N] for a) concentric, b) static c) dynamic eccentricity

When the rotor magnets or stator teeth are skewed, multiple axial segments are needed. The amount and placement can be freely chosen by the user, as seen with three segments in Figure 14. Each segment is implemented as a coupling in the simulation model with its own lookup tables previously calculated by solving Maxwells equations in 2D. The necessary parameters are set in the graphical user interface in “xPre” (preprocessor of *FIRST*).

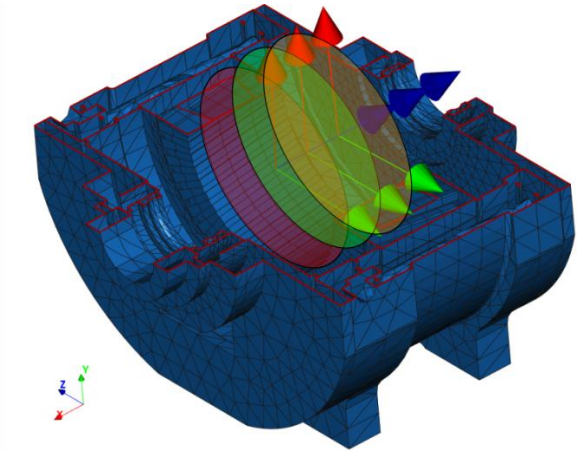

Figure 14: Concept of multiple axial segments defining the electromagnetic force interfaces for the consideration of stator teeth/rotor magnet skew.

Since the rotor is very stiff in the modelled application, the resulting tangential forces are applied as torque with the leverage l_i on the rotors center line in form of Eq. 4.

$$m_{\mathrm{rotor}}(v,\varepsilon,\phi) = \sum_{i=1}^{n_t} F_{\tan}(v,\varepsilon,i,\phi) l_i \qquad \textbf{Eq. 4}$$

The axial forces caused by skewed stator teeth or skewed rotor magnets are approximated via applying the skew-angle to the tangential electromagnetic forces (Eq. 5).

$$F_{axial}(v,\varepsilon,\phi) = \sum_{i=1}^{n_t} F_{\tan}(v,\varepsilon,i,\phi) tan(\alpha) \qquad \textbf{Eq. 5}$$

3 Multi-Body-Simulation Model

The finite element elastic multibody simulation model contains the structures, which underwent mixed static/modal reduction [FIR25], the EM-force coupling interface [DOM22] as well as roller bearing coupling interfaces. The housing is fixed at eight node groups via RBE3 elements located at the areas where the specimen will be held in place at the test-bench. The fixation is implemented by using a stiff spring damper (SD) coupling element. An overview of the setup is given in the concept schematic in Figure 15.

3.1 Material Model and Mass

The stator and rotor sheet stacks as well as the copper windings of the electric drive train can be modelled homogeneous and possibly anisotropic materials using different approaches. The chosen approaches are according to [FRA22] and [MIL15] respectively. The influence of the winding material on the velocity of the nodes on the outer housing surface can be seen in Figure 16.

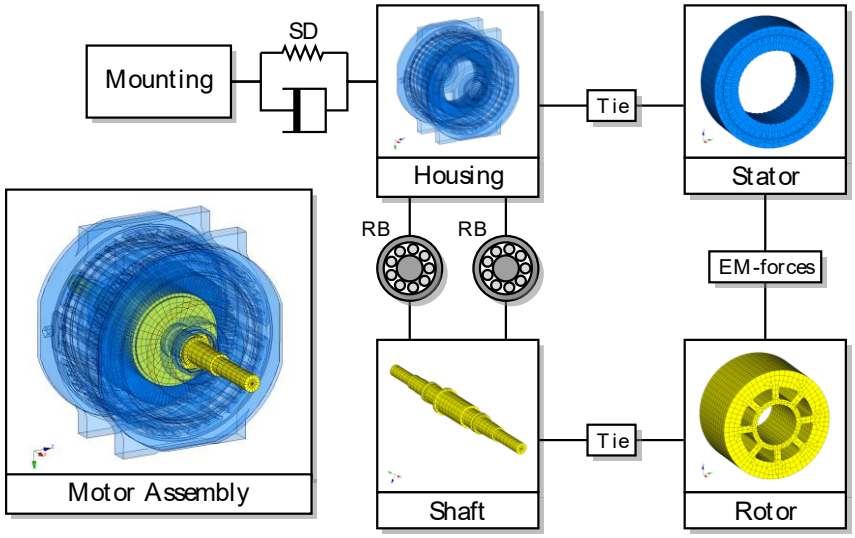

Figure 15: FE model schematic with RB=roller bearing coupling, SD=spring damper coupling.

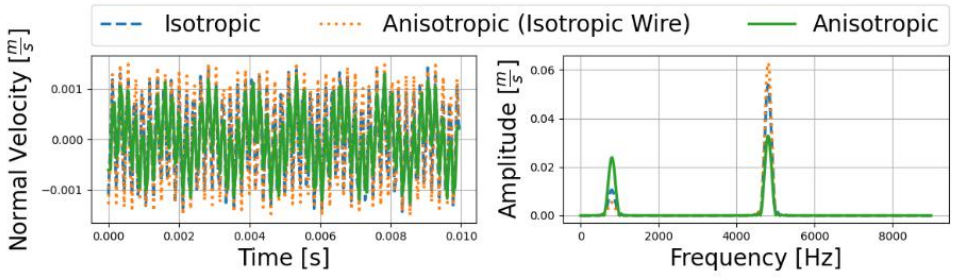

Figure 16: Node velocity for different combination of material models of sheet stacks and copper windings.

Since the real-world model (i.e. test bench) requires hardware to measure different result values such as surface velocities, the corresponding masses of lasers and cables as well as clutch are modelled as additional mass points.

3.2 Automation

Both the calculation of electromagnetic forces, as well as the multi body simulation have been automated by the use of the scripting language Python. MotorCAD has an existing interface with Python bindings to set up and control multiple calculations. Additionally, a script was implemented to enable sensitivity analyses of the FEM simulation.

4 Roller Bearing Model

The standard *FIRST* roller bearing coupling calculates the roller bearing forces for each rolling body according to a hertzian contact stiffness, which are in turn applied locally at the rolling element's position. The interface has been validated by comparing it to tools like Schaeffler's "Easy E-Maschine" online tool [SCH23], the software package MESYS [MES25] and roller bearing calculations according to [NGU16]. The radial forces on the roller bodies have been compared in Figure 17. Additionally, MESYS is able to calculate the radial forces caused by axial forces on a roller bearing from the resulting contact between roller body and bearing groove for arbitrary roller bearing geometries and types. Thus, the implemented MESYS interface in *FIRST* and its effect on the surface vibration is discussed in the subsequent results section (see chapter 5).

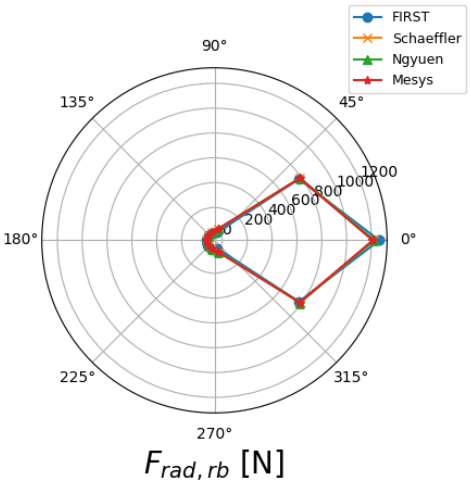

Figure 17: Radial forces acting on 10 roller bodies in a groove ball bearing: Comparison between FIRST, Schaeffler roller bearing tool, Mesys and calculations according to [NGU16].

5 Results

To test the influence of the roller bearing model multiple run-ups have been simulated for different eccentricity cases (concentric, static eccentricity $\varepsilon = 28.5\%$ and dynamic eccentricity $\varepsilon = 28.5\%$,). To get an understanding of the general effect of eccentricity Figure 18 shows the spectrogram of the acceleration of a node on the housing surface over the run-up duration. The diagonals with the highest amplitude marked in yellow show the harmonic orders that relate to multiples of rotor poles (8) and stator teeth (48), with the teeth order being the most pronounced. Since in the concentric case the radial forces cancel each other out, the load on the roller bearing is only caused by gravitational force on the rotor acting in the y-axis direction. In the static eccentricity case, the radial forces are not cancelled out and act in the direction of eccentricity (smallest air gap). Additional

harmonic orders become more visible (e.g. 32nd, 64th). In the dynamic eccentricity case, the radial roller bearing forces rotate with the position of the smallest air gap and the spectrogram shows additional harmonic orders that are placed at +/-1 of the pole/teeth orders, especially visible at orders 8, 24 and 48. The effect of eccentricity on the NVH behavior and the roller bearing forces is therefore working as expected. The previously used *FIRST* roller bearing model is compared to the Mesys roller bearing in Figure 19. As indicated by the region in the red circle, the calculation with Mesys changes the position of the amplitude maxima along the harmonic orders, in this case the 24th order. This shift of the amplitude maxima might be explained by the differences of force application in the two roller bearing models. While the *FIRST* roller bearing applies the forces locally, the MESYS roller bearing applies the forces as a sum in a center-point-coupling. Additionally, the MESYS interface takes into account the radial forces which are caused by the roller bodies being pushed into the grooves and can therefore alter the resulting radial forces due to axial forces stemming from stator tooth or rotor magnet skew. The comparison with the measured data from the test bench is shown in Figure 20. The figure shows the comparison of amplitude along the harmonic orders for the simulations using FIRST roller bearing model, the Mesys roller bearing model and the test bench measurements. While the simulations with Mesys roller bearings show a difference in some of the order amplitudes, the roller bearing model does not seem to be the missing factor to reach the measured test bench results. As seen from previous work however [ZIM24], the measurement strategies for the testbench were previously untested for this application and the measurements therefore remained with some uncertainty regarding the interpretation.

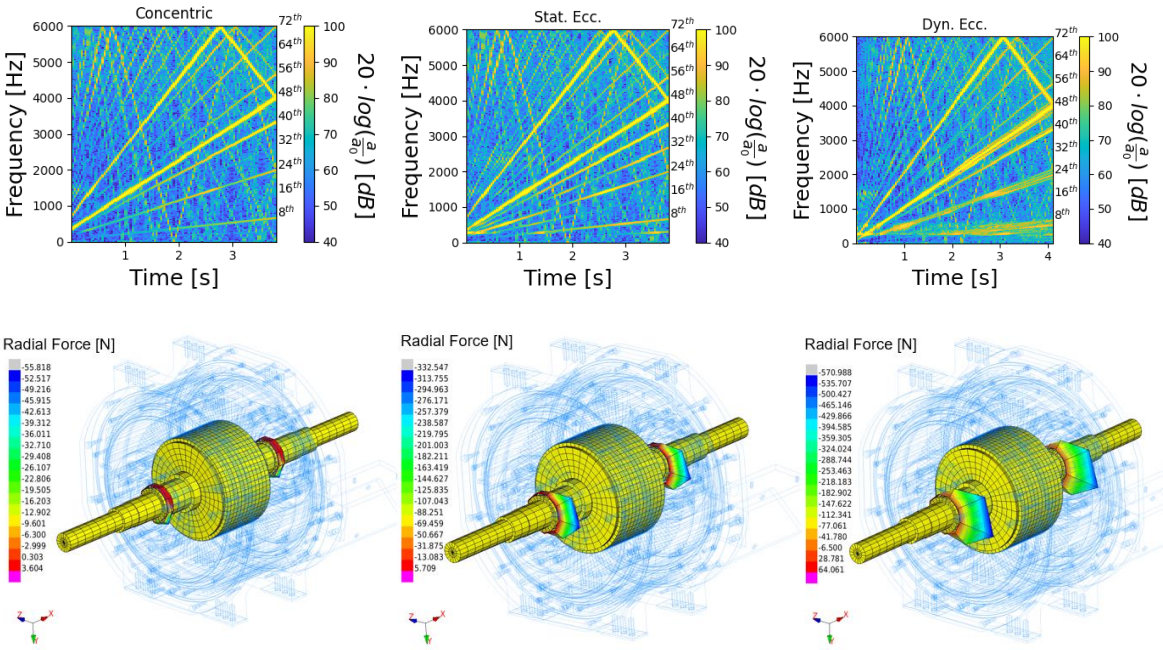

Figure 18: Top row: Spectrogram of runup simulations for different eccentricity cases. Bottom row: Resulting radial forces on (FIRST) roller bearings.

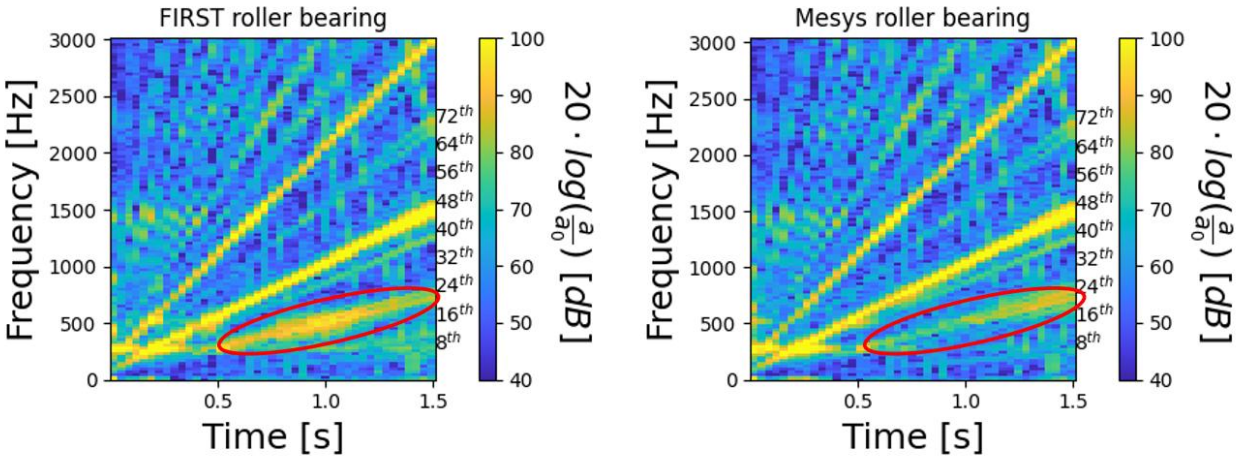

Figure 19: Comparison between FIRST and Mesys roller bearing: shift of amplitude maxima along of 24th order in frequency spectrum of the runup.

Figure 20: Order cut in spectrogram for one measurement point and comparison of roller bearing models with test bench data.

6 Conclusion

The workflow process of simulating an electric drive train with an electromechanical coupling using an elastic multi body simulation and look up tables for the electromagnetic forces has been demonstrated. Different roller bearing models have been presented and compared. The use of these roller bearing models with the implemented *FIRST*-Mesys interface has been found have a significant impact on the results, even though the measurement data did not allow defining a modeling priority for this application.

7 Bibliography

[DOM22] Dombrovskij, Tamir: Mehrkörpersimulation elektromagnetisch gekoppelter Antriebssysteme
ATZLive Expertenforum Powertrain, 2022

[FIR25] FIRST - Multibody System Simulation Software
https://www.ist-aachen.de
accessed: 08.01.25

[FRA22] Franck, Marius: Strukturdynamische Werkstoffdämpfung von Blechpaketen elektrischer Maschinen.
In: e & i Elektrotechnik und Informationstechnik volume 139, pages 167–175
Springer, 2022

[NGU16] Hung-Nguyen-Schäfer: Numerische Auslegung von Wälzlagern
Springer Verlag, 2016

[MIL15] Millithaler, Pierre: Dynamic behavior of electric machine stators: Modelling guidelines for efficient finite-element simulations and design specifications for noise reduction.
HAL open science, Université de Franche-Comté, 2015

[MOT25] Ansys MotorCAD: Electromechanical Design Software
https://www.ansys.com/de-de/products/electronics/ansys-motor-cad
accessed: 08.01.25

[SCH25] Schaeffler Tool zur Berechnung von Wälzlagern: „Bearinx-online Easy E-Maschine“
https://bearinx-online-easy-emachine.schaeffler.com/
accessed: 08.01.25

[ZIM24] ZIM research project: EleSim
IST mbh, MSE Institute RWTH, IEM Institute RWTH
2024

Drivetrain Technology:

Predictive Maintenance and Condition Monitoring

Fiber Optical Sensing solution for powertrain design validation and condition / performance monitoring

G. Angelis[1], M. Kolsteeg[1], W. Joosten[2], G. Angelis[1]

[1]Sensing360 B.V., Vondellaan 106 Utrecht, The Netherlands

[2]Damen, Avelingen-West 20 Gorinchem, The Netherlands

Keywords: *Fiber Optical Sensing (FOS), Design Validation, Condition Monitoring, Gears, Bearings, Powertrain*

Abstract: It is important to understand the operating conditions and health status of a driveline. With detailed information on the loads acting on machine elements like bearings and gears, driveline designs can be improved and the modelling assumptions can be validated. One needs to rely on sophisticated software packages and modelling assumptions to compute detailed stress and strain distributions to understand the implications of bearings arrangements and gear configurations.

To achieve the next level of reliability and performance there is a need to verify the design calculations with measurements covering real operating conditions.

This paper summarizes a novel Fiber Optical Sensing (FOS) solution that makes it possible to measure crucial performance indicators suitable for driveline design verification and qualification. At the core of the technology is a FOS sleeve instrumented with a single fiber comprising about 9-13 sensors (Bragg gratings) around its circumference. The sleeve is installed on the outer ring of a bearing to measure accurately and real-time the detailed strain patterns following from the transmitted bearing loads in the application.

As an example the design is shown of a FOS system with a number of bearings instrumented on the low speed shaft of a marine propulsion gearbox. A comparison is made between the output from the FOS system and a drive train design and simulation SW package. The measurements are taken on a dedicated test bench. The axial and radial loads acting on the bearings are visualized for several operating conditions and compared to the loaded zones calculated by the SW package.

It is illustrated that the ability to measure the transmitted load in real-time and high accuracy with a FOS system opens up the opportunity to optimize the operational efficiency of the vessel and to detect non-optimal operating conditions and premature failures of a drivetrain being operated before they cause severe failure.

1 Introduction

This paper shows a novel Fiber Optical Sensing (FOS) Solution that makes it possible to measure, quantify and visualize important performance indicators for driveline design verification and qualification. At the core of the technology is a FOS sleeve instrumented with a single fiber comprising about 9-13 sensors (Bragg gratings) around its circumference. A sleeve is installed on the outer ring of a bearing to measure accurately and real-time the detailed strain patterns following from the transmitted bearing loads in the application.

The design of a FOS system is illustrated with an example, i.e. a number of bearings instrumented on the low speed shaft of a marine propulsion gearbox. A comparison is made between the output from the FOS system and a drive train design and simulation SW package. The FOS measurements are taken on a dedicated test bench and also compared with a reference torque and speed sensor.

The axial and radial loads acting on the bearings are visualized for several operating conditions and compared to the loaded zones calculated by the SW package.

It is further illustrated that besides design validation and qualification the ability to measure the transmitted load in real-time with a FOS system opens up the opportunity to optimize the operational efficiency of the vessel and to detect non-optimal operating conditions and premature failures of a drivetrain being operated before they cause severe failure.

2 Application

A marine transmission is the reduction device which generates ship's propulsion and consists of several main functional components, see Figure 21. The high speed input shaft is interconnected via a flexible coupling with the engine. A clutch is applied for ahead and astern operation. The input shaft is rotated in the same direction as that of engine, and the output shaft in the opposite direction during ahead actuation but in the same direction during astern actuation. The low speed output shaft is connected with the propellor shaft. The motor torque and speed are controlled to deliver the propellor thrust force needed for achieving the desired power (ship speed) under various operating conditions. The motor torque induces the gear mesh forces, i.e. an axial and radial force at the gear mesh locations as a fraction of the tangential force between pinion and gear. The magnitude of these forces are a function of gear geometry (i.e. helix angle and normal pressure angle) and of course the input torque and direction (ahead or astern). The resultant (reaction) forces at the bearings at the low speed shaft follow from the force and moment balance equations. Note that besides the thrust force also the helix gear geometry introduces axial forces at the bearing locations.

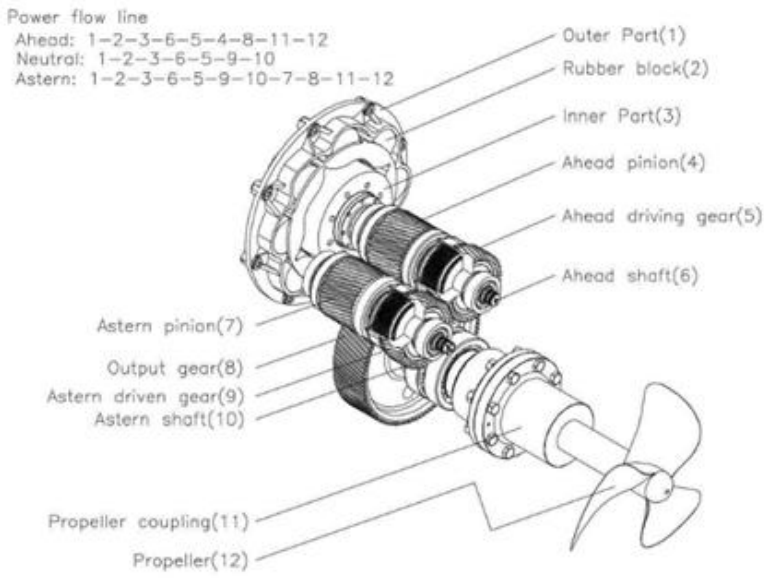

Figure 21: An illustrative example of a drive line system of a marine transmission, picture from DMT manual [DMT20].

The propulsion system is instrumented with a FOS system on the low speed output shaft. The low speed shaft of the gearbox is equipped with three FOS sleeves that hold the outer ring of the bearings to measure the strain related to the transmitted motor torque and propulsion force, see Figure 22. From the strain signals, the real-time transmitted torque, thrust force and shaft speed are computed. With the already available SCADA (Supervisory Control And Data Acquisition) measurements such as fuel consumption and ship speed it becomes than possible to determine the fuel

efficiency and separate the engine efficiency from the propellor efficiency and from the hull resistance. This allows for further optimizing the vessel operation and scheduling predictive maintenance actions and inspections in compliance with ISO 19030 and ISO 140001 as part of an environmental regulation and management policy.

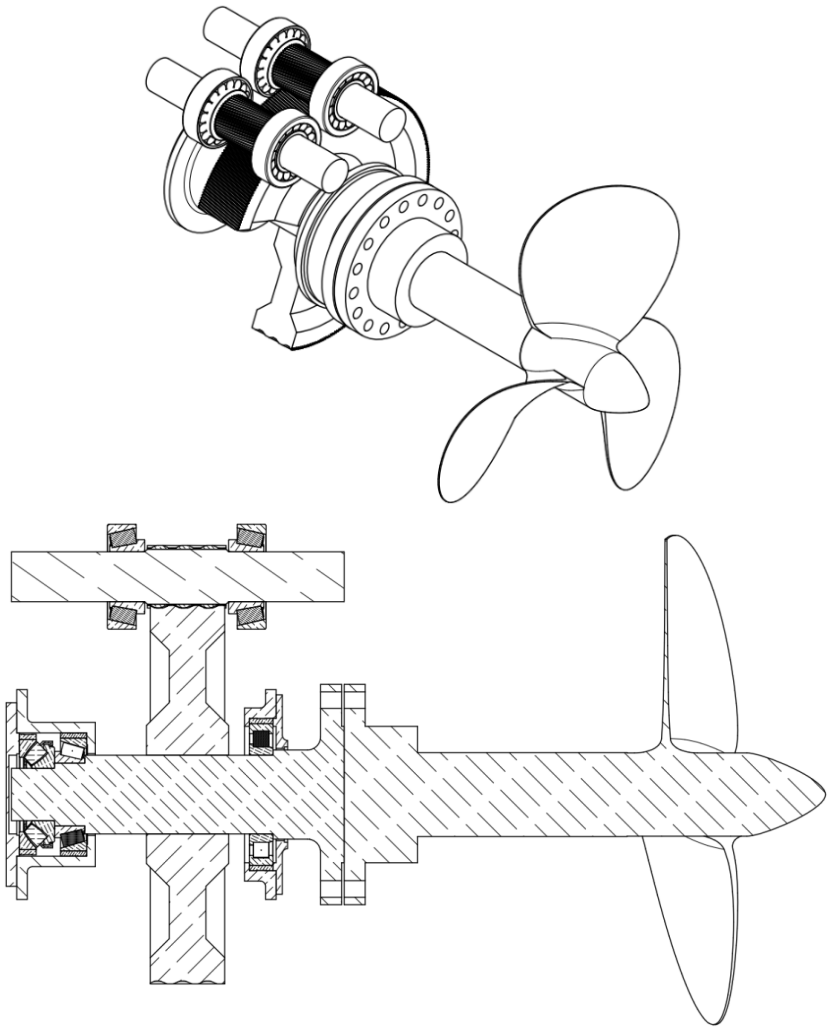

Figure 22: A marine propulsion system including a gearbox with pinion (ahead and astern) at the high speed shaft and a gear ring at the low speed shaft. The cross section of the low speed propellor shaft shows three bearings, i.e. a STRB (far left), TRB (left) and CRB (right) instrumented with a FOS sleeve. The sensors are uniformly distributed around the circumference of the bearings.

2.1 Measurement setup

2.2 Fiber Optical Sensing solution

For this application three bearings on the low speed shaft are instrumented with standardized FOS sleeves that fit on the outer ring of the bearings. The sleeves are developed and productized by Sensing360 B.V. and cover a wide range of bearings of different size and type. This includes the bearings relevant in this application, i.e. a Cylindrical Roller Bearing (CRB) and a Tapered Roller

Bearing (TRB) that transfer mainly the radial load and a Spherical Trust Roller Bearing (STRB) that transfers only axial load on the low speed shaft.

A steel sleeve is instrumented with an array of 13 fiber-optic strain sensors in a measurement groove. The sensors used are so-called Fiber Bragg Gratings (FBGs). A FBG sensor is a section of the optical fiber with a periodic variation of its refractive index. This section acts like a mirror, reflecting specific wavelength while transmitting others. The reflected wavelength variation is caused by temperate and/or strain variation. The reflected center wavelengths of the Bragg gratings in a single fiber are chosen such that they do not interfere with each other. Benefits of FBGs compared to traditional strain gauges are that they offer a higher signal-to-noise ratio, are immune to electromagnetic interference and that a single optical fibre can accommodate multiple sensors as shown in Figure 3.

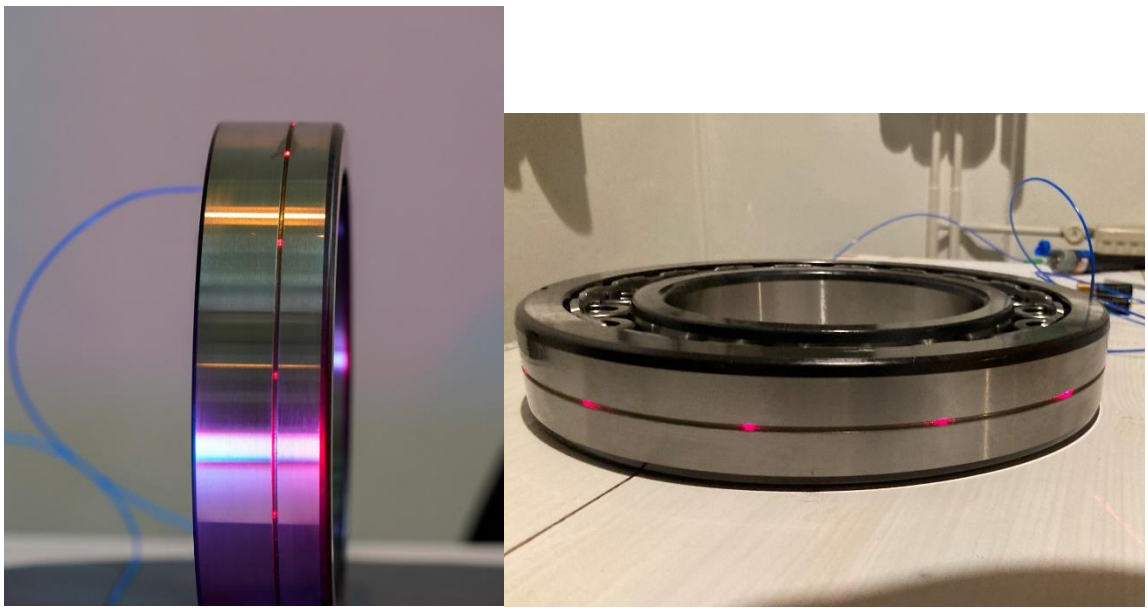

Figure 23: A TRB (left) and CRB (right) instrumented with a FOS sleeve comprising 13 sensors in a single fiber in a dedicated measurement groove. In this case the sensors are uniformly distributed around the circumference.

The radial and axial bearing forces are transferred from the rotating world, i.e. the low speed shaft, through the inner ring via the rolling elements to the instrumented sleeve that holds the outer ring. When a rolling element passes the location of a sensor, the forces between the rolling element and the outer ring cause a deformation pattern on the sleeve proportional to the force and at a pace by which the rolling elements pass the sensor. This deformation causes strains on the FBG sensor, which is picked up by a fiber optic interrogator, which analyzes the wavelengths reflected by the FBGs. The interrogator and data acquisition system are able to continuously log the strain up to 24 kHz sample rate. Sensing360 B.V. delivered the FOS solution.

3 Measurement results

The measurement of the FOS system are compared to a reference speed and torque sensor on the test rig. The test rig is a back-to-back end-of-line test rig that runs at a controlled reference speed and torque profile. Furthermore, the FOS measurement results are compared to the calculated output from the gearbox design report of a state-of-the-art SW package [FVA24] that calculates the bearing loads given the reference operating conditions from the test under consideration.

3.1 Torque and speed estimation

A number of tests are executed with different torque and speed levels for ahead as well as astern gear mode. In Figure 24 a torque estimate from the FOS system for increasing reference torque levels from 2000-6000 [Nm] at a fixed reference speed of 450 [RPM] is shown. Both the speed and input torque levels are estimated accurately with the FOS system.

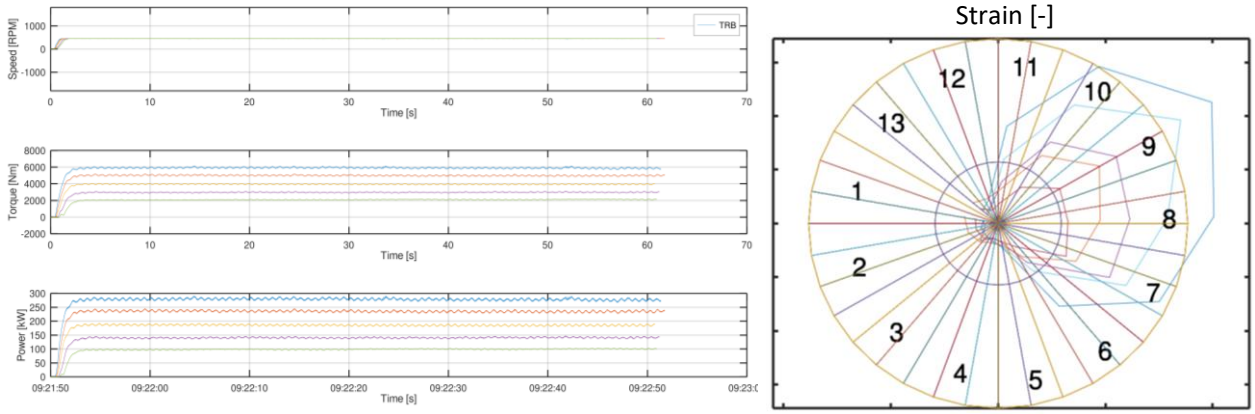

Figure 24: The torque estimate from the FOS system for different reference torque levels from 2000-6000 [Nm] at a fixed reference speed of 450 [RPM] for ahead gearbox operation mode. At the right the spatial strain distribution at the sensor locations (1,2,..,13) for the different torque levels is shown.

In Figure 25 the result is shown of a test with constant reference torque and increasing speed followed by a decreasing speed profile. The torque estimate from the FOS system (yellow) is compared to the reference torque sensor (blue) and shows a close fit. The upper figure shows the speed calculated from the induced strain on the FOS sleeve by the CRB roller passings. The estimated speed closely match the reference speed, see also Table 1. Some background on the algorithms used to combine and decompose the FOS sensor signals into variables of interest (Torque, Speed etc..) can be found in [ANG21].

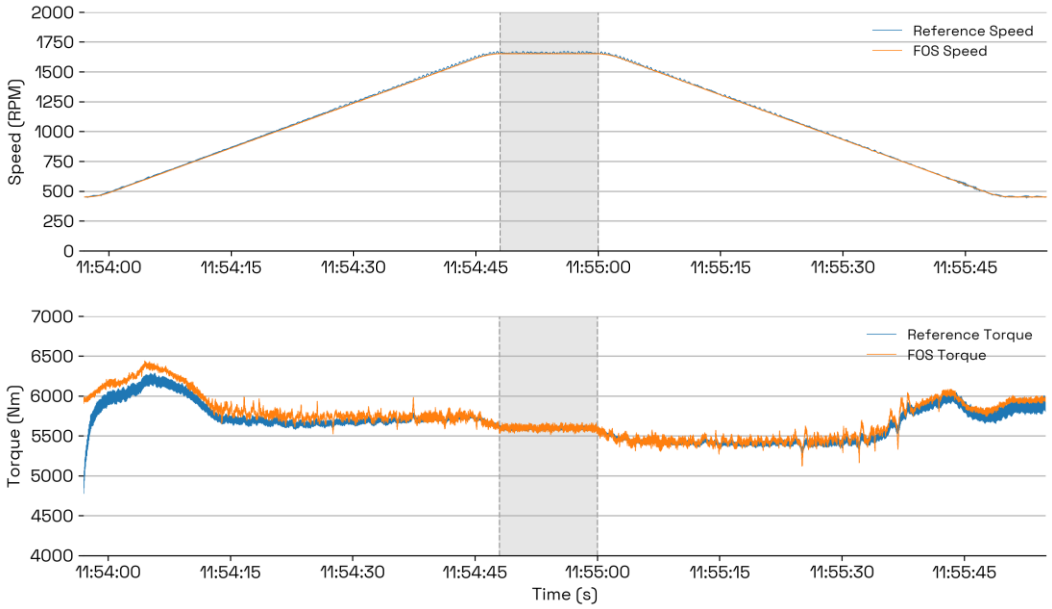

Figure 25: The torque estimate from the FOS system (orange) compared to the reference torque sensor (blue). The upper most figure shows the speed calculated with the CRB and the input power.

	Reference	FOS
Torque [Nm] (mean ± SD)	5598.0 ± 23.6	5594.4 ± 16.4
Speed [RPM] (mean ± SD)	1652.1 ± 00.6	1658.9 ± 05.0

Table 3: Mean and standard deviation for reference and FOS torque and speed.

3.2 Loaded zone measurements

A comparison study is made between the loaded zone calculation from the SW package and the FOS measurements for both radial bearings, i.e. the CRB and TRB. Since the strain levels at 13 locations on the circumference of the bearing sleeves are available, it is possible to construct a loaded zone in real-time for a specific operating condition of interest. In Figure 24 also the spatial strain distribution is shown for the measurement data. A strain distribution on the TRB sleeve at the 13 sensor locations at a moment in time for reference torque levels ranging from 2000-6000 [Nm] at a fixed reference speed of 450 [RPM] is shown. A loaded zone is estimated from these instant strain measurements.

The loaded zones are calculated also with the design calculation SW package so it is possible to compare these results with the measurement data as well. In Figure 26 the loaded zones on the bearings and resulting force vectors for a torque of 6000 [Nm] at a fixed reference speed of 450 [RPM] are shown. On the top row the loaded zone from the FOS system is shown for both the CRB (left) and the TRB (right). On the bottom row the calculation results are shown from the design SW. Qualitatively there is a good match between the simulation results and the real FOS measurements. The resulting force vectors are also close in magnitude and direction. The width of the loaded zone is a well-known indicator for the radial clearance. A load zone of about 180 degrees indicates zero clearance whereas a larger loaded zone indicates preload and a narrower loaded zone indicates clearance. With the FOS system we are able to quantify the bearing clearance/preload condition in real-time under varying operating conditions. The FOS measurement indicates a preloaded condition for the CRB (loaded zone width of 220 degrees) and the TRB shows some clearance (loaded

zone width of 170 degrees). If the bearing play is not optimal, this will affect the function and lifespan of the bearing. The clearance (and loaded zone width) as calculated by the design SW differs significantly from the measured clearance condition, see Figure 26.

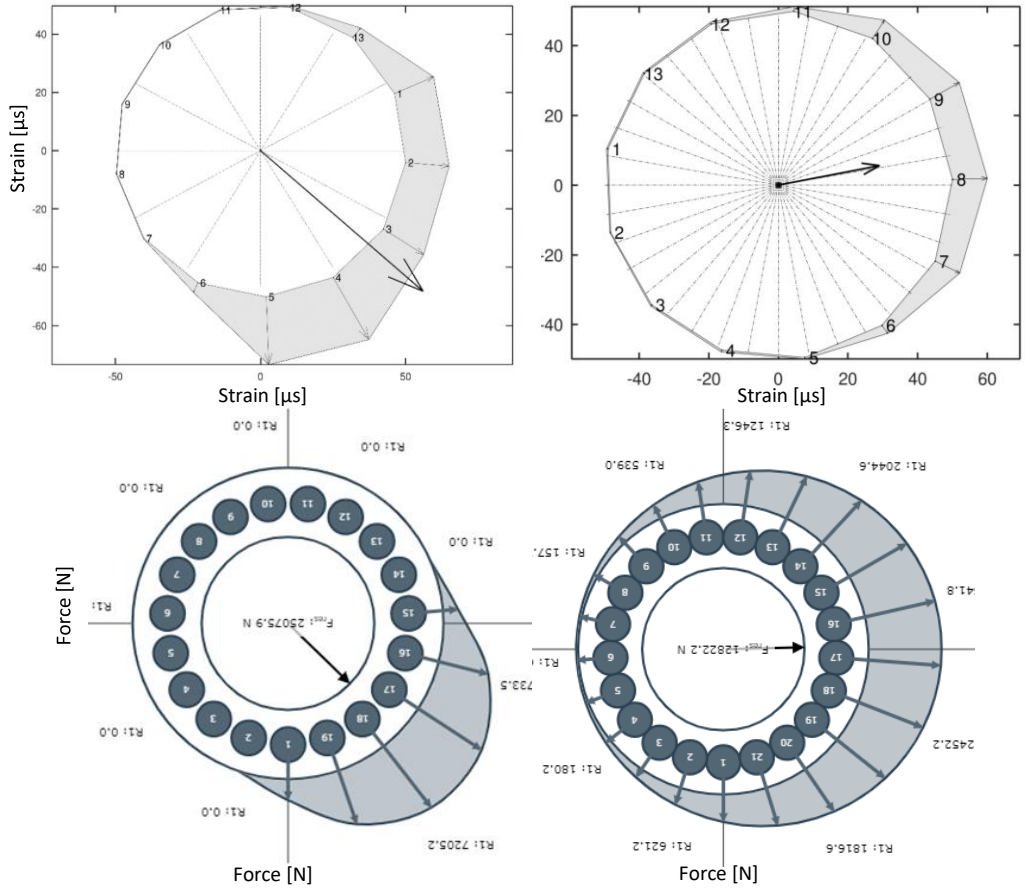

Figure 26: The loaded zones and resulting force vectors for a torque of 6000 [Nm] at a fixed reference speed of 450 [RPM] are shown. On the top row the loaded zone from the measured FOS system is shown for both the CRB (left) and the TRB (right). On the bottom row calculation results are shown from the design SW [FVA24].

3.3 Condition Monitoring

Since the FOS data is available at a high sample rate it is also illustrative to check if it is possible to detect bearing and gear related characteristic (and potential fault) frequencies in the frequency spectrum of the FOS data. The spectrum of the FOS data is used for the same underlying data as used in Figure 26 to construct the loaded zones.

A spectrum of a healthy marine gearbox with spectral components observed by the FOS sleeve related to gear mesh frequencies, ball pass frequencies, shaft frequencies (of low speed gear shaft and high speed pinion shaft) is shown in Figure 7. The spectra shows modulated frequencies around the gear mesh frequency and around the ball pass frequency and also the higher harmonics. The energy content in these frequencies as reflected by the amplitudes are potential indicators for faults that are being developed. Faults can be gear tooth faults or bearing wear at the outer ring, inner ring or rolling elements. Besides gear or bearing related faults also non-optimal (unfavorable) operating conditions can be detected since the energy content at the shaft running frequencies and higher harmonics is also clearly visible in the spectrum.

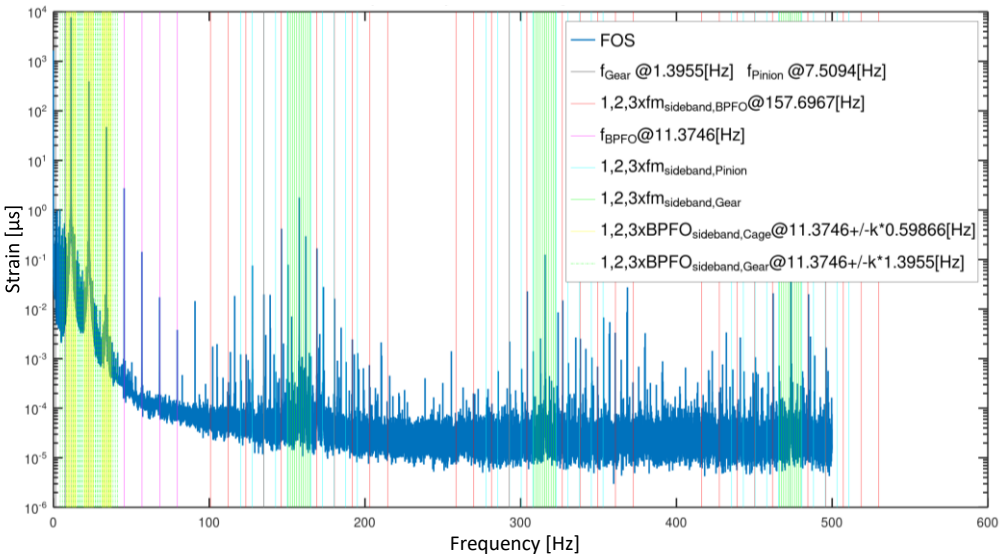

Figure 27: A FOS amplitude spectrum of a healthy gearbox that shows the characteristic frequencies related to the gear mesh and bearing (fault) frequencies.

4 Conclusion

It is shown that a FOS system can be used in different ways to support the life cycle of a marine gearbox/powertrain. In the design phase it can be used to prove the feasibility of the design and to validate the design and modelling assumptions. In the qualification phase it can be used to fingerprint each transmission as part of an end-of-line qualification test in the factory. The fingerprint will reveal some crucial manufacturing tolerances of the components (gears and bearings) and the resulting full assembly. In the operating phase the FOS system can be used to deliver a real-time measurement of torque, speed and trust load to support a fuel efficient and more sustainable optimized operation. The FOS system can also be used as a condition monitoring system to support a predictive maintenance strategy to detect and diagnose degradation of hull efficiency and/or thruster related inefficiencies in combination with already available SCADA parameters. Furthermore, the FOS system can be used to detect early gear teeth defects and bearing faults that are being developed before they cause more catastrophic failures.

5 Bibliography

[ANG21] Angelis, Georgo: GB201904221D0 Method of decomposing a load of interest associated with bearing-supported equipment

European Patent Office, United Kingdom, 2021

[DMT20] MARINE TRANSMISSION INSTRUCTION MANUAL, http://d-i.co.kr/eng/ (2025-01-20)

[FVA24] FVA-WORKBENCH, https://www.fva-service.de/fvaworkbench/ (20250120)

Machine Elements:

Design & Tribology

Machine learning-based prediction of friction losses in textured journal bearings

Yujun Wang[1], Georg Jacobs[1], Benjamin Klinghart[1], Florian König[1], Dennis Bosse[1]

[1]Institute for Machine Elements and Systems Engineering, RWTH Aachen University

Keywords: *Surface textures; Journal bearings, Machine learning, Friction losses*

Abstract: Adequately designed and positioned surface textures are considered to be a promising way to reduce friction losses of journal bearings. However, the high degree of freedom in design parameters for surface textures and various operation conditions poses challenges to accurately and efficiently predict the friction losses in textured journal bearings. To address this issue, the machine learning (ML)-based surrogate model for textured journal bearings is developed in this study. Computational fluid dynamics (CFD) models of textured journal bearing are built up to generate the datasets. Furthermore, three ML methods, including the Artificial Neural Network (ANN), Support Vector Regression (SVR), and Gaussian Process Regression (GPR) are compared to select a suitable prediction algorithm. The results show that, the ANN model demonstrates the best performance in the prediction of friction performance of textured journal bearings in this study. Moreover, the prediction accuracy of the ANN surrogate model is further enhanced through the cross-validation-based hyperparameter optimization. Eventually, a prediction accuracy of over 97% is achieved.

1 Introduction

Journal bearings have attracted much attention for its widely used applications, including various subsystems in engines and powertrains. The growing demand for energy efficiency of machinery requires lower friction and higher load-carrying capacity in journal bearings [1]. Surface textures have been proven to be a promising way for improving tribological behaviors of journal bearings [2]. Several beneficial effects have been identified experimentally and numerically. However, textures also can be detrimental if designed wrong [3]. Therefore, with the aim of enhancing the lubrication performance of journal bearings, surface textures should be properly designed. To properly design the texture parameters, the friction performance of textured journal bearings should be efficiently and accurately predicted.

To analyze the flow fields in textured journal bearings, two numerical methods are commonly used: the Reynolds equation method and the computational fluid dynamics (CFD) method [4]. The Reynolds equation is a simplified version of the Navier-Stokes equations, derived by neglecting the inertia effect and the flow in the film thickness direction [5]. Despite its higher computational efficiency compared to the CFD method, various studies have reported that the Reynolds equation's simplified assumptions limit its accuracy in predicting textured contacts [6]. Consequently, a CFD model based the N-S equations is required to accurately predicting textured journal bearings.

Nevertheless, the CFD method compromises computational efficiency, due to the dramatic increasing of mesh cell numbers when capturing the texture-induced microflow inside the textures [7]. In addition, the multiple design parameters of surface textures mean that a large amount of simulation

cases is required, which further leads to increased time requirements. To cope with these challenges, machine learning (ML) algorithms have been developed in the field of tribology [8]. However, the high degree of freedom in design parameters of surface textures requires a large amount of training data from the CFD model. In order to further reduce the high computational cost and improve the prediction efficiency, it is crucial to explore methods that can improve prediction accuracy without the need for additional datasets.

For this purpose, CFD models of textured journal bearings are first built to prepare the datasets for the ML-based surrogate model in this study. With the training datasets, three different ML methods are trained and compared to determine the most suitable prediction algorithm. Furthermore, aiming for a higher prediction accuracy, the surrogate model is further optimized with the identical datasets. This methodology can be abstracted for other application.

2 Methods

2.1 Numerical model

In this study, CFD models of textured journal bearings are built up. The dynamic mesh algorithm based on the load balance equations is implemented to predict the friction performance for textured journal bearings under different operation conditions, which is as Figure 1 shows. More details of this CFD model are introduced in Ref. [9].

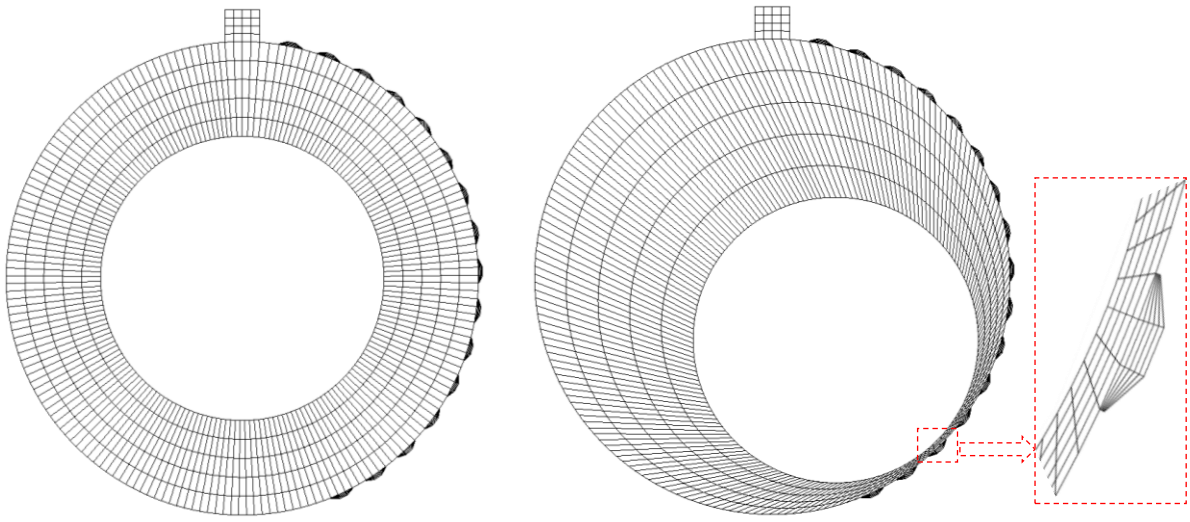

(a) Initial mesh model (b) Updated mesh model

Figure 2. Results of dynamic mesh algorithm

2.2 Machine learning-based surrogate model

2.2.1 Generation of datasets

The machine learning-based surrogate model is trained for a wide range of texture parameters and operation parameters. The input parameters include the texture geometry parameters, texture distribution parameters, as well as the external load, as Table 1 shows. 170 design points with different input parameter combinations are executed with the CFD model. Among these 170 sets of data, 150 sets of data are used to train ML models. The remaining 20 sets of data are used to evaluate the prediction accuracy of the trained surrogate model.

Parameters	Minimum value	Maximum value
Textured width ratio	0.2	0.96
Texture depth ratio	0	3
Texture coverage	0	170
Start position	5	180
External load	100	450

Table 4: Design range of input parameters

2.2.2 Machine learning methods

To determine the most appropriate prediction algorithm for the textured journal bearing, three commonly used ML methods, including the Artificial Neural Network (ANN), Support Vector Regression (SVR), and Gaussian Process Regression (GPR), are trained and compared based on the identical datasets. To estimate the prediction performance of the ML-based models, the mean square error (*MSE*) and the correlation coefficient (*R*) are calculated, which are two common parameters for the model evaluation [10].

2.2.3 Cross-validation-based hyperparameter optimization

Generally, the accuracy of the surrogate model can be enhanced by employing a larger number of training datasets. However, considering the high computational cost of CFD simulations, an alternative approach should be investigated. In this study, the surrogate model is optimized based on the cross-validation-based hyperparameter optimization with the identical datasets. The cross-validation method is used to evaluate various architecture parameter combinations [11]. Each combination undergoes 5-fold cross-validation to be evaluated. The optimal ANN architecture combination with the best prediction accuracy is outputted and determined.

3 Results and discussion

3.1 Comparison of different ML methods

The prediction performance of three aforementioned ML methods is illustrated in Figure 1. It can be found that the *R* value of ANN is higher than those of SVR and GPR, which means a higher prediction accuracy. Meanwhile, the *MSE* value for ANN is smaller than SVR and GPR, which means a better estimation performance. Besides, GPR depicts a better prediction performance than SVR. From the comparison of both *R* and *MSE* values, it can be observed that ANN method demonstrates a higher prediction performance in comparison to the other two methods under the current hyperparameters.

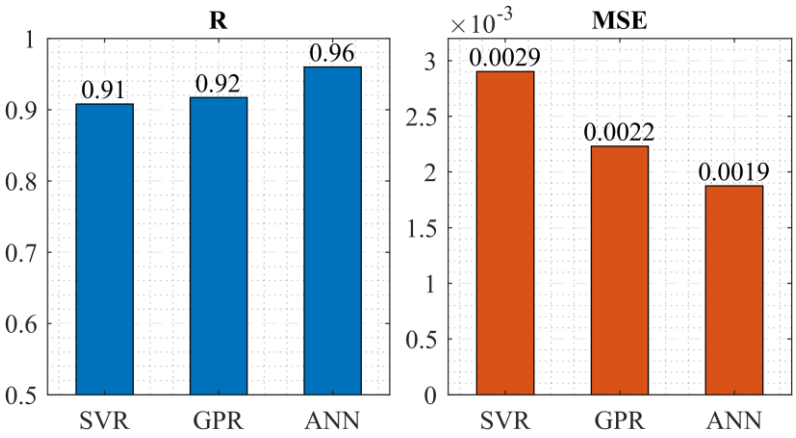

Figure 1: Prediction performance of the three ML models

Furthermore, to evaluate the prediction accuracy of the trained ANN model more intuitively, the friction losses of 20 evaluation datasets are predicted. The comparison of the predicted values with the true values, is depicted in Figure 2. It can be seen that the overall trend of the predicted values by the ANN model is consistent with the true values. The average prediction accuracy stands at 95.89%. However, as observed from Figure 2b, the maximum deviation approaches to nearly 14%, which indicates the necessity for further optimization of the prediction accuracy of the ANN-based surrogate model.

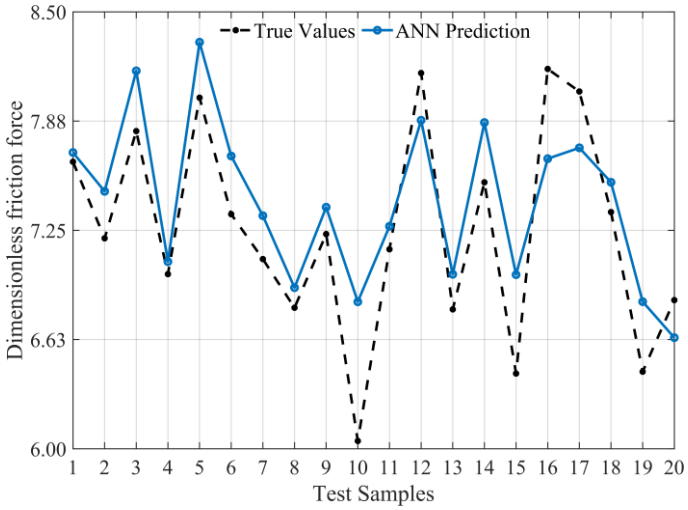

(a) Comparison with the true values

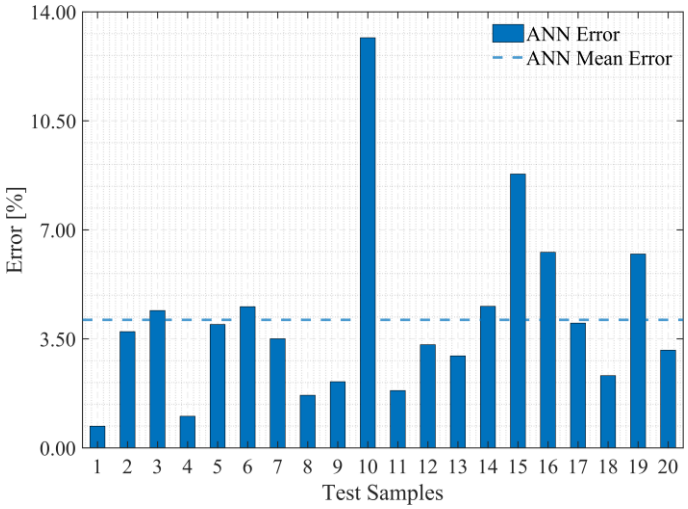

(b) Prediction errors of ANN model

Figure 2: Comparison between predicted and true values for initial ANN model

3.2 Optimization of the surrogate model

To further reduce the computational cost, the ANN surrogate model is optimized with the identical datasets based on the cross-validation-based hyperparameter optimization. Four key parameters influencing the performance of ANN are selected in this work, including the number of hidden layers, number of neurons in each hidden layer, the learning rate of the ANN model, as well as the type of activation function in hidden layers. The optimization range of each parameter is shown in Table 2.

Parameter	**Range**
Number of hidden layers	1-3
Number of neurons in hidden layer	2-20
Learning rate	10^{-1}-10^{-5}
Activation function on hidden layers	*tanh*, *sigmoid*, *ReLU*

Table 2: Optimization range of architecture parameters

After the hyperparameter optimization through the cross-validation, the selected number of hidden layers is 2. The number of neurons for each hidden layer are 12 and 4. The learning rate is 10^{-2} and the activation function in hidden layers is *ReLU*. The *R* values for the ANN model with the determined architecture by cross-validation (shortly CV-ANN) shows a notable improvement, with the *R* value for all datasets increasing from 0.957 to over 0.974.

The comparison between the true and predicted values by the ANN and CV-ANN models is intuitively depicted in Figure 3. Compared to the initial ANN model, CV-ANN model exhibits a higher accuracy in predicting the friction of textured journal bearings. In terms of average prediction accuracy, it increases from 95.89% to 97.82%. Notably, the prediction error can be consistently kept below 6% for each set of data.

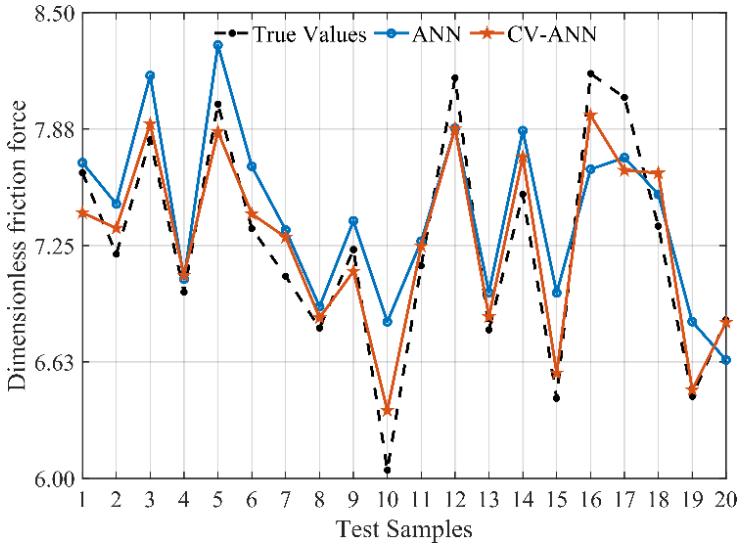

(a) Comparison with the true values for ANN and CV-ANN

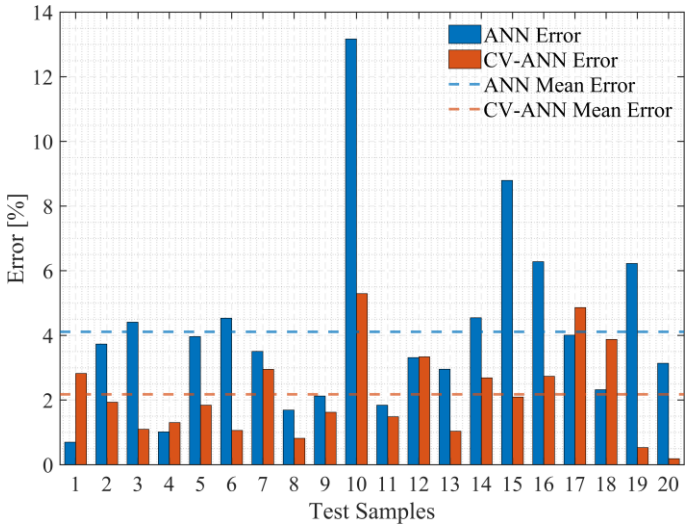

(b) Prediction errors of ANN and CV-ANN models

Figure 3: Comparison of predicted and true values for ANN and CV-ANN models

4 Summary

In the present work, a ML-based surrogate model is developed to accurately and efficiently predict the friction losses of textured journal bearings. The CFD models are built up to generate datasets for the ML algorithms. By comparing three ML models, ANN holds the best prediction performance. Considering the high computational cost of CFD simulations when preparing the datasets, the prediction accuracy of the surrogate model is optimized with the identical datasets through the cross-validation-based hyperparameter optimization. After the optimization, a prediction accuracy of over 97% is achieved. This work provides the reference and knowledge to build up a highly efficient surrogate model based on machine learning, particularly in cases with high computational costs for the generation of datasets.

5 Bibliography

[1] König F, Sous C, Jacobs G. Numerical prediction of the frictional losses in sliding bearings during start-stop operation. Friction 2021;9(3):583–97. https://doi.org/10.1007/s40544-020-0417-9.

[2] Gachot C, Grützmacher P, Rosenkranz A. Laser surface texturing of TiAl multilayer films—Effects of microstructure and topography on friction and wear. Lubricants 2018;6(2):36. https://doi.org/10.3390/lubricants6020036.

[3] Gropper D, Wang L, Harvey TJ. Hydrodynamic lubrication of textured surfaces: A review of modeling techniques and key findings. Tribology International 2016;94:509–29. https://doi.org/10.1016/j.triboint.2015.10.009.

[4] König F, Rosenkranz A, Grützmacher PG, Mücklich F, Jacobs G. Effect of single- and multi-scale surface patterns on the frictional performance of journal bearings – A numerical study. Tribology International 2020;143:106041. https://doi.org/10.1016/j.triboint.2019.106041.

[5] Liang X, Liu Z, Wang H, Zhou X, Zhou X. Hydrodynamic lubrication of partial textured sliding journal bearing based on three-dimensional CFD. Industrial Lubrication and Tribology 2016;68(1):106–15. https://doi.org/10.1108/ILT-04-2015-0055.

[6] Keller D, Jacobs G, Neumann S. Development of a low-friction radial shaft seal: using CFD simulations to optimise the microstructured sealing lip. Lubricants 2020;8(4):41. https://doi.org/10.3390/lubricants8040041.

[7] Wang Y, Jacobs G, König F, Zhang S, Goeldel S von. Investigation of microflow effects in textures on hydrodynamic performance of journal bearings using CFD simulations. Lubricants 2023;11(1):20. https://doi.org/10.3390/lubricants11010020.

[8] Marian M, Tremmel S. Current trends and applications of machine learning in tribology—A review. Lubricants 2021;9(9):86. https://doi.org/10.3390/lubricants9090086.

[9] Wang Y, Jacobs G, Zhang S, Klinghart B, König F. Development of a machine learning-based surrogate model for friction prediction in textured journal bearings. Friction 2024. https://doi.org/10.26599/FRICT.2025.9441051.

[10] Ostasevicius V, Paleviciute I, Paulauskaite-Taraseviciene A, Jurenas V, Eidukynas D, Kizauskiene L. Comparative analysis of machine learning methods for predicting robotized incremental metal sheet forming force. Sensors 2021;22(1). https://doi.org/10.3390/s22010018.

[11] Isler Y, Narin A, Ozer M. Comparison of the effects of cross-validation methods on determining performances of classifiers used in diagnosing congestive heart failure. Measurement Science Review 2015;15(4):196–201. https://doi.org/10.1515/msr-2015-0027.

Machine Elements:

Bearing Technology: Lifetime

Prediction of Rolling Bearing Life Applying Ultrasonic Testing

Keita Yamada[1], Dr. Sho Hashimoto[1], Ralf Petersen[2]

[1]NSK Ltd., 1-5-50, Kugenuma Shinmei, Fujisawa-shi, Kanagawa 251-8501, Japan

[2]NSK Deutschland GmbH, Harkortstrasse 15, Ratingen, 40880, Germany

Keywords: flaking, non-metallic inclusion, stress intensity factor, rolling contact fatigue

Abstract:

Flaking is one the most common forms of damage affecting rolling bearings. It can be generally divided into two types, that originating in the subsurface, and that in the surface. When rolling bearings operated in conventional condition, then we are usually talking about subsurface originating flaking, often as a result of non-metallic inclusions in the bearing steel. In recent years, improvements in the cleanliness of bearing steel mean that this sort of flaking isn't causing as many bearings to fail, resulting in a large discrepancy between the actual bearing life and that suggested by calculations under ISO 281. Evaluating bearing steel using ultrasonic testing, however, allows for the gathering of statistical data on the size and quantity of non-metallic inclusions that cause subsurface-initiated flaking. In addition, a method for evaluating bearing life and fatigue limit was developed based on the results of durability tests and simulation analyses of rolling bearings with artificial defects. By combining these technologies, a method to predict rolling bearing life caused by non-metallic inclusions with high accuracy has been suggested.

1 Introduction

When properly selected and handled, rolling bearings can be used until they reach their rolling contact fatigue (RCF) life. In this case, bearing life is defined as the total number of revolutions or the time before flaking (also called as spalling) occur in the rolling bearings. One form of RCF is subsurface fatigue, which is caused by non-metallic inclusions in the bearing steel. In this paper, bearing life is defined as the time or number of revolutions before flaking occurs due to non-metallic inclusions in the bearing steel. A countermeasure to inclusion-initiated flaking is to improve the bearing steel cleanliness (quantity and size of inclusions in the steel). In the past, bearing manufacturers have worked with steelmakers to reduce the amount of oxygen in steel to reduce oxide-type inclusions and improve material cleanliness. In recent years, inclusion-initiated flaking has become less of a cause of premature damage.

Basic rating life L_{10} of a rolling bearing is expressed as

$$L_{10} = \left(\frac{C}{P}\right)^{p} \qquad \textbf{Eq. 2}$$

using the basic dynamic load rating C, bearing load P, and load coefficient p. This formula was proposed in the fatigue life theory established by Lundberg and Palmgren and is still widely used today as the most basic rolling bearing life calculation method. However, this life calculation formula includes experimental constants obtained from durability test results of bearings manufactured between 1940 and 1950, and thus includes the effect of material cleanliness at that time. The formula does not include material cleanliness as a parameter, so even if a rolling bearing is made of high cleanliness steel manufactured using the latest technology, the effect of this material cleanliness

cannot be reflected in the calculated life. Therefore, the length of time it takes bearings manufactured with modern steel-making technology to flake tends to be longer than calculations with the formula in Eq. 1. This suggests that bearings often have excessive durability under clean lubrication conditions. Therefore, highly accurate prediction of bearing life for inclusion-initiated flaking will be possible to use smaller rolling bearings than before, contributing to machine weight reduction and resource conservation.

To predict the bearing life for inclusion-initiated flaking, it is necessary to quantitatively evaluate the material cleanliness of the steels used in the rolling bearings and the effects of inclusions. However, conventional material cleanliness evaluation methods use optical microscopes, which limit the analysis range and detect very small inclusions of just a few micrometers. They do not detect relatively large non-metallic inclusions of several tens of micrometers or more, which have the low probability of detection and are actually the cause of subsurface flaking under the conventional operating conditions. In addition, it is extremely difficult to observe the process of fatigue crack initiation and propagation, and it is difficult to quantitatively evaluate the effect of inclusions on bearing life.

To solve these problems, originally developed ultrasonic testing technology (NSK Micro-UT) was used to evaluate non-metallic inclusions with sizes that have a strong correlation with fatigue life. The results of rolling contact fatigue tests and simulation analyses of rolling bearings with artificial defects of the same size as the inclusions have shown that this is an effective method for evaluating the bearing life and fatigue limit. By combining these technologies, a method for highly accurate rolling bearing life prediction caused by non-metallic inclusions have been suggested. In this paper, a new life model using stress intensity factor is proposed based on the actual condition of inclusions in steel using NSK Micro-UT and the results of tests using micro drill holes.

2 Actual condition of inclusions

2.1 Overview of NSK Micro-UT

NSK Micro-UT enables to non-destructively evaluate non-metallic inclusions inside steel bars of several tens of mm in diameter and several hundred mm in length. The schematic of NSK Micro-UT is shown in Fig.1. The steel is placed in a water tank and rotated, then the probe is scanned in the axial direction to inspect the entire circumference of the steel. Ultrasonic waves emitted from the probe propagate inside the steel, and if non-metallic inclusions are present in the steel, reflected waves are detected. Echo image of inclusions detected by NSK Micro-UT is shown in Fig. 2. The intensity of the echoes from the ultrasonic waves is indicated by the color of each pixel, with red, yellow, and blue indicate greater echo intensity in that order. The actual size of the inclusions is estimated from these detection results, and the cleanliness of the material is used as an index to determine the cleanliness of the material.

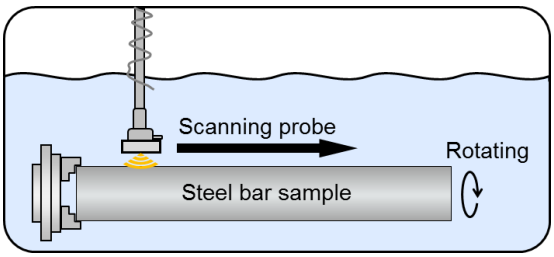

Figure 28: Schematic of NSK Micro-UT

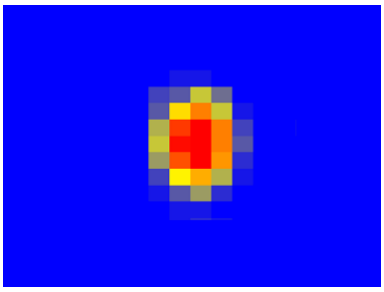

Figure 29: The echo image by NSK Micro-UT

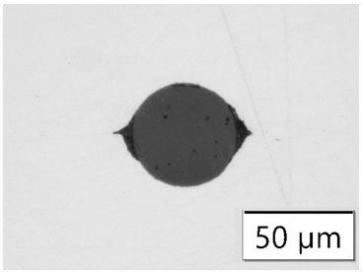

Figure 30: The inclusion image corresponding to the echo image in Fig.2

2.2 Size estimation of non-metallic inclusions using NSK Micro-UT

The area of the echo detected by ultrasonic testing does not necessarily correspond to the size of the inclusion that was the source of the echo. For example, differences in ultrasonic focus position and attenuation caused by differences in the depth of inclusions can change the echo intensity, which in turn changes the dimensions of the inclusions in the ultrasonic testing data. Therefore, an estimation equation was developed to accurately estimate the size of each non-metallic inclusion from the ultrasonic testing data. To develop the estimation equation, (i) the actual size of non-metallic inclusions in steel was measured and (ii) factors that affect the apparent inclusion size were identified and corrected.

(i) Measurement of actual size of inclusions in steel

After determining the location of non-metallic inclusions detected from the ultrasonic testing data, the cross section of the location was observed using a optical microscope to determine the dimensions of the actual inclusions. After cutting and removing the area around the detected position to observe the exact position, the maximum size of the actual inclusion was measured by repeating polishing and observation of a few micrometers while measuring the amount of polishing. N = 50 different non-metallic inclusions were evaluated. As an example, Fig. 3 shows the observation results of non-metallic inclusions corresponding to the echo image in Fig. 2.

(ii) Identification of factors affecting apparent inclusion dimensions

The following factors were considered as influencing factors: inclusion area (number of echo masses), echo intensity, location of non-metallic inclusions (depth from the steel surface), echo noise due to the microstructure of the material, and steel diameter. An estimation equation was developed based on multiple regression analysis considering these five factors and the dimensions of actual inclusions obtained in (i). Fig. 4 shows a comparison of the size of non-metallic inclusions calculated from the estimation equation and the actual size of inclusions. It can be seen that the estimated dimensions of actual inclusions can be accurately estimated by using the estimation equation. The correlation coefficient was 0.90, indicating a positive correlation. This estimation equation enables an accurate understanding of the distribution of inclusions in the steel. In addition, the cleanliness of the material can be quantitatively determined by using these indexes.

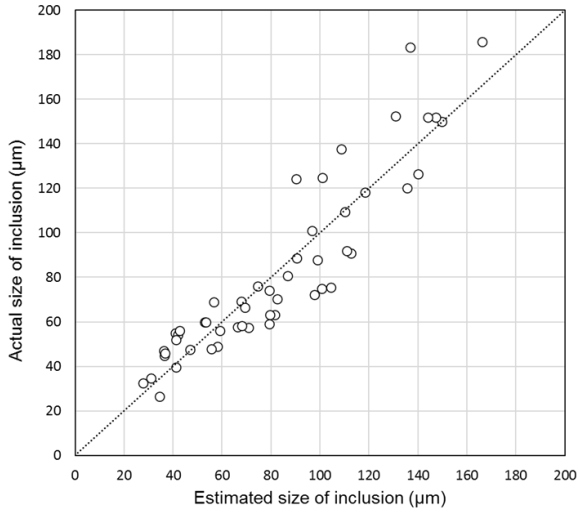

Figure 31: The comparation between estimated inclusion size and actual inclusion size

2.3 Relationship between material cleanliness and bearing life evaluated by NSK Micro-UT

After the cleanliness of the material was quantified using NSK Micro-UT, the correlation between the cleanliness of the material and the life of the bearing was verified. Fig. 5 shows the results of durability tests on 6206 deep groove ball bearings manufactured from bearing steel (JIS-SUJ2) of different cleanliness as evaluated by NSK Micro-UT. The durability test conditions were radial load of 13.8 kN and speed of 3900 min^{-1}. The lubrication method was forced circulation lubrication and ISO-VG68 lubricant. Bearings made from steel A, which is inferior in cleanliness, are to the left of bearings made from steel B, which is better in cleanliness, indicating a shorter life. This indicates that there is a correlation between the material cleanliness evaluated by NSK Micro-UT and the rolling bearing durability test results.

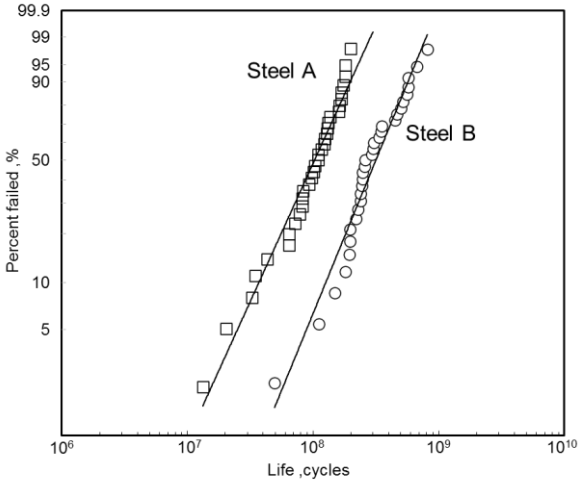

Figure 32: Weibull plots for different cleanliness index

3 New bearing life for inclusion-initiated flaking model using stress intensity factor

3.1 Rolling contact fatigue (RCF) tests using rolling bearings with micro drill holes in the raceway

RCF tests were conducted using deep groove ball bearings with small drill holes introduced into the inner ring raceway. The material of the test bearings was JIS-SUJ2 with a hardness of 740 to 760 *HV.* The dimensions of the drill holes were in the range of diameter *d* = 0.050 ~ 0.100 mm and edge depth *h′* = 0.050 ~ 0.175 mm. A schematic of the drill holes is shown in Fig. 6, and the test conditions are shown in Table 1. In this test, fatigue cracks initiated at the edge of the drill hole and propagated through the material before flaking. Hashimoto et al. investigated Mode II stress intensity factor $\Delta K_{\mathrm{II,drill}}$ at the edge of an annular crack of length a' originating from the edge under Hertzian contact using FEM and obtained the following approximate equation. [1]

$$\Delta K_{\mathrm{II,drill}} = (-1.56 \cdot d + 0.82) \cdot \frac{8}{(2-\nu)\pi} \tau_{\mathrm{a}} \sqrt{\pi\left({}^{d}/_{2} + a'\right)} \qquad \textbf{Eq. 3}$$

τ_{a} is the shear stress amplitude acting horizontally and vertically on the raceway at the crack edge depth. As shown in Fig. 7, there is a good correlation between the bearing life and the value of $\Delta K_{\mathrm{II,drill}}$ calculated by Eq. 2. This suggests that the bearing life for inclusion-initiated flaking can be expressed using ΔK_{II} at the initial crack edge originated from the inclusion.

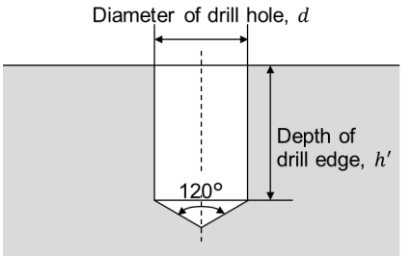

Figure 33: Geometry of drilled hole

Bearing dimension	Outer diameter [mm]	62
	Inner diameter [mm]	30
RCF test conditions	Max. contact pressure for inner ring [GPa]	2.50 – 3.45
	Rotational speed [min^{-1}]	3900
	Lubricating oil	ISO-VG68

Table 5: Details of RCF test conditions

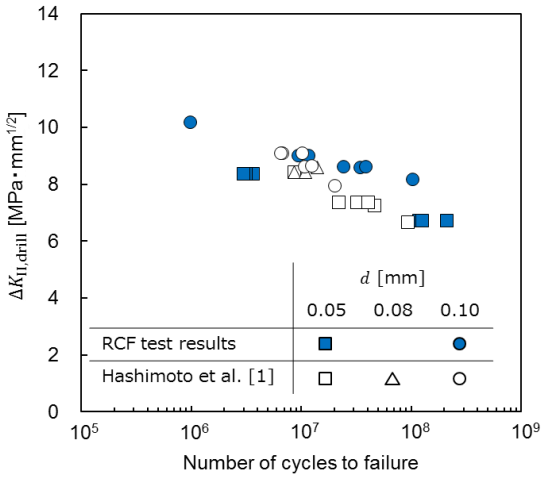

Figure 34: Relationship between $\Delta K_{\mathrm{II,drill}}$ and bearing life

3.2 Derivation of bearing life for inclusion-initiated flaking model

Flaking is mainly classified into two types: sub-surface originated flaking and surface originated flaking. In the case of sub-surface originated flaking, there is a type that caused by the material structure in addition to the non-metallic inclusion initiated. These are considered to be independent phenomena, and the life model is expressed as following.

$$\ln\frac{1}{S} = A_{\mathrm{nmi}} \cdot N^{e_1} \int \frac{\left(\sigma_{\mathrm{nmi}} - \sigma_{\mathrm{th,nmi}}\right)^c}{z_0^h} dV_{\mathrm{ss}} + A_{\mathrm{ss}} \cdot N^{e_2} \int \frac{\left(\sigma_{\mathrm{ss}} - F_{\mathrm{env}} \cdot \sigma_{\mathrm{th,ss}}\right)^c}{z_0^h} dV_{\mathrm{ss}} + A_{\mathrm{s}} \cdot N^{e_3} \int \left(\sigma_{\mathrm{s}} - \sigma_{\mathrm{th,s}}\right)^c dV_{\mathrm{s}} \quad \textbf{Eq. 4}$$

where S is the survival probability, N is the number of stress cycles, z_0 is the depth of the maximum orthogonal shear stress, σ is the driving force of flaking, σ_{th} is the material strength (fatigue limit), V is the stress volume, e_1 to e_3 are Weibull slopes, A, c and h are constants. The subscripts refer to the flaking type, where the first term on the right-hand side of Eq. 3 represents the inclusion initiated, the second term is due to the material microstructural change related, and the third term is the surface originated type. $F_{\mathrm{env}}$is a coefficient that represents the strength reduction due to environmental effects, such as hydrogen embrittlement. In this paper, only the first term on the right-hand side of Eq. 3, which represents inclusion originated flaking, is considered. Since the driving force of flaking is considered to be ΔK_{II}, σ_{nmi} is replaced by ΔK_{II}, and using the lower limit of stress intensity factor ΔK_{IIth}, $\sigma_{\mathrm{th,nmi}}$ is replaced by ΔK_{IIth}, the life model is expressed as follows

$$\ln\frac{1}{S} = A_{\mathrm{nmi}} \cdot \frac{N^{e_1}(\Delta K_{\mathrm{II}} - \Delta K_{\mathrm{IIth}})^c V_{\mathrm{ss}}}{z_0^h} = A_{\mathrm{nmi}} \cdot \left(\frac{\Delta K_{\mathrm{II}} - \Delta K_{\mathrm{IIth}}}{\tau_0}\right)^c \frac{N^{e_1}\tau_0^c V_{\mathrm{ss}}}{z_0^h} \quad \textbf{Eq. 5}$$

τ_0 is the maximum orthogonal shear stress amplitude. For the life at 10% at a given value of ΔK_{II}, the similarity with the Lundberg - Palmgren theory, Eq. 4 can be described as follows

$$L_{\mathrm{mean}} = A'_{\mathrm{nmi}} \cdot \left(\frac{\Delta K_{\mathrm{II}} - \Delta K_{\mathrm{IIth}}}{\tau_0}\right)^{\alpha} \left(\frac{C}{P}\right)^{\beta} \quad \textbf{Eq. 6}$$

C is the basic dynamic load rating of the bearing, P is bearing load, A'_{nmi}, α and β are constants.

Next, using the results in Fig. 7, the values of each constant are examined with a focus on the life of the inner ring where flaking occurs. The life data obtained as a result of the test is considered to be the average life $L_{\mathrm{mean,i}}$ of the inner ring in each $\Delta K_{\mathrm{IIth,drill}}$. Based on the results of Okazaki et al., on the lower limit of shear-type growth of elliptical cracks, the lower limit of growth of a crack originating from a drill hole $\Delta K_{\mathrm{IIth,drill}}$ is expressed by the following equation using the projected area of the drill hole $area_{\mathrm{drill}}$.

$$\Delta K_{\mathrm{IIth,drill}} = 1.49\left(\sqrt{area_{\mathrm{drill}}}\right)^{1/3} \qquad \textbf{Eq. 7}$$

Based on the results of Figure 7 and Equation 5, the logarithmic results are shown in Figure 8, with $L_{\mathrm{mean,i}}/(C_{\mathrm{i}}/P)^{\beta}$ on the vertical axis and $\left(\Delta K_{\mathrm{II,drill}} - \Delta K_{\mathrm{IIth,drill}}\right)/\tau_0$ on the horizontal axis. When $A'_{\mathrm{nmi}} = 1.40 \times 10^3$, $\alpha = -5.51$, and $\beta = 1.11$, both values showed a good correlation. The unit of τ_0 is GPa.

To predict the bearing life of inclusion-initiated flaking, ΔK_{II} of the initial crack originating from the inclusion and its threshold $\Delta K_{\mathrm{IIth,drill}}$ must be considered. Using the results of Okazaki et al. study,[2] ΔK_{II} of inclusions and $\Delta K_{\mathrm{IIth,drill}}$ under Hertzian contact can be expressed by the following equation using the projected area of the inclusion,$area_{\mathrm{nmi}}$.

$$\Delta K_{\mathrm{II}} = F_{\mathrm{nmi}} \cdot 1.16\tau_{\mathrm{a}}\sqrt{\pi\sqrt{area_{\mathrm{nmi}}}}, \qquad \Delta K_{\mathrm{IIth}} = 2.61\left(\sqrt{area_{\mathrm{nmi}}}\right)^{1/3} \qquad \textbf{Eq. 8}$$

τ_{a} is the shear stress amplitude acting at the crack initiation inclusion depth. F_{nmi} is a correction factor to account for this effect. The results of the above study show that Equations 5 and 7 can be used to determine the average bearing life of flaking originating from inclusions size.

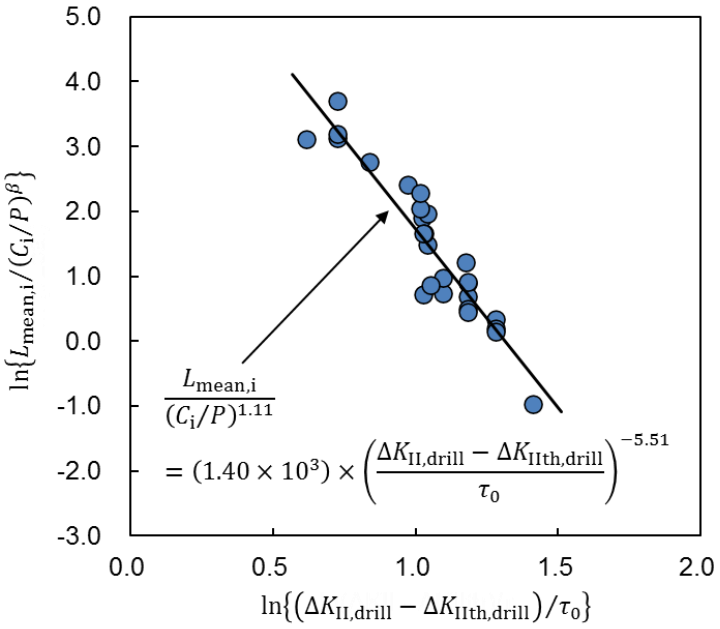

Figure 35: Relationship between $L_{\mathrm{mean,i}}/(C_{\mathrm{i}}/P)^{\beta}$ and $\left(\Delta K_{\mathrm{II,drill}} - \Delta K_{\mathrm{IIth,drill}}\right)/\tau_0$

4 Weibull plot prediction of bearing life

Based on the statistical data of material cleanliness evaluated from NSK Micro-UT, the largest inclusion size that can be included in the stress volume per bearing of M bearings is estimated. If the process of randomly extracting m data from M bearings and arranging them in ascending order is repeated multiple times, the average of the maximum inclusion size in each order is $\sqrt{area_{\mathrm{nmi}_k}}$. It is possible to predict a Weibull plot by applying value of $\sqrt{area_{\mathrm{nmi}_k}}$ to Equations 5 and 7.

Based on the durability test results of 6206 deep groove ball bearings made of steel of different purity as shown in Fig. 5 and the statistical data from NSK Micro-UT purity evaluation of the same steel, the inclusion size was calculated and compared with the Weibull chart, predicted by the above method. Fig. 9 shows the bearing life results compared with experimental and predictive methods. The comparison between the Weibull plot based on durability tests and the Weibull plot based on the bearing life prediction for inclusion-initiated flaking model showed a good correlation for both steel A and B.

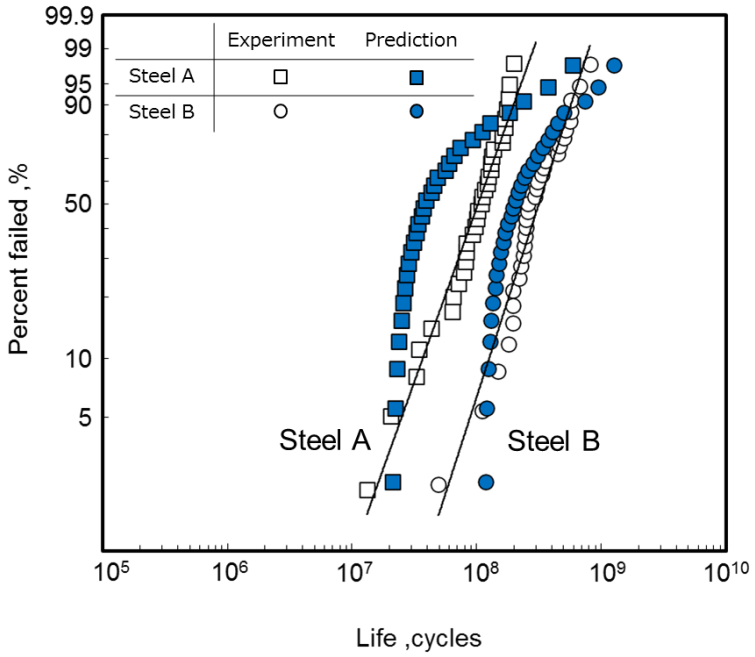

Figure 36: Comparison in Weibull plots of experiment and prediction of steel A and B

5 Summary / Conclusion

NSK Micro-UT enables evaluation of the size of inclusions that may cause inclusion-initiated flaking. The results of rolling contact fatigue tests on rolling bearings with small drill holes indicate that the driving force of flaking is the stress intensity factor range ΔK_{II} of cracks initiated by inclusions. Based on this knowledge, a life model was derived using ΔK_{II} and its threshold ΔK_{IIth}.

By combining the statistical data of material cleanliness evaluated using NSK Micro-UT and a new bearing life for inclusion-initiated flaking model using stress intensity factors, it was possible to predict Weibull plots of a bearing life.

6 Bibliography

[1] Hashimoto S., et al.: Quantitative evaluation of the flaking strength of rolling bearings with small defects as a crack problem

Int. J. Fatigue, 119, 195-203

Elsevier, Netherlands, 2019

[2] Okazaki S., et al.: A practical expression for evaluating the small shear-mode fatigue crack threshold in bearing steel

Theor. Appl. Fract. Mech., 73, 161-169

Elsevier, Netherlands, 2014

TEHL Film Thickness Measurements in Roller Bearings Using Electrical Impedance Methods

Manjunath Manjunath[1,2], Patrick De Baets [1,2], Dieter Fauconnier [1,2]

[1]Soete Laboratory, Department of Electromechanical, Systems & Metal Engineering, Faculty of Engineering and Architecture, Ghent University, Technologiepark 903, 9052 Ghent, Belgium;

[2]Flanders Make @ UGent-Core Lab MIRO, 9000 Ghent, Belgium

Keywords: *Electrical Impedance Spectroscopy; EHL film thickness, roller bearings, lubrication regime identification.*

Abstract: In this research, we focus on utilizing Electrical Impedance Spectroscopy (EIS) for the assessment of global and contact impedances in roller bearings. Our primary objective is to establish a quantitative prediction of lubricant film thickness in Elasto-Hydrodynamic Lubrication (EHL) and investigate the impedance transition from ohmic to capacitive behaviour as the system shifts from boundary lubrication to EHL. To achieve this, we conduct measurements of electrical impedance, bearing and oil temperature, and frictional torque in a cylindrical roller thrust bearing (CRTB) subjected to pure axial loading across various rotational speeds and supply oil temperatures. The measured impedance data is analysed and translated into a quantitative measure of lubricant film thickness within the contacts, using the impedance-based and capacitance-based methods. For EHL, we observe that the measured capacitance of the EHL contact deviates from the theoretical value based on a Hertzian contact shape by a factor ranging from 3 to 11, depending on rotational speed, load, and temperature. The translation of complex impedance values to film thickness, employing the impedance and capacitance method, is then compared with analytically estimated film thickness using Moes correlation, corrected for inlet shear heating effects. This comparison demonstrates a robust agreement within 2% for EHL film thickness measurement. Monitoring the bearing resistance and capacitance via EIS across rotational speeds clearly shows the transition from boundary to mixed lubrication as well as the transition from mixed lubrication to EHL. Finally, we have observed that monitoring the electrical impedance appears to have potential to perform the run-in of bearings in a controlled way.

1 Introduction

Energy efficiency and durability of machines and powertrains are crucial for a sustainable economy, with minimizing frictional losses and wear in bearings being a key strategy [DOL23]. Bearings ideally operate in the Elasto-Hydrodynamic Lubrication (EHL) regime [GOH01][DOW06], where a pressurized lubricant film separates surfaces, minimizing friction and wear. However, at high loads, low speeds, or low lubricant viscosity, mixed or boundary lubrication can occur, reducing efficiency. At very high speeds, shear heating raises oil temperature, decreasing viscosity and thinning the lubricant film, increasing the risk of mixed lubrication [MAN23].

The transition between lubrication regimes is dynamic and depends on factors like speed, load, temperature and viscosity, which vary during operation. Accurate knowledge of instantaneous lubricant film thicknesses is critical for energy efficiency and bearing longevity. In EHL contacts, spanning a few square millimetres, film thicknesses range from 50 nm to 1.5 µm, with roller pass-by times as short as 10^{-5} to 10^{-3} seconds, making in-situ measurement challenging.

This research explores in-situ measurement techniques, particularly electrical impedance spectroscopy, to determine film thickness in EHL conditions and identify oil film breakdown in mixed lubrication. By applying AC voltage across a lubricated cylindrical roller thrust bearing (Figure 1), the complex impedance Z is measured, providing insights into ohmic and capacitive contributions to distinguish between full-film and mixed lubrication regimes.

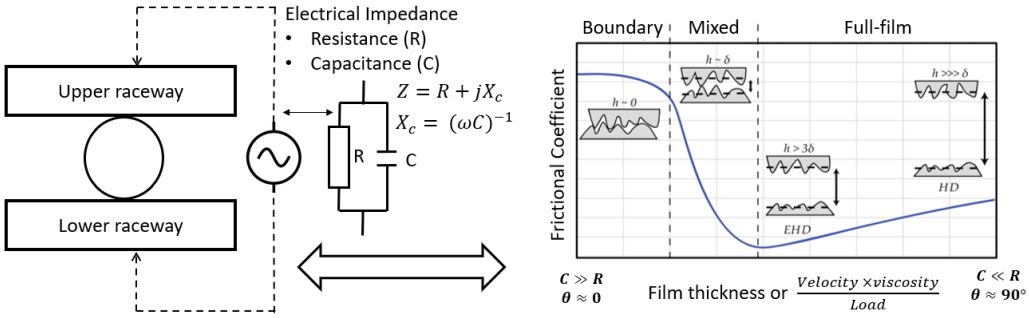

Figure 37: Lubrication condition and its electrical properties in rolling bearing.

2 Methodology and Results

In current research we focus on the direct comparison between the capacitance-based approach of Jablonka et al. [JAB23][JAB13] and the impedance-based approach of Maruyama et al. [MAR18][MAR19][MAR23] for determining the film thickness in the identical EHL line contacts of a cylindrical roller thrust bearings (CRTB). The results of both approaches are compared and their accuracy and reliability were evaluated. The reconstructed film thickness results were compared to Moes' EHL film thickness equation. The investigations also consider a parametric analysis of the effect of axial load, speed, and supply oil temperature on the measured impedance.

2.1 Maruyama's method

Maruyama et al. [MAR18][MAR19][MAR23] analytically derived the equations (1-3) for line contact EHL. The oil film breakdown parameter α represents the resistive contribution to the entire impedance (Equation 1). h_c denotes the film thickness within the loaded zone of the EHL contact (Equation 2) whereas h' denotes the average film thickness which is calculated using Equation (3). If $\alpha = 0$ (EHL) than average film thickness (h') is equal to h_c. However, in mixed lubrication ($\alpha \neq 0$), the average film thickness is less than h_c.

$$\alpha = \frac{2R_{10}cos\theta}{N|Z|} \qquad \textbf{Eq. 9}$$

$$h_c = \frac{8(1-\alpha)^2 b^2}{\pi^2 r}\left(\frac{1+\sqrt{1+\varphi}}{\varphi}\right)^2 \qquad \textbf{Eq. 2}$$

$$h' = (1-\alpha)h_c \qquad \textbf{Eq. 3}$$

where $\boldsymbol{\varphi}$ represents the dimensionless number (Equation 4).

$$\varphi = -\frac{8(1-\alpha)b\ sin\theta}{\pi^2 \varepsilon N L r \omega |Z|} \qquad \textbf{Eq. 4}$$

The electrical impedance $Z = |Z|e^{j\theta}$, with magnitude $|Z| = \frac{|V|}{|I|}$ and phase angle θ, given in the formula's above, is obtained by measuring the electrical current as response to an imposed alternating voltage. The electrical base resistance R_{10} in Equation (5) is defined as

$$R_{10} = \frac{N|Z_0|}{2cos\theta_o} \qquad \textbf{Eq. 5}$$

in which $|Z_0|$ and θ_o in Equation (5) are respectively the magnitude and phase of the initial impedance Z_0 for a stationary lubricated contact where the oil film breakdown factor α is unity. Once these parameters are determined at standstill, monitoring the impedance during operation provides directly an estimation for the central and averaged oil film thickness during EHL and/or mixed lubrication (Equation 3) as well as for the breakdown ratio (Equation 1).

First we use the method of Maruyama et al. [MAR18][MAR19][MAR23], to calculate the central film thickness, taking into account the full impedance $Z_{bearing}$, including the capacitive and resistive contributions. Besides the film thickness also the breakdown of the lubricant film has been assessed. Figure 2 presents the measured impedance and phase angle for varying rotational speed. Additionally, the bearing frictional torque M_t and bearing temperature were measured simultaneously.

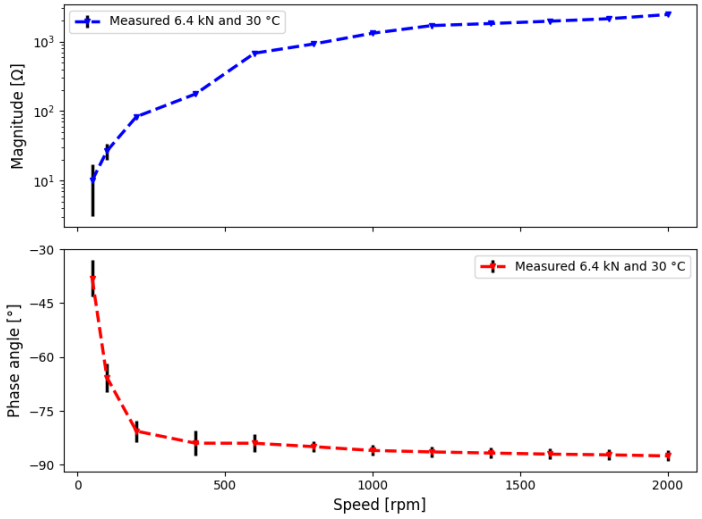

Figure 2: Measured impedance, magnitude(top) and phase angle (bottom), for varying speeds

The measured global bearing impedance ($Z_{bearing}$) and phase angle were used to calculate the average oil film thickness and breakdown ratio using Equations 1- 5 of Maruyama et al. [MAR18] [MAR19][MAR23]. The values for the oil film breakdown factor α are shown in Figure 3a as a function of speed and load whereas the reconstructed central film thickness, as well as the values obtained with the correlations of Moes, are shown in Figure 3b.

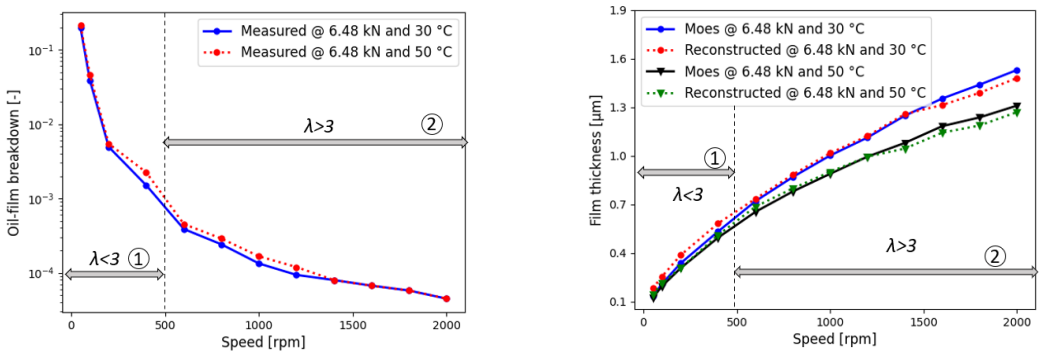

(a) (b)

Figure 3: (a) Oil-film breakdown and (b) Comparison of reconstructed and Moes' film thickness

At high rotational velocities, an adequate lubricant film is established, separating the roller and raceway surfaces. Hence the oil film breakdown factor α is very low, with values in the order of 10^{-4}, indicating full-film EHL. At low rotational velocities, however, the lubricant film is too thin to fully separate the surfaces. Thus, direct metallic contact of opposite asperities occurs resulting in a fast increase of the value of the oil film breakdown factor α with several orders of magnitude up to 0.2 for the lowest rotational speed. It is worth noting that there isn't a clear cut distinction between boundary lubrication and mixed lubrication, as evident in Figure 3a. This suggests that the α parameter may not be particularly sensitive to this transition.

For mixed lubrication conditions (Figure 3b, Zone 1), the central film thickness, obtained by Maruyama's method, was found to be 6-8% higher in comparison to the values obtained by the correlations of Moes. We emphasize, however, that the Moes correlation is no longer valid, and hence reliable, in mixed-lubrication for which corrections would be needed. However, for full-film EHL (Figure 3b, Zone 2), the measured film thickness in the speed range $600rpm$ to $800rpm$ was observed to be only 2% higher than the analytically calculated film thickness. Meanwhile, from higher speeds of $1500\ rpm$ onwards, Maruyama's film thickness was 4-5% lower than the calculated one (Moes).

2.2 Jablonka Method

The method of Jablonka et al. [JAB23][JAB13], initially developed via a ball-on-glass test setup, has been applied to ball bearings (point contacts) as discussed in [SHE22]. Since Jablonka et al. [JAB23][JAB13] considered only the capacitive contribution of the contacts, equation (6), can be rewritten as

$$C_{bearing} = \lim_{R\to\infty}\left[\frac{1}{Z_{bearing}}\right] = \sum_{k=1}^{N}\frac{C_{k,u}.C_{k,l}}{C_{k,u}+C_{k,l}} = \frac{N.(C_H + C_0)}{2} \qquad \textbf{Eq. 6}$$

the total bearing capacitance $C_{bearing}$ for a bearing with equal contact conditions for each roller/ball, is defined as

$$C_{bearing} = \frac{N}{2}(\varepsilon_{r,Oil}\varepsilon_O\frac{A_H}{h_C} + C_0) \qquad \textbf{Eq. 7}$$

from which the central film thickness h_c can be obtained. Note that implicitly, the assumption is made that the film thickness in the loaded area of the contact is uniform for both the upper and the lower raceways such that in this region, the surfaces are nearly parallel.

The capacitance $C_0 = C_{inlet} + C_{cav}$ in the region outside of the loaded zone of the contact is given by [JAB23] [JAB13],

$$C_O = \int_{A_{Flooded}} \frac{\varepsilon_O \varepsilon_{r,Oil}}{h_C + h_{gap}(x,y)} dxdy + \int_{A_{Cav}} \frac{\varepsilon_O}{\frac{h_C}{\varepsilon_{r,Oil}} + \frac{h_{gap}(x,y)}{\varepsilon_{r,Air}}} dxdy \quad \textbf{Eq. 8}$$

Equations 7 and 8 are adjusted to accommodate the line contact model [FUR17], incorporate the Hertzian area A_H for a line contact and capacitance in the outside of the loaded zone C_O.

A direct comparison of the film thickness reconstruction by Jablonka et al. [JAB23] [JAB13], using capacitance measurements, with the values obtained via the correlations by Moes, is shown in Figure 4a. Similarly to the impedance-based results of Maruyama et al., we observe a reasonably good correlation between the film thickness values based on the capacitance measurements and those obtained via the Moes fit with inlet shear factor (Figure 4b). In the EHL regime, deviations between both range between -1.5% at lower rotational speeds, to maximum 1.6% at high rotational speeds.

The results of the comparison indicate that both methods, the electrical approach and Moes' correlation, exhibit strong performance in predicting EHL film thickness. This suggests a high level of reliability and accuracy in the proposed electrical approach for EHL film thickness measurements.

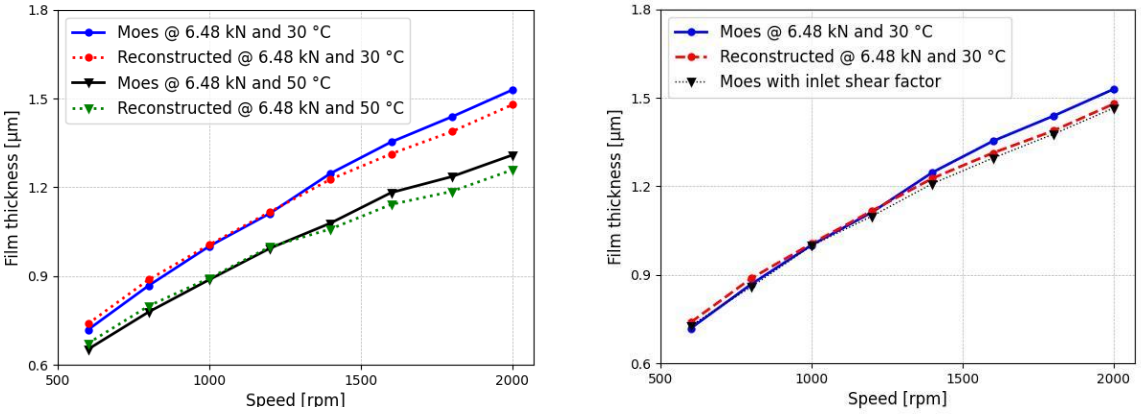

(a) (b)

Figure 4: (a) Reconstructed and Moes film thickness comparison and (b) Film thickness with inlet shear factor

2.3 Transition From Ohmic to Capacitive Behaviour over Lubrication Regimes

In order to ascertain the transition from mixed to full-film lubrication, it is imperative to understand the variation in the ohmic to capacitive transition across different operating conditions. Therefore, impedance measurements were recorded in a large frequency range of 100 Hz to 1 MHz at different rotational speeds as depicted in Figure 5. As the film thickness increases, the impedance magnitude $|Z|$ increases (Figure 5a) while the impedance phase angle θ decreases (Figure 5b).

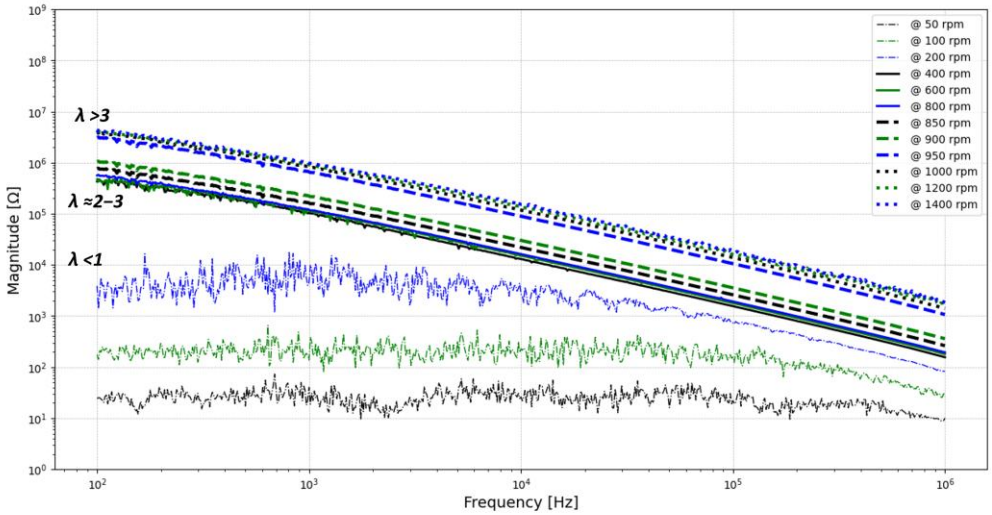

(a)

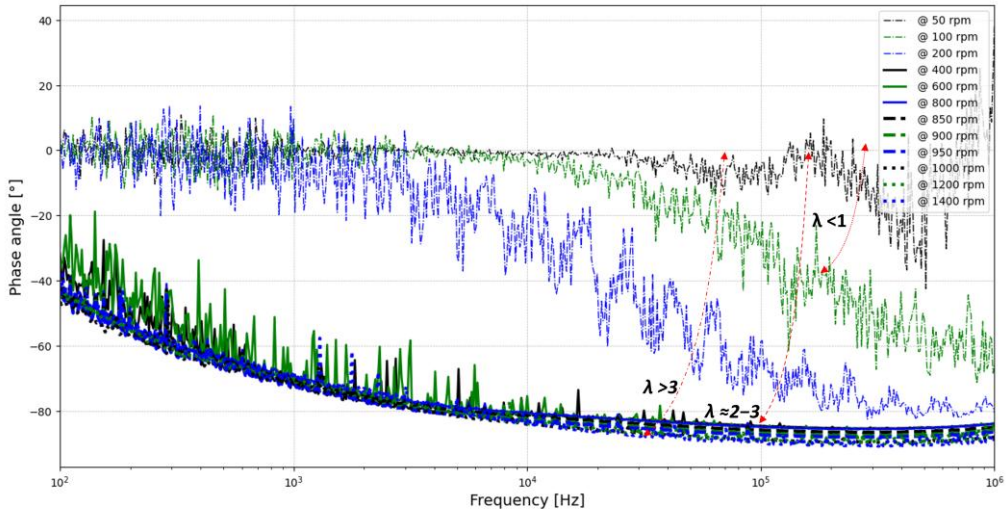

(b)

Figure 5: Measured magnitude (a) and phase angle (b) for varying frequencies and speeds.

3 Summary

In this research we focused on the use of Electrical Impedance Spectroscopy to measure the global and contact impedances in a cylindrical roller thrust bearing, with the aim to determine a quantitative prediction of the lubricant film thickness and analyse the transition from ohmic to capacitive nature of the impedance when evolving from boundary lubrication to Elastohydrodynamic lubrication (EHL). Besides the electrical impedance, the bearing temperature and frictional torque, are measured in a test bearing, undergoing a pure axial loading for various rotational speeds and oil temperatures. The measured impedance is translated into a quantitative measure of the lubricant film thickness in the contacts, using both the methods of Maruyama et al. [MAR18] [MAR19][MAR23] and Jablonka et al. [JAB23] [JAB13]. Moreover, the obtained film thicknesses are compared to the analytical film thickness obtained from the correlation of Moes, taking into account shear heating effects at the

inlet. Additionally, we investigated the transition from boundary (ohmic) to full film EHL lubrication (capacitive) behaviour in bearings. The main conclusions in this work are enlisted in the following:

- An analogous trend was observed when migrating from boundary lubrication to mixed lubrication and finally towards EHL lubrication. Indeed, inspection of the bearing or contact impedance, and more specifically the contact resistance and capacitance for various bearing speeds clearly shows the transition from boundary to mixed lubrication as well as the transition from mixed to EHL lubrication.
- Monitoring the film breakdown indicator α, proposed by Maruyama et al.[MAR18] [MAR19][MAR23], as function of increasing rotational speed, and hence film thickness, very small values ($< 10^{-4}$) were observed during EHL, whereas the value increases quickly with several orders of magnitude during mixed lubrication up till order 10^{-1} in boundary lubrication. The breakdown indicator α, however, did not show a very clear distinction once transitioning from mixed to boundary lubrication.
- Comparison of the impedance-based and capacitance-based film thickness estimations of respectively Maruyama et al. [MAR18][MAR19][MAR23] and Jablonka et al. [JAB23][JAB13] to the analytically estimated film thickness by Moes' correlation, corrected for inlet shear heating effects, revealed that both methods perform very well for EHL film thickness measurements. Deviations of both methods to the values of Moes were in the order of 2-3%, which is near the measurement uncertainty.

4 Bibliography

[DOL23] Doll, G.L: Causes and Effects of Bearing Damage
Roller Bearing Tribology 2023 ,205–231,
doi:10.1016/B978-0-12-822141-9.00011-X.

[DOW06] Dowson, D.; Higginson, Reflections on Early Studies of Elasto-Hydrodynamic Lubrication. Solid Mechanics and its Applications 2006, 134, 3–21, doi:10.1007/1-4020-4533-6_1.

[FUR17] Alexander Furtmann's. Elektrisches Verhalten von Maschinenelementen Im Antriebsstrang, Leibniz Universitat Hannover, 2017

[GOH01] Gohar, R. *Elastohydrodynamic*.
World Scientific, 2001; ISBN 1-86094-170-2

[JAB12] Jablonka, K.; Glovnea, R.; Bongaerts ,J Evaluation of EHD Films by Electrical Capacitance. J Phys D Appl Phys 2012, 45, 385301, doi:10.1088/0022-3727/45/38/385301

[JAB13] Jablonka, K.; Glovnea, R.; Bongaerts, J: Morales-Espejel, G: The Effect of the Polarity of the Lubricant upon Capacitance Measurements of EHD Contacts. Tribol Int 2013, 61, 95–101, doi:https://doi.org/10.1016/j.triboint.2012.11.016.

[MAN23] Manjunath, M.; Fauconnier, D.; Ost, W.; De Baets, P. Experimental Analysis of Rolling Torque and Thermal Inlet Shear Heating in Tapered Roller Bearings.
Machines 2023, 11, 801, doi:10.3390/machines11080801.

[MAR18] Maruyama, T.; Nakano, K. In Situ Quantification of Oil Film Formation and Breakdown in EHD Contacts.
Tribology Transactions 2018, 61, 1057–1066,
doi:10.1080/10402004.2018.1468519.

[MAR19] Maruyama, T.; Maeda, M.; Nakano, K. Lubrication Condition Monitoring of Practical Ball Bearings by Electrical Impedance Method.
Tribology Online 2019, 14, 327–338, doi:10.2474/trol.14.327.

[MAR23] Maruyama, T.; Radzi, F.; Sato, T.; Iwase, S.; Maeda, M.; Nakano, K Lubrication Condition Monitoring in EHD Line Contacts of Thrust Needle Roller Bearing Using the Electrical Impedance Method.
Lubricants 2023, 11, doi:10.3390/lubricants11050223.

[SHE22] Shetty, P.; Meijer, R.J.; Osara, J.A.; Lugt, P.M. Measuring Film Thickness in Starved Grease-Lubricated Ball Bearings: An Improved Electrical Capacitance Method.
Tribology Transactions 2022, 65, 869–879,
doi:10.1080/10402004.2022.2091067.

Systems Engineering:

Seamless Model-Based Product Development

Automated Generation of Drivetrain Components with Model-Based Systems Engineering, Variant Modeling and FVA-Workbench

I. Schulz[1]

[1]SKF GmbH, Gunnar-Wester-Straße 12, 97421 Schweinfurt

Keywords: *Drivetrain components, MBSE, FVA-Workbench, SysML*

Abstract: Drivetrain components and their application are of huge importance for the German industry. Therefore, to increase effectiveness and efficiency of their engineering processes is a continuous effort. One possibility to do so is the use of Model-Based Systems Engineering MBSE. With a high-precision gearbox as example, this paper shows how MBSE supports qualitative and quantitative variant generation, enables efficient simulation in the FVA-Workbench in terms of automated update of the geometry, load cases and test case verification, as well as the automated design generation and tolerancing in PTC Creo & Sigmetrix CETOL. The presented engineering environment is not a theoretical concept, but an executable practical implementation.

1 Introduction

Drive and automation technology form a strong basis for the performance of the German industry. The variety of applications and thus the design of drive technology components leads to a high quantitative, dimensional variance as well as a qualitative variance, which is reflected in differences in the design structure. Mastering these variances both technologically and economically efficiently is one of the key success factors of the German economy.

To make these variances manageable, SKF developed an approach using a high-precision gearbox, e.g. for robotics industries. This product has been chosen due to its variety of different drive technology components, their demand for technical excellence and high precision, and the need to develop such challenging systems in very short time at a competitive cost level. Within this project various patents could be filed, e.g. for a new family of ball bearings, the Cross-Ball Bearing [SCH20], a new principle solution for backlash-free gearboxes [SCH18], and new ways of how to monitor the condition of such gearboxes have been developed [AMI22]. Figure 38 shows the system and the technological inventions done.

The high-precision gearbox is based on model-based systems engineering with SysML, variant modeling with the VAMOS method, automated simulation with the FVA-Workbench [FVA25], and automated design and tolerance analysis in PTC Creo [PTC25] and Sigmetrix CETOL [SIG25]. At the same time, the resulting data model provides an ideal basis for methods of artificial intelligence.

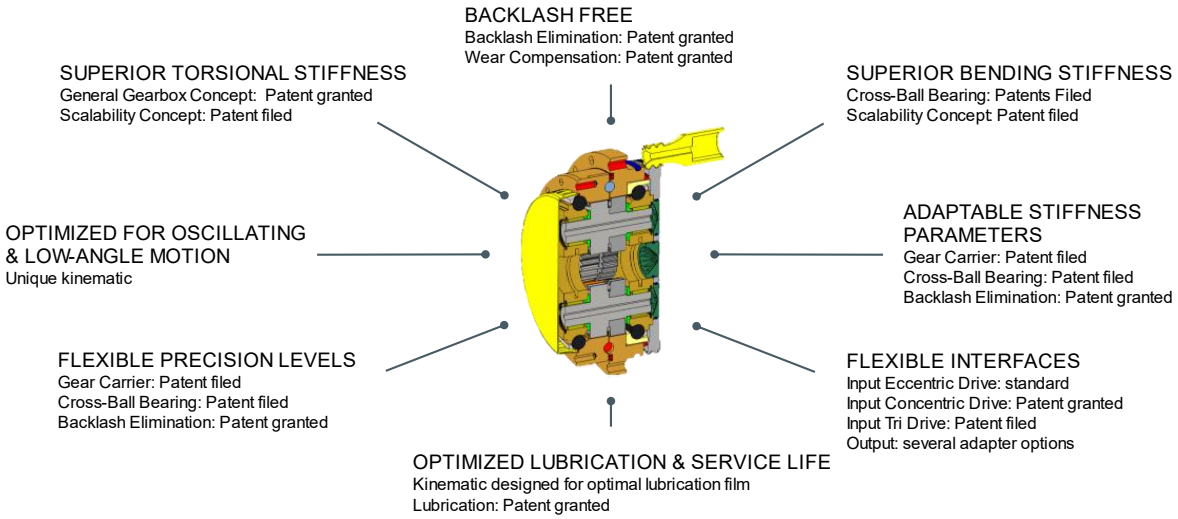

Figure 38: High-precision gearbox SKF Gear Bearing Unit

2 Principles guiding the system model

In the beginning of the project several basic principles have been created to orientate the development work in the most effective way. Even if the below described principles have been evolved over time and show their final status, the fundament has existed already in the beginning of the work.

2.1 The system data model $(n+1)^n$

The shown systems model is based on a system data model, inspired by Prof. Feldhusen from RWTH Aachen [FEL13]. Within the system data model $(n+1)^n$, method n uses system data n to instantiate product model n, so that system data n is available for work step n+1 as a result, Figure 39. This process is repeated continuously, generating a more advanced model in each iteration.

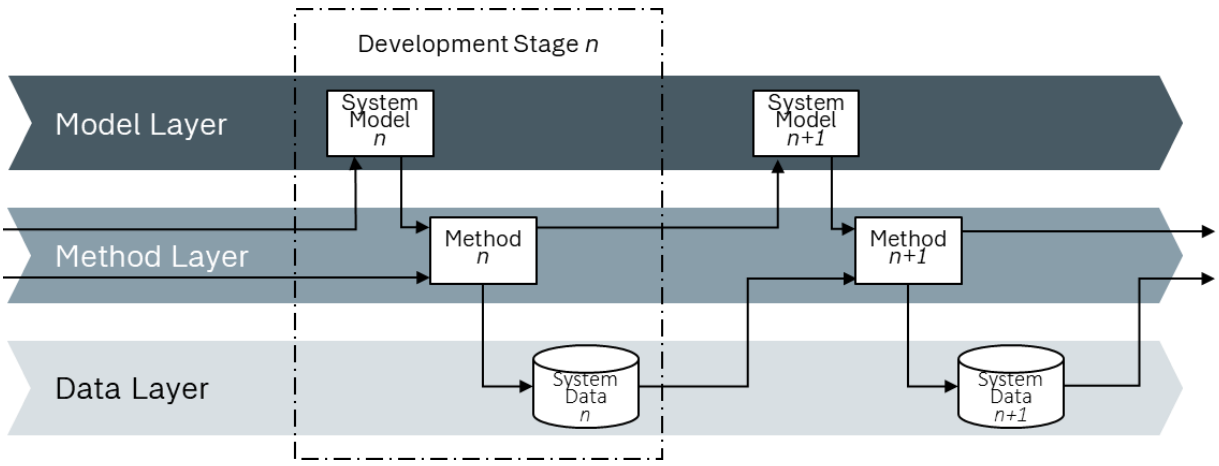

Figure 39: System data model $(n+1)^n$ [SCH23]

2.2 The FR²LP² process model

A typical framework in MBSE is the so called RFLP, bringing the Requirements Model, the Functional Model, the Logical Model, and the Physical Model in a sequence [EIG21]. Although this framework is widely used and well perceived, observations of the author within the area of drivetrain

solutions indicate that an adapted model fits better to the specific needs of this industry. This advanced model is called FR²LP² (Figure 40). Since the drivetrain industry is usually dealing with well-known products, often standardized components, that are configurated in a new, maybe innovative way, the starting point of a new development is the Functional Model. Here the purpose of the system-of-interest is defined. Based on this purpose, the boundary conditions given by the application, the Customer Requirements Model is created. Nevertheless, there are more boundaries to be considered, e.g. specific design rules or regulations, that are described in the Company Requirements Model. All three models are part of the analysis of the system, what leads to the synthesis of the Logical Model, in which the principle components and sub-systems are defined. When these artifacts are used in a certain well-defined context they become the Physical Model, e.g. connected by interfaces. Finally, the elements described in the physical model are available to become the input elements of the Process Model, in which manufacturing and assembly, but also purchasing and operation processes can be modeled.

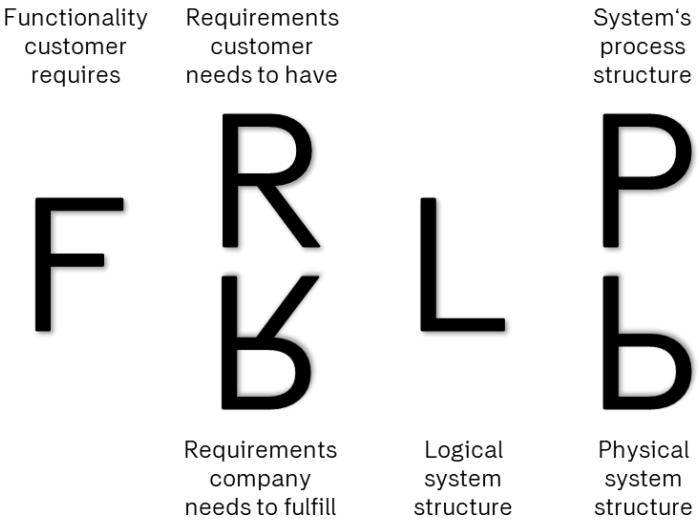

Figure 40: The development process model Function-Requirements (external/internal)-Logic-Physic-Process FR²LP²

2.3 Design patterns used

During the development of the system model of the high-precision gearbox several best practices or design patterns have been used. Two of them, that turned out to be crucial for the system model, are the Variant Pattern and the Connection Pattern.

One of the objectives of the development project has been to create a highly efficient environment for the customization of high-precision gearboxes, for which the methodology VAMOS has been applied [WEI16]. This pattern is integrated e.g. in the functional model, in which the variation point is the actual input drive of the gearbox, and the variants are the eccentric, concentric, and TriDrive solutions. Within the physical model one variation point is the planet’s bearing type, with its variations ball, needle, and tapered roller bearing. The criteria, which variant to choose is dependent on loads and geometry and modeled as a variation constraint.

The connection pattern lives in both the logical and physical model. It provides interface blocks, to type ports, and association classes to type connections. With this powerful pattern interfaces between functional surfaces can be clearly specified, like bolt connections, gear flange contacts and rolling element to raceway contacts.

Within the described project the model, and therefore the design patterns, have been implemented using SysMLv1.6. These implementations have been customizations, special stereotypes and own instructions, how to use these patterns. It's very promising to see, that these and more patterns became part of the standard framework of the SysMLv2.0, so that interoperability between different tools, but also interchangeability of specifications between customers and suppliers can become more flawless and efficient.

3 Realization of the system model and development environment

Within this chapter a brief overview of the implementation of the system model into an engineering environment and the connection to several development tools is given.

3.1 MBSE product model and python-based engineering environment

One of the most important aspects of modeling the high-precision gearbox model in MBSE was the visualization of the development activities, the artifacts that had to be created, and the decisions that have been made. Both the process model FR²LP² and the MBSE tool enabled an efficient development workflow for this purpose.

It is important to consider that the described automated design generation process is taking place after the system has been developed e.g. according to the V-model [EIG21]. After the first phase of system development, all needed partial models are defined, all variation points are identified, and all instance tables are implemented. These tables are the central data source of the $(n+1)^n$ data model, to feed all methods needed to engineer a customized high-precision gearbox solution.

The interaction between the different methods and tools used in this process are orchestrated by a set of python scripts. According to the system model n these scripts extract the needed system data n-1 for the method n from the instance tables and process them, e.g. by calculating geometries based on design rules documented in public standards or company specific knowledge. Then, the scripts store the results back into the instance tables as system data n and provide the data as input to the next process step n+1, e.g. for a simulation.

3.2 Automated verification in FVA-Workbench

The FVA-WB model (Figure 41) is set up by three parts:

1. Templates for the standard Eccentric Drive, the eccentric TriDrive, and the Concentric Drive
2. A master script, implemented in each of the templates
3. A set of executing sub-scripts, that are called by the master script

Based on the initially selected variant of the high-precision gearbox in the functional model, the respective template is selected. By executing the master script, all needed sub-scripts are called to update the geometry, implement the loads, and assigning e.g. the required safety factors. As first calculation step an iterative definition of e.g. the helix angle modification $c_{H\beta}$ based on the required operative load set and a minimum requirement on the face load factor $K_{H\beta}$ is done. This geometrical set up acts than as the starting point for the optimization of both gear and bearing geometries for the operative, the acceleration, and the overload case.

Important to note is, that all geometrical attributes and all test case results, as they are defined in the system model, are stored in instance tables, even, if the geometry of the system has not fulfilled

the test case. Background of this is, that all calculations contribute to a data basis that can be used to train algorithms of artificial intelligence.

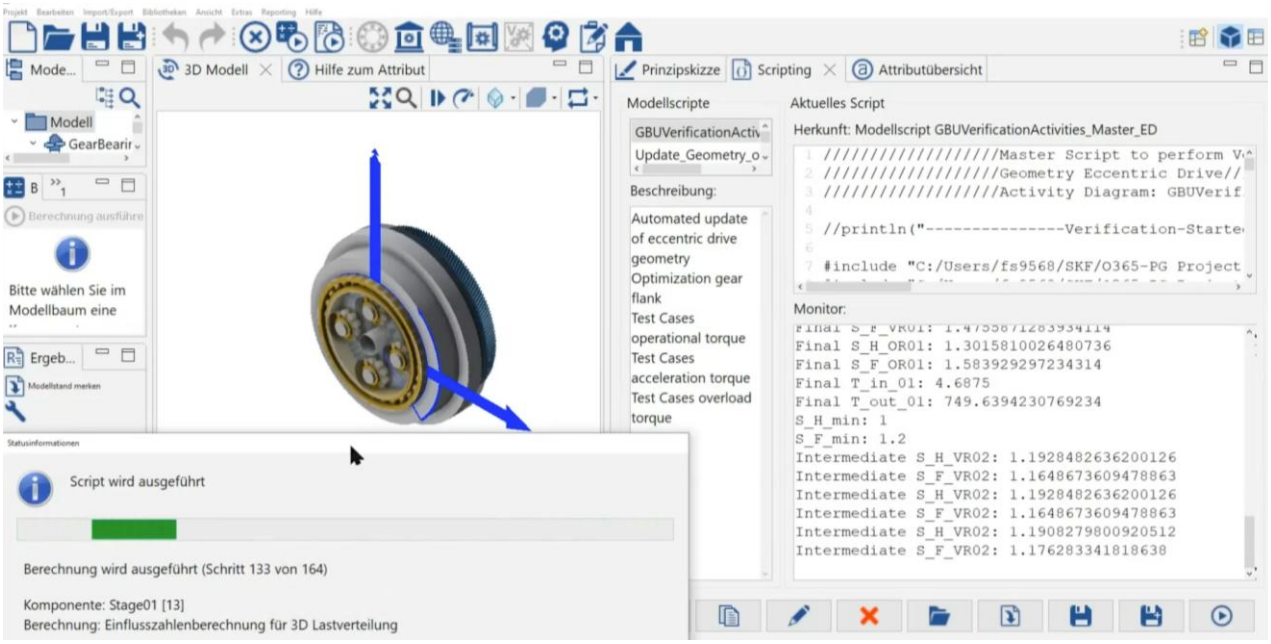

Figure 41: FVA-Workbench model during execution of optimization

3.3 Automated design and tolerancing in PTC Creo and Sigmetrix CETOL

Once the design team has approved the test case results of the verification work step, the automated design and tolerancing in a CAD environment can be initiated. Again, a python script is started that collects the relevant data from the instance tables and ‘injects’ these data into the target CAD template. Within this project the CAD system is PTC Creo and the interface between the python engineering environment and CAD has been implemented using the python library Creopyson [CRE25].

Similar to the verification step there is a set of pre-defined templates for the standard Eccentric Drive, the eccentric TriDrive, and the Concentric Drive available. Each of these templates consists of several geometrical representations, covering the states raw-material, soft-machining, heat treatment and hard-machining. The transition from one state to the next is guided by specific design rules.

After creation of the geometry models, the functional viability of the system design is investigated, considering both customer’s functional requirements like bending stiffness, and company’s requirements like cost and reliability. For this, part of the CAD model is a pre-defined tolerance model, here realized with the analysis software CETOL. Within this model, tolerance test cases transfer requirements into geometrical attributes, e.g. the bending stiffness of the high-precision gearbox into clearance and intersection of the bearings, respectively. Equipped with data from real manufacturing processes, the results give an answer, which geometrical parameters are critical-to-quality and which machines are required for manufacturing.

Important to mention is that after the regeneration of all geometrical representations the CAD model has 100% functionality, but some geometrical features may intersect and still need to be detailed by the CAD designer.

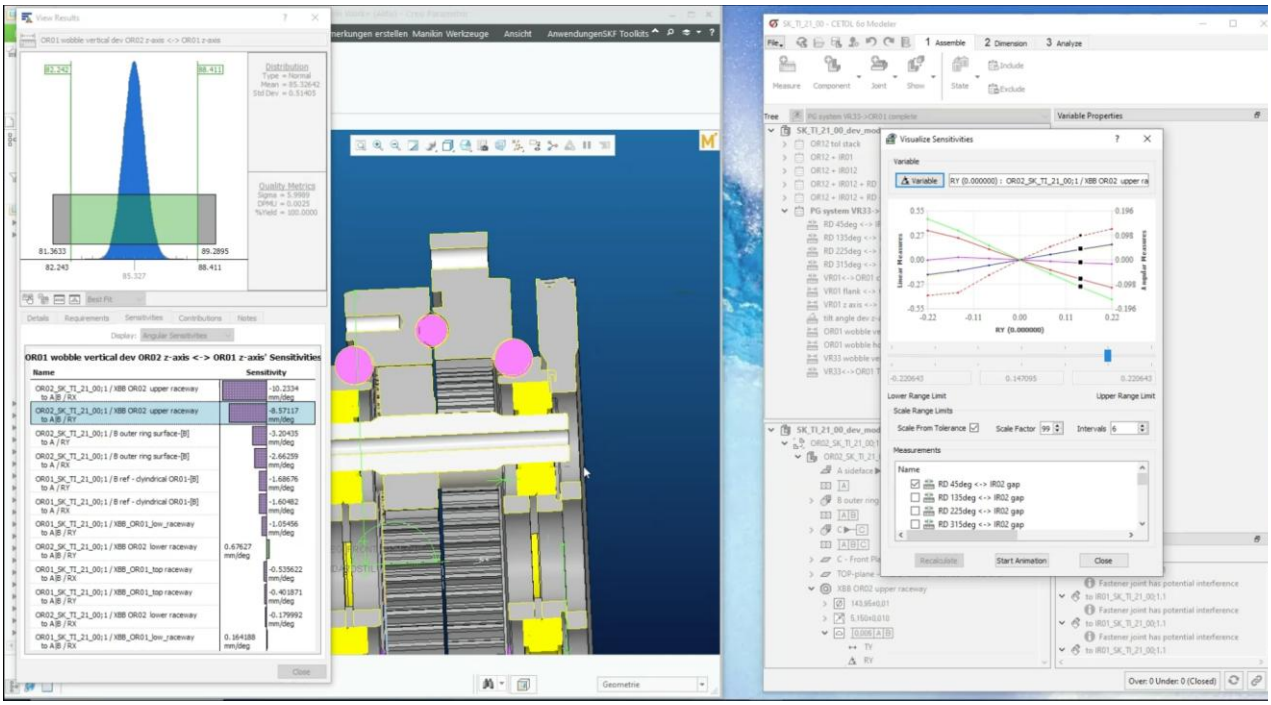

Figure 42: 1.1 Automated design and tolerancing in PTC Creo and CeTol

4 Achievements and further development

Following the known three dimensions of project management, quality, time, and cost, the project has shown the following advantages:

During the project the described high-precision gearbox has seen two major designs, and within the designs up to three iterative steps. Each major design took around 9 months from first sketches to the first test run, the iterative steps have been realized in around three and a half months. But even that the development team has been distributed across Europe and the design team has sat in India, none of the produced prototypes had a failure preventing the assembly or test run. The team members agreed on that one of the most important aspects achieving this high level of quality and robustness was the consequent data and model driven design approach.

Additionally, based on the modeling done within the prototype phases, the shown engineering environment has been proven to deliver a new high-precision gearbox configuration within 24 minutes. Of course, in a real development process the development would be structured by design review meetings, discussing and judging carefully the calculations results, design decisions and the fulfillment of customer requirements. Nevertheless, the time span to start manufacturing the first prototype will be a matter of a few weeks, rather than several months.

Finally, realizing a “first-time-right” development approach with high speed allows spending less resources for development, and faster integration in the final system-of-interest. Both lowers the cost tremendously, since not only cost spent will be reduced but also time-to-market for the end customer is improved significantly.

5 Bibliography

[AMI22] Amin Al Hajj, M.; Quaglia, G.; Schulz, I.:
Condition Based Monitoring on High Precision Gearboxes for Robotic Applications.
In: Shock and Vibration, Volume 2022
Hindawi, https://doi.org/10.1155/2022/6653723, 2022

[CRE25] Creopyson
https://pypi.org/project/creopyson/, 27.01.2025

[EIG21] Eigner, M.: System Lifecycle Management.
Springer Vieweg, Wiesbaden, 2021

[FEL13] Feldhusen, J.; Grote, K.-H.: Pahl/Beitz Konstruktionslehre.
Springer Vieweg, Berlin, 2013

[FVA25] FVA Software & Service: FVA-Workbench
https://www.fva-service.de/fvaworkbench, 27.01.2025

[PTC25] PTC: Creo
https://www.ptc.com/en/products/creo, 27.01.2025

[SCH18] Schulz, I.; Gläntz, W.; Haar, T., Reck, D.: Planetary Transmission.
US10823258B2, Earliest Priority Date: 03.01.2018

[SCH20] Schulz, I.; Cao, L.; Zeug, C.: Bearing Assembly.
US2023313837A1, Earliest Priority Date: 09.09.2020

[SCH23] Schulz, I.; Köping, L.; Reck, D.: KI-unterstützter Digitaler Zwilling für Hoch-Präzisionsgetriebe.
In: Wilke, Daria: Tag des Systems Engineering
Gesellschaft für Systems Engineering e. V., Bremen, 2023

[SIG25] Sigmetrix: CETOL
https://www.sigmetrix.com/software/cetol, 27.01.2025

[WEI16] Weilkiens, T.: Variant Modeling with SysML.
MBSE4U, 2014-2016

Enabling broader access to MBSE system models using collaborative engineering platforms and SysMLv2

M. May[1], T. Zerwas[1]

[1]Institut für Maschinenelemente und Systementwicklung, RWTH Aachen, Schinkelstr. 10, 52062 Aachen

Keywords: *SysMLv2, 3DExperience, data continuity*

Abstract: High data availability is essential in large engineering projects to ensure consistent information access across stakeholders. Model-Based Systems Engineering (MBSE) addresses this by using central system models as a Single Point of Truth (SPoT), connecting requirements and architectures to improve traceability and collaboration. Platforms like the 3DExperience (3DX) enhance data continuity by linking MBSE models to numerous engineering tools through standardized interfaces. While these interfaces streamline data exchange with simulation tools, the interfaces can only be accessed from the MBSE tool, not outside tools, limiting direct access to the information for engineers not working with the system model.

To address this challenge, a concept inspired by SysMLv2 is explored. SysMLv2 introduces a standardized API and centralized database, potentially enabling external tools to directly access system model data without relying on the MBSE tool. This approach could improve data availability, transparency, and cross-domain collaboration in large-scale projects.

1 Introduction

Large and complex projects face significant challenges that require effective management and coordination. In large collaborations, ensuring access to consistent information is crucial but often hindered by:

- Distributed data sources (Information is stored in various tools and databases)
- Lack of Accessibility (Stakeholders have no access to relevant information from others)
- Tool and system incompatibility (Seamless data transfer between different systems impaired)

These challenges result in a core issue: Involved stakeholders do not have a consistent level of information.

An example for projects facing these challenges is the Einstein Telescope, a next-generation gravitational wave detector. These instruments detect ripples in spacetime caused by massive cosmic events using laser interferometry, measuring movements with amplitudes smaller than a proton’s diameter [LIG20]. The Einstein Telescope will have 10-kilometer-long arms, built 200 to 300 meters underground to reduce seismic noise [MAG20], with estimated costs of €1.8 billion for construction

and €40 million annually for operation [PHY24]. Over 1,700 researchers across Europe collaborate to realize this project [ETI24].

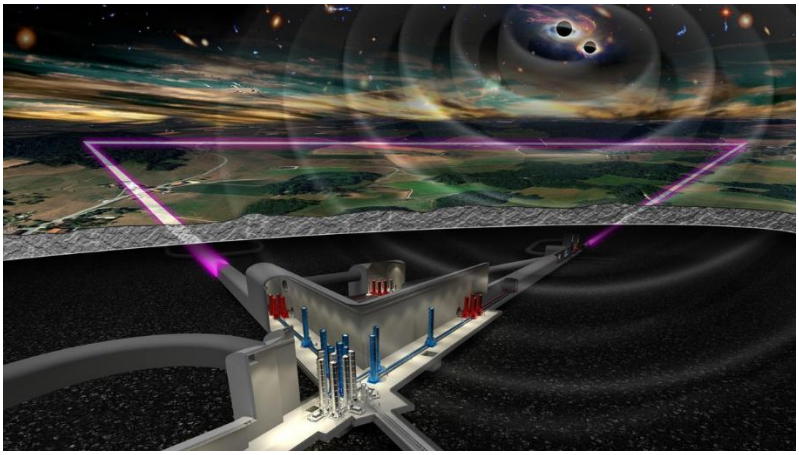

Figure 43: Artistic depiction of the underground Einstein Telescope [LUE25] ©NIKHEF

To address information continuity, Model-Based Systems Engineering (MBSE) is essential. MBSE consolidates project information into a central system model, enabling direct data exchange with simulation models for requirement verification. These central system models serve as repositories connecting all engineering information, such as requirements, functional architectures, and behavioral aspects, across domains. These models emphasize traceability, linking abstract functional descriptions to concrete system components, thereby fostering efficiency and consistency in multidisciplinary projects [JAC21]. However, these models are expert tools; extracting information and interfacing with other simulation and engineering tools remain challenging and often require custom solutions. This presentation explores how experts' access to MBSE system models and the extraction of data from these models can be improved.

2 Enabling access to central system models

Providing involved stakeholders with seamless access to central system models is crucial for enhancing collaboration and ensuring data continuity. To address this challenge, we focus on the use of collaborative engineering platforms, such as the 3DExperience, which connect MBSE system models with a large amount of engineering tools across different domains.

2.1 Collaborative Engineering Platforms and their limitations

The 3DExperience (3DX) platform provides a comprehensive environment to link MBSE central system models with various engineering tools, enabling efficient data exchange across domains. MBSE models serve as the Single Point of Truth (SPoT), connecting requirements, functional architectures, and physical and logical system elements in a unified architecture. This centralized approach ensures that engineering decisions across disciplines are based on consistent and up-to-date information, improving traceability and reducing errors compared to document-based processes. These advantages, as outlined in Chapter 1, are crucial for maintaining data continuity and enhancing project efficiency.

To facilitate integration with external tools, the 3DX platform uses simple and standardized interfaces, offering platform-wide tool compatibility. By incorporating the industry-standard MBSE tool Catia Magic, the system model becomes a uniform data source for connected tools. Notably, the

Process Composer app provides a significant advantage over standalone MBSE models by enabling direct parameter transfer between simulation tools and Catia Magic. This ready-to-use interface connects to numerous simulation tools, allowing for the automation of workflows, reducing manual data handling, and streamlining cross-disciplinary engineering activities. Additionally, requirements are managed in dedicated expert tools with synchronization to the system model, ensuring consistency.

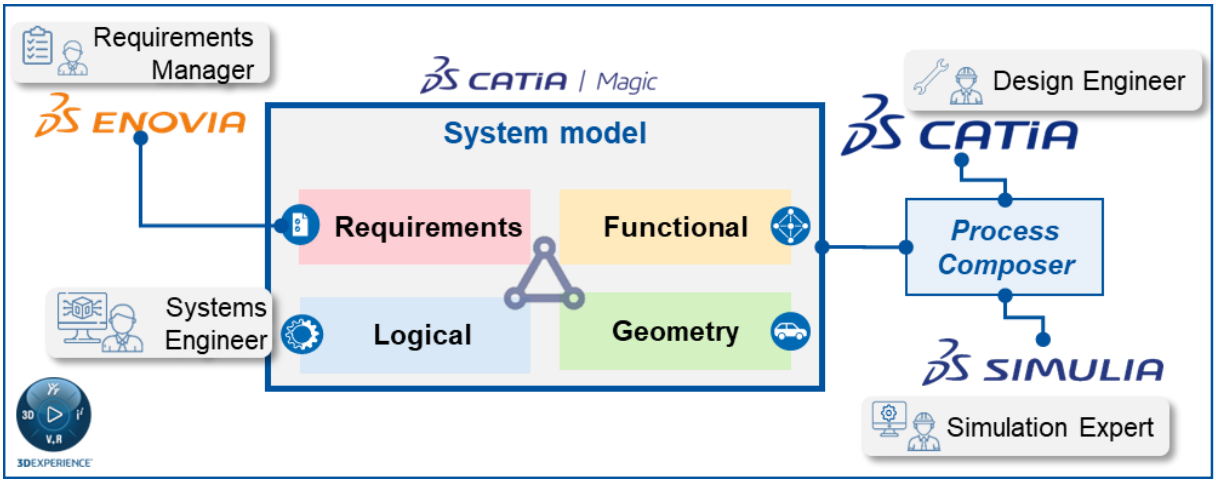

Figure 44: Overview of the possible interfaces such as Process composer and Enovia requirements between the 3DExperience platform and central system models in Catia Magic

Despite these benefits, a significant limitation of the 3DX platform lies in its restricted accessibility. Interfaces to access the system model data can only be activated from within the MBSE tool itself, preventing direct data retrieval from external tools. This limitation hinders transparency and slows cross-domain collaboration. This raises the central question: How can we enhance the platform to enable access to system model data from outside the MBSE tool?

2.2 Integration of the SysMLv2 database approach

One potential approach to addressing the limited accessibility of the 3DExperience platform is to draw inspiration from the SysMLv2 database concept. SysMLv2 introduces a standardized API and a central database, which could offer a unified framework for extracting data from MBSE system models. While not a fully developed solution, this approach presents a conceptual direction to improve accessibility by enabling external tools to access the system model without requiring direct interaction with the MBSE tool.

The integration of a standardized database and API could provide a cross-tool parameter space where data and parameters from all connected engineering tools are accessible. This setup would allow involved stakeholders to retrieve system data directly through the database, reducing reliance on the MBSE tool operator. For example, simulation experts might pull parameter values directly from the system model database, and design engineers could update CAD models without additional manual data requests. Such an integrated, function-oriented system architecture could enhance data continuity in large projects.

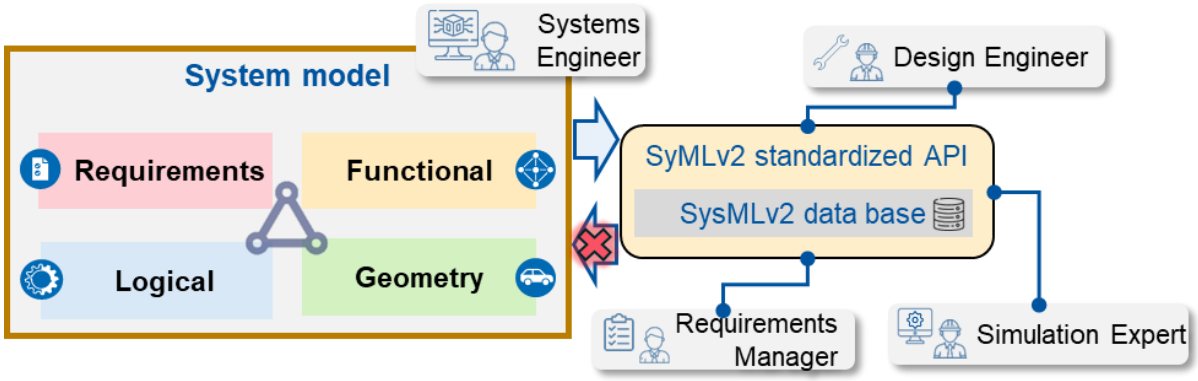

Figure 45: the standardized SysMLv2-API and database allow for simulation experts to access the information and data stored in system models in interpretable formats

3 Conclusion

In large and complex engineering projects, seamless access to consistent and transparent system information is crucial yet challenging. Collaborative engineering platforms like the 3DExperience (3DX) establish MBSE models as the Single Point of Truth (SPoT), improving data continuity, traceability, and cross-domain collaboration. Interfaces like the Process Composer enable ready-to-use connections to various simulation tools, streamlining workflows and reducing manual data handling. However, a key limitation remains: Data interfaces in 3DX can only be activated from within the MBSE tool, restricting direct access for external stakeholders.

To address this limitation, the SysMLv2 database approach offers an interesting approach. By introducing a standardized API and centralized database, this idea envisions a unified data source accessible from external tools, enabling engineers to directly retrieve system data for simulations or CAD updates. While this concept is not a fully developed solution, combining 3DX's extensive tool integration with SysMLv2's standardized data access could enhance collaboration, transparency, and data consistency across engineering domains, pointing toward a promising direction for future development.

4 Bibliography

[ETI24] Einstein Telescope Collaboration: In Warsaw, the third annual meeting of ET Scientific Collaboration.
INFN, Italy, 2024
https://www.einstein-telescope.it/en/2024/11/11/in-warsaw-the-third-annual-meeting-of-et-scientific-collaboration
(25 January 2025)

[JAC21] Jacobs, Georg et al.: Function-Oriented Model-Based Product Development.
In: Krause, Dieter; Heyden, Emil (eds.): Design Methodology for Future Products: Data Driven, Agile and Flexible., 243–262
Springer International Publishing, 2021

[LIG20] LIGO Scientific Collaboration: LIGO's Interferometer.
California Institute of Technology, Pasadena, 2020
https://ligo.caltech.edu/page/ligos-ifo
(25 January 2025)

[LUE25] Lück, Dr. Harald: Einstein-Teleskop
https://www.aei.mpg.de/einsteinteleskop
(28.01.2025)

[MAG20] Maggiore, Michele et al.: Site selection criteria for the Einstein Telescope.
In: Review of Scientific Instruments, 91, 094504
American Institute of Physics, 2020

[PHY24] Phys.org: Einstein Telescope ushers in a new era of astronomy.
Science X Network, 2024
https://phys.org/news/2024-06-einstein-telescope-era-astronomy.html
(25 January 2025)

Systems Engineering:

MBSE in Practical Application

Realizing Multidisciplinary Verification: Synchronizing System Architecture and Electrical Simulation Domains

Morten Huber[1], Marcel Plonka[1]

[1]Dassault Systemes Deutschland GmbH

Keywords: *System Architecture, Requirements Verification, Simulation, Integration*

Abstract: Analyzing and managing complex systems across multiple levels of abstraction remains a fundamental challenge in systems engineering. In the early stages of product design, verifying that a system meets its requirements is crucial to ensuring overall accuracy, functionality, and long-term reliability. This is particularly true for systems that integrate electrical and electronic components, where the close collaboration between electrical and systems engineering disciplines becomes essential. In such cases, the effective integration of tools that bridge System Architecture and Electrical Simulation plays an important role in streamlining the verification process. These tools not only facilitate clearer communication among multidisciplinary teams but also enhance the overall design process by allowing for comprehensive simulation and analysis. This paper explores the impact of these integrative tools on the development process, detailing how they contribute to optimized workflows, improved testing, and robust system design. By adopting a collaborative approach and leveraging specialized tools, engineering teams can better address complex design challenges and deliver systems that perform reliably in real-world applications.

1 Introduction

The rise of specialized software and platforms, particularly Software-as-a-Service (SaaS), for addressing engineering challenges has made it increasingly difficult for companies to manage and monitor software in active use [FOR24]. The resulting heterogeneity of the IT landscape—characterized by the interaction of numerous tools and architectures—introduces complexity that often impedes development processes. Consequently, companies frequently encounter challenges in establishing integrated and efficient workflows [HEL22, CAP14]. The implementation of Model-Based Systems Engineering (MBSE) further underscores the difficulties arising from a heterogeneous tool landscape. MBSE strives to connect traditionally siloed engineering domains at the organizational level, but also demands the integration or migration of various applications and data. This process often entails significant efforts in tool harmonization, personnel training, and change management, frequently leading to staffing challenges and high spending for software consultancy [LUC24]. This application paper demonstrates the integrity of workflows enabled by Dassault Systèmes' 3DEXPERIENCE platform, using the domains of Electrical Engineering and Systems Engineering as examples.

2 Use Case of On-Board-Diagnosis System in Vehicle

A typical touchpoint between Systems Engineering and Electrical Engineering occurs in the domain of Electrical & Electronics (E/E) engineering. In this context, engineering teams must ensure that stakeholder requirements are met within the highly complex environment surrounding the use of Electrical Control Units (ECUs). The example of an On-Board Diagnostics (OBD) system is selected to demonstrate how interoperability between different tools can be achieved, specifically focusing

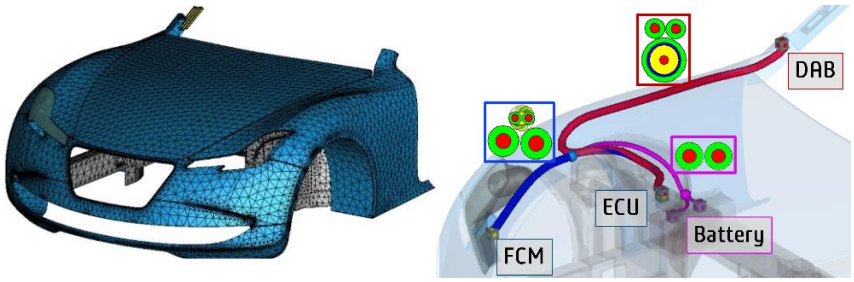

Figure 46: Vehicle CAD model with electrical harnesses

on the ECU that controls the Digital Audio Broadcast (DAB) and the Front Control Module (FCM) unit, ensuring that these devices work correctly. As shown in Figure 1 (right), this is accomplished by installing a wire harness to electrically connect all system parts and provide a power supply to them from a typical 12V battery. In this use case, the ECU establishes a connection with other units and performs a check for any issues associated with that link and the power supply.

Should any issues be detected, the ECU will dispatch an error message to inform the driver. Failure of this system can be considered as mechanical damage to the connectors or wire harness itself, caused by animal, natural elements, or by simple but unavoidable "wear and tear". Therefore, the system shall launch a system analysis, verifying the integrity of the components of the electronic control unit (ECU), the digital audio broadcast (DAB) system and the front control module (FCM). In the presented application, a failure was emulated, in which the wire harness between ECU and DAB got physically damaged. Consequently, no communication with DAB unit is possible. The application paper describes the IT infrastructure and the process to set up a connected simulation environment, including the Model-based Systems Engineering (MBSE) tool of CATIA Magic, the 3D electromagnetic analysis software CST Studio Suite® and the 3DEXPERIENCE® Platform.

2.1 System Architecture

The application of MBSE usually follows methodological guidelines to guarantee a consistent and integrated architecture. Therefore, the MagicGrid® methodology [MOR21] is applied (Figure 47). This is instrumental in guiding the early stages of system design, from defining stakeholder needs to exploring conceptual subsystems and their functionality and establishing implementation requirements. Usually, the method is conducted for every level of hierarchy of a product, i.e. starting with the whole vehicle and ending with the specification of individual components. As shown in the matrix in Figure 47, it links requirements to behaviors, structures and measures of effectiveness. The

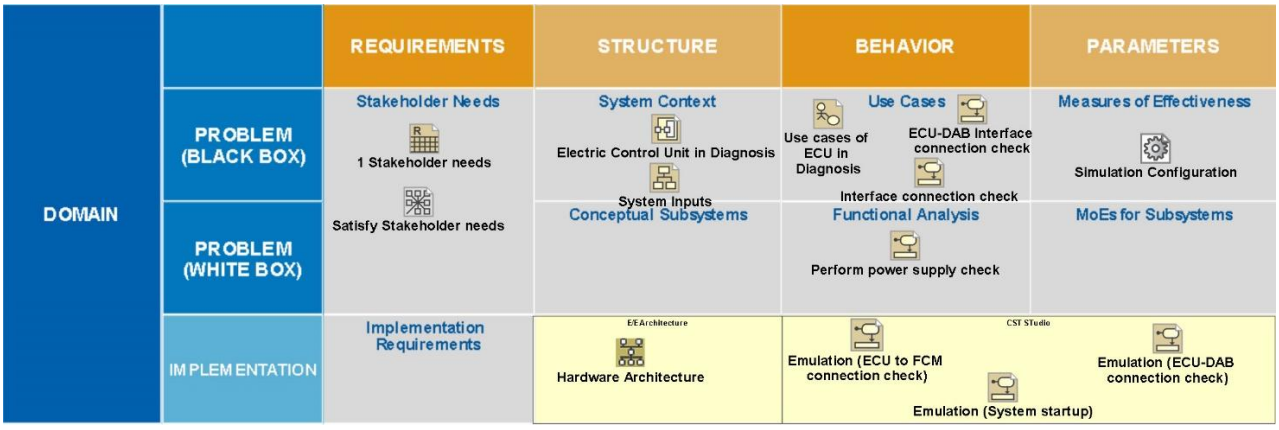

Figure 47: Applied MagicGrid® methodology on the example.

latter describe the parameters that are used for validation and verification purposes later on in the process. Thereby, it is advised to structure the system development into separate domains: problem domain, solution domain (not shown in this example) and the implementation domain. The first domain motivates the applicant to focus on understanding the problem and its facets. The second domain describes the precise functional specification of the systems and how it is going to solve the problem. The third domain provides the means to implement the required systems. In general, the modelling language SysML [SYS23] can be used to conceptualize complex systems and it is part of the MagicGrid® methodology description. However, certain aspects of the methodology can be provided outside of the scope of what SysML can cover, such as the hardware topology applied by the usage of the EE-Architect profile of Catia Magic or the electrical simulation that shall be covered by the CST Studio in the detailed implementation phase. To address the problem domain effectively, it is essential to begin with a specification of the system requirements. At this stage, the level of specification is already focused on the component; therefore, the requirements outlined in Figure 48 refer specifically to the system level instead of stakeholder requirements. These requirements contain detailed parameters, such as voltage and current specifications, for individual components like the Digital Audio Broadcast (DAB) unit and the Front Control Module (FCM). Such precise specifications ensure that the devices can operate reliably within the broader system architecture. Additionally, the System of Interest (SoI) is required to consume specific Diagnostic Trouble Codes (DTCs) for maintenance personnel. DTCs play a critical role in fault detection and isolation, offering clear and standardized error codes that enable efficient troubleshooting and system repairs. By defining this functionality at an early stage, the integration and behavior of the subsystems can be developed systematically to meet both functional and performance objectives. These requirement specifications also form the foundation for subsequent validation and verification processes (see Chapter 2.4). Verification ensures that the system has been built correctly according to its defined requirements, while validation confirms that the system fulfills its intended purpose. Establishing this clear link between requirements and verification processes is vital to achieve a robust and reliable system design. Following the requirements elicitation and formulation, understanding the system's structure and composition is fundamental to analyze the problem at hand. Figure 49 illustrates a breakdown of the Electric Vehicle System, showing how the On-Board Diagnostics (OBD) system functions as the System of Interest (SOI). This perspective makes it easier to see the role of OBD within the broader system architecture.

#	△ Name	Text
1	SN-1 System startup	System check shall work without failure at vehicle startup
2	SN-1.1 FCM Current	The FCM Current shall be above 3 A and below 4.4 A.
3	SN-1.2 ECU Current	The ECU Current shall be above 1.74 A and below 2.6 A.
4	SN-1.3 Battery_Current	The Battery Current shall be above 5.5A and below 8.2 A.
5	SN-1.4 DAB_Current	The DAB Current shall be above 0.86A and below 1.3A.
6	SN-1.5 Battery_Voltage	The Battery Voltage shall be above 9 V.
7	SN-2 Response to failure	System shall send Diagnostic Trouble Codes (DTC) in case of emulated failure
8	SN-2.1 ECU to DAB COAX cable connection check	The system shall monitor the connection between the (FCM) and the (ECU) via the COAX cable and send messages in case of a connection loss.
9	SN-2.1.1 ECU to DAB Interface shorted	The shorted interface failure check for DAB to ECU shall be 0, i.e false (no failure)
10	SN-2.1.2 ECU to DAB Interface opened	The opened interface failure check for DAB to ECU shall be 0, i.e false (no failure)

Figure 48: Excerpt of System-level requirements specification.

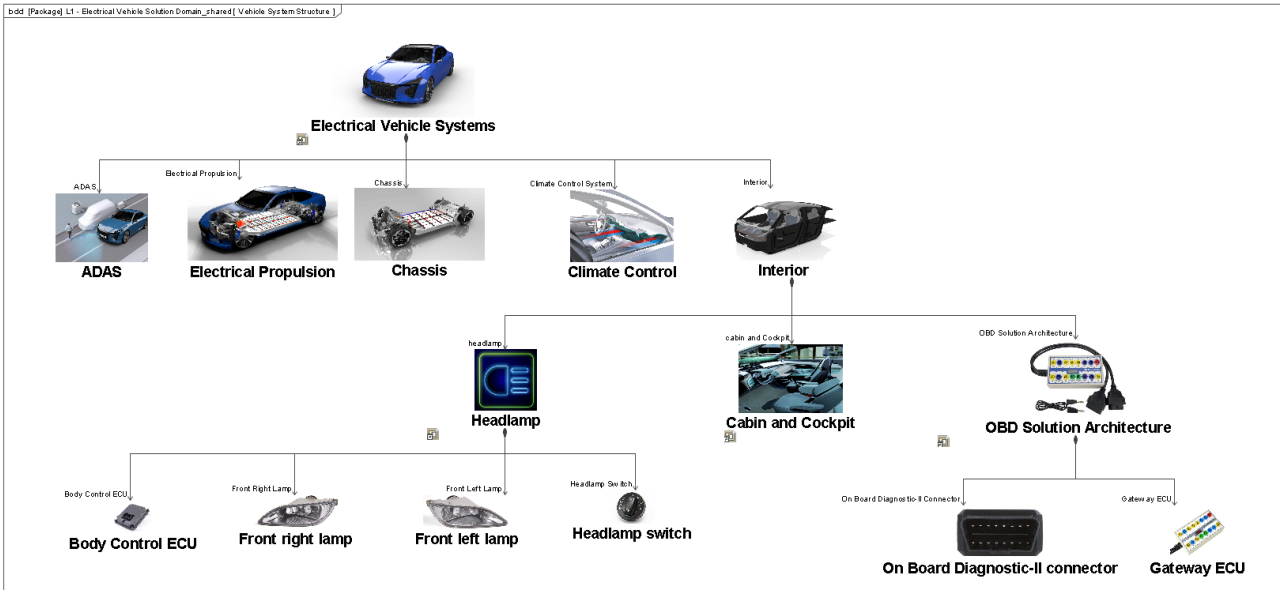

Figure 49: Illustration of System Architecture.

As illustrated in Figure 50, the OBD system connects to the Electrical Control Unit (ECU), which generates the Diagnostic Trouble Codes (DTCs). These codes are essential for identifying faults and assisting maintenance personnel with troubleshooting. The ECU is responsible for facilitating communication between itself and the FCM module via a standardized automotive protocol, CAN Bus. This protocol enables the ECU to control the standard FCM functions, such as the operation of the on-board camera or headlights. Additionally, the ECU manages the RF link with the DAB unit. The ECU also controls the power rail stability to ensure the reliable operation of all devices in the system. By examining these interconnections and communication pathways, the system's overall architecture and functional relationships become clear. In line with the MagicGrid® methodology, the system's use cases are to be specified in the given context. In the application presented, the focus is on the first use case which is specified in the SysML activity diagram in Figure 51. Within the specified activity diagram, it describes what the individual devices contribute to the overall functionality that is needed to check whether the ECU system is connected to the DAB system. In the conceptual phase, it is determined that the ECU initiates a power-supply check and a connection health check to the DAB unit (see blue actions in the activity diagram in Figure 51). However, it is not yet specified how this shall be accomplished. Later on, in the development phase it is then decided to carry out the two indicated actions using a tooling for electromagnetic simulation – CST Studio Suite. For this, a corresponding model is set up to allow for the electrical simulation in combination with the 3D ECAD model for the wire harness.

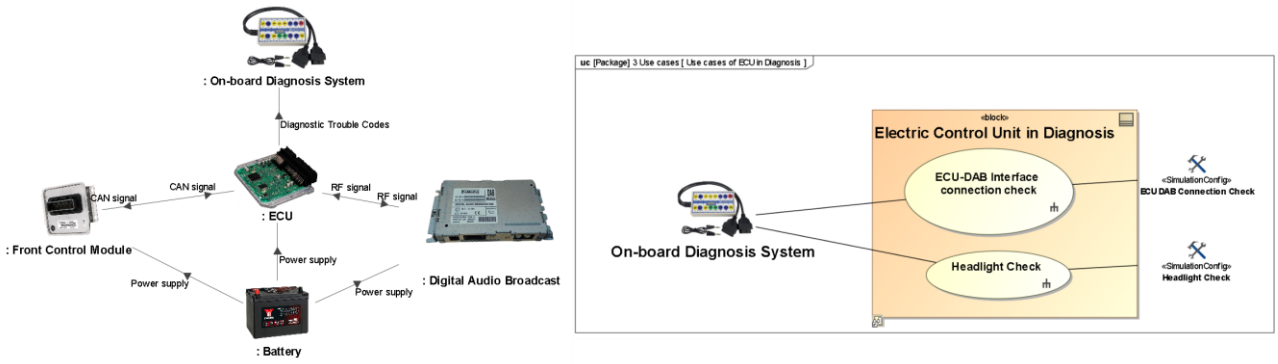

Figure 50: Illustration of System Context (left) and Use Cases (right)

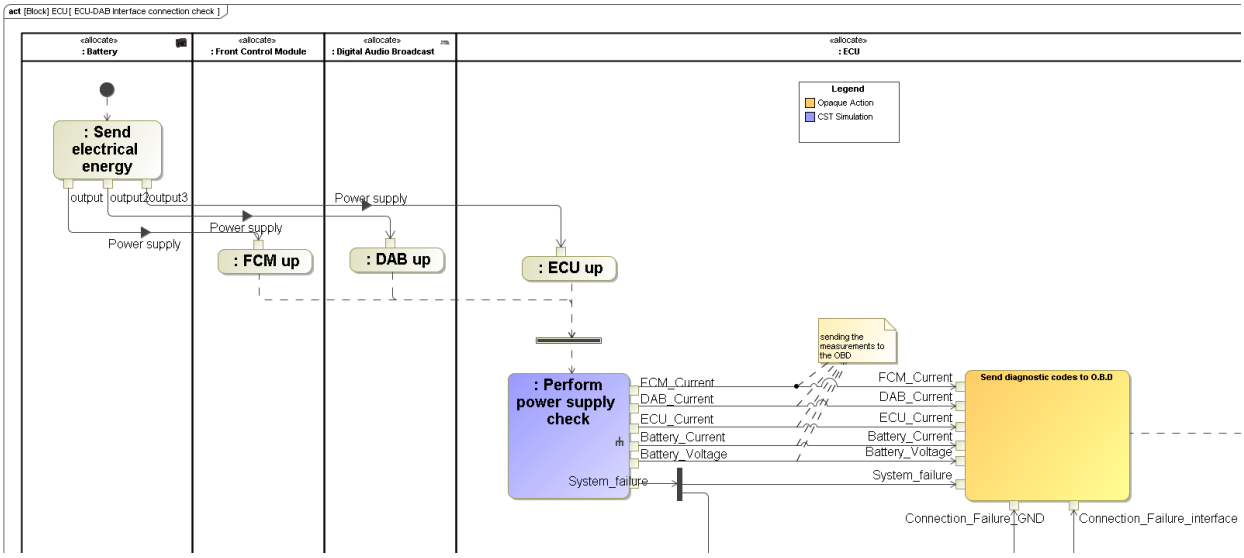

Figure 51: Excerpt of activity simulation with CST Design Studio simulations highlighted in blue color.

2.2 Electrical Simulation

In order to identify the appropriate cabeling dimensioning in the context of electrical signal integrity containing the electromagnetic investigations, as for Electromagnetic Compatibility (EMC) an electrical representation of the system is desired. Figure 53 illustrates the simulated electrical system. A 3D wire harness, which facilitates the power supply and digital communication between the ECU, DAB, and FCM units, was designed on the 3DEXPERIENCE platform. The harness is transferred from the 3DEXPERIENCE platform to CST Studio Suite and translated into a transmission line model. All units are modeled in a simplified manner. This means that they load the power supply network only as resistors to simulate their active or inactive states, and the loading conditions for digital systems (CAN bus and ECU-DAB link) are met solely using matching resistors. The electrical model uses the logical components (shown in Figure 52 as SPICE blocks) as basic blocks to monitor the electrical signals within the system and set the warning flags in the event of faults. The model is configured so that the results of the logical evaluation can be utilized as global output parameters of the model. This is the fundamental setup to begin using the electrical model as a black-box model to incorporate into the integrated simulation framework for the electrical and systems engineer.

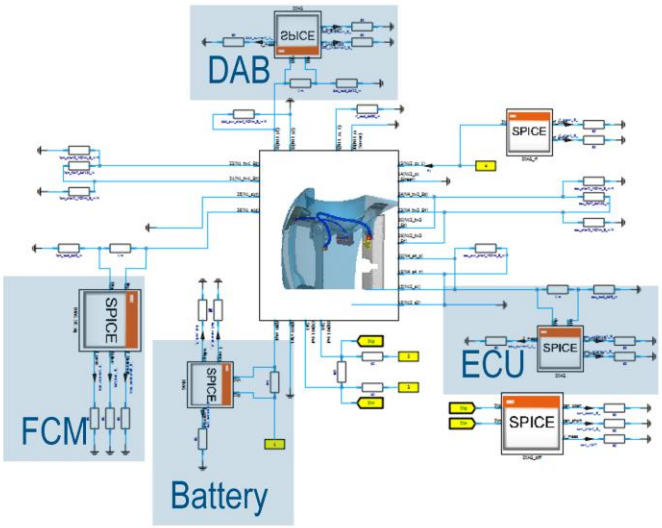

Figure 52: Illustration of electrical schematic model in CST Design Studio

2.3 Simulation Framework

As the system architecture model and the implemented electrical simulation are in place, it must be defined how to connect the two domains of Systems Engineering and Electrical Engineering. With the out-of-the-box connectivity of both tools to the 3DEXPERIENCE Platform, the individual models can be made visible. In the following step, the electrical simulation is utilized in the process orchestration where the previously defined parameters can be utilized and controlled without the necessity of opening an instance of CST Studio Suite [DAS24]. It is possible to use this process setup within the system architecture (shown on the right-hand side of Figure 53), utilizing the simulation engine of the Model Analyst plugin. For that, the electrical simulation, can be used in activity or parametric diagrams as a black-box, providing all input and output parameters to CATIA Magic (see blue box in Figure 51).

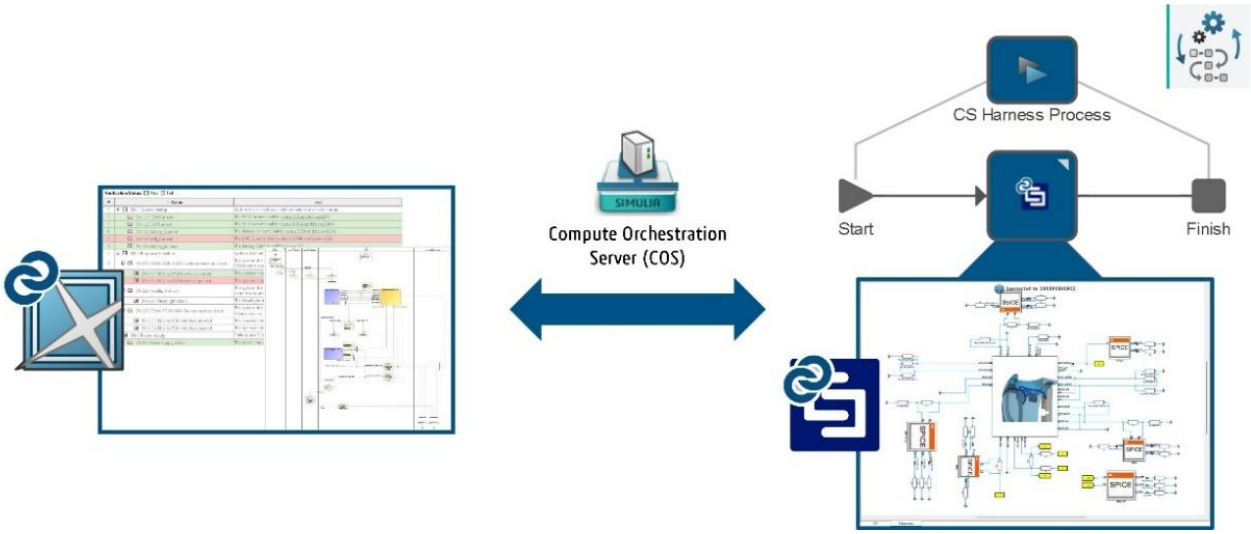

Figure 53: Illustration of the simulation framework

2.4 Results

Following the setup of the interfacing between the system architecture and the electrical simulation, the aforementioned use case scenario can be launched to verify the system-level requirements.

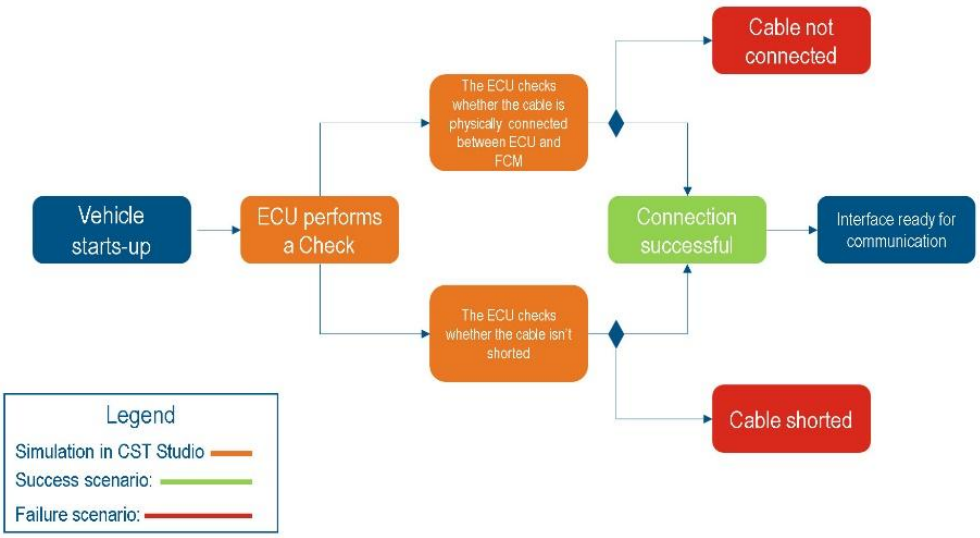

Figure 54: Scenario description for the integrated simulation.

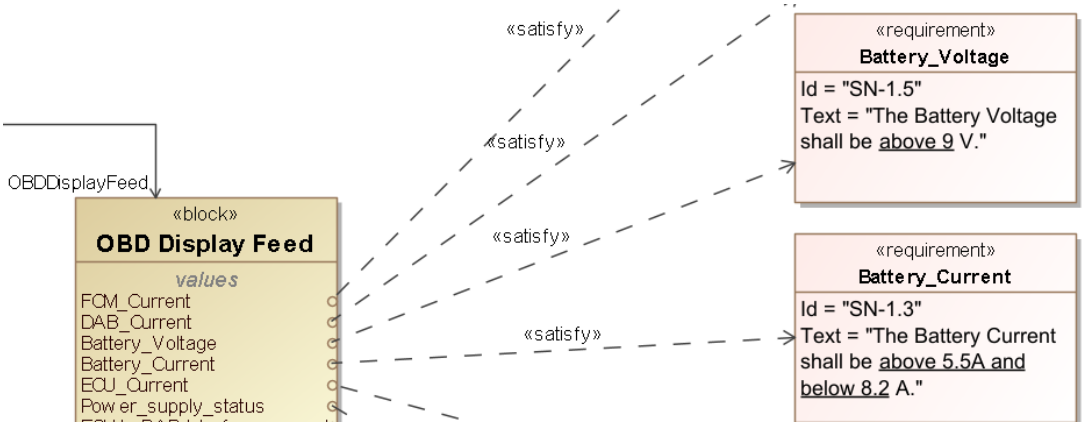

Figure 55: Satisfy relationships between value properties and requirements used for verification**.**

For the sake of simplicity, the activity diagram from Figure 51 is broken down into the flow visualized in Figure 54 that clearly states which steps are conducted in the electrical simulation. Referring to the requirements specification from Figure 48, the system is expected to launch a check after vehicle startup and verify whether the connection between the ECU and the DAB system is functional. As the parameters from the system architecture are connected with the requirements used for verification (see Figure 55), it is possible to conduct an in-the-loop verification while running integrated simulations. Hereby, the numerical results from each simulation are stored in an instance, which serves as the context for the requirements matrix, as seen in Figure 56. This means the tool automatically reviews all the stored values, compares them against the predefined requirements and generates a pass or fail status based on that comparison. It can be seen that the system is able to detect the failure in the connection between ECU and DAB unit and additionally, that the current flow is significantly lower than expected; close to zero, i.e. indicating an open connection, and therefore a disconnected cable.

Verification Status: Pass Fail

#	Name	Text	Bounds	Value
1	SN-1 System startup	System check shall work without failure at vehicle startup		
2	SN-1.1 FCM Current	The FCM Current shall be above 3 A and below 4.4 A.	(3;4.4)	3.6658
3	SN-1.2 ECU Current	The ECU Current shall be above 1.74 A and below 2.6 A.	(1.74;2.6)	1.1013
4	SN-1.3 Battery_Current	The Battery Current shall be above 5.5A and below 8.2 A.	(5.5;8.2)	5.864
5	SN-1.4 DAB_Current	The DAB Current shall be above 0.86A and below 1.3A.	(0.86;1.3)	1.0968
6	SN-1.5 Battery_Voltage	The Battery Voltage shall be above 9 V.	>9	11.1204
7	SN-2 Response to failure	System shall send Diagnostic Trouble Codes (DTC) in case of emulated failure		
8	SN-2.1 ECU to DAB COAX cable connection check	The system shall monitor the connection between the (FCM) and the (ECU) via the COAX cable and send messages in case of a connection loss.		
9	SN-2.1.1 ECU to DAB Interface shorted	The shorted interface failure check for DAB to ECU shall be 0, i.e false (no failure)	=0	0
10	SN-2.1.2 ECU to DAB Interface opened	The opened interface failure check for DAB to ECU shall be 0, i.e false (no failure)	=0	0

Figure 56: Requirements Verification results

3 Conclusion

This application paper clearly demonstrates the key challenges of connecting multiple domains to create multidisciplinary simulation environments. In the example of an on-board-diagnostics system, it was shown that a connected and integrated simulation can quickly demonstrate the developed capabilities and allow introspection of specific failures within the model. However, it should be noted that this represents a simplified view of the actual process. More sophisticated examples are currently under research and will be presented at a later stage.

4 Bibliography

[CAP14] Tangled web of IT applications stunts digital transformation – Crowded application landscape is overwhelming IT departments and eroding competitive edge (2014), Capgemini Application Landscape Report

[DAS24] SIMULIA Process Composer Integration, Dassault Systemes (2024)

https://docs.nomagic.com/display/MSI2024xR2/SIMULIA+Process+Composer+Integration (accessed 18.12.2024)

[FOR24] Bhargava, Rajat. The Hidden Costs Of Unmanaged IT: Best Practices To Eliminate Sprawl, Gaps And Waste (2024), Forbes Technology Council https://www.forbes.com/councils/forbestechcouncil/2024/04/04/the-hidden-costs-of-unmanaged-it-best-practices-to-eliminate-sprawl-gaps-and-waste/ (accessed 17.12.2024)

[HEL22] Helle, P., Richter, S., & Schramm, G. (2022). Implementing and Deploying an Execution Environment for Multidisciplinary-Analyses in a Heterogeneous Tool Landscape. *The Eighth International Conference on Fundamentals and Advances in Software Systems Integration (FASSI 2022).* Lisbon.

[LUC24] Lucarelli, Christian. How the channel helps organizations curb software sprawl by focusing on process (2024) https://www.itpro.com/business/digital-transformation/how-the-channel-helps-organizations-curb-software-sprawl-by-focusing-on-process (accessed 17.12.2024)

[MOR21] Morkevicius, Aurelijus; Aleksandraviciene, Aiste. MagicGrid® Book of Knowledge – A Practical Guide to Systems Modeling using MagicGrid from Dassault Systemes. 2nd edition (2021)

[SYS23] OMG Systems Modeling Language™(SysML®)

https://www.omgsysml.org/ (accessed 17.12.2024)

Lightweight User Interface for Model-Based Systems Engineering of Product Architecture

A Maithripala[1]

[1]Vestas Wind Systems A/S, Hedeager 42, 8200 Arhus

Keywords: *MBSE, SysML, User Interface,*

Abstract: Model Based Systems Engineering (MBSE) is promoted as the promising alternative to document-centric product development in a world of ever-increasing complexity. However, its practical adoption in the industry falls short of expectations [CAM23], [CED23]. In this paper, we discuss one contributor to this slow adoption and propose a light-weight application of MBSE for developing a modular product architecture for wind energy systems.

The technical elements crucial in the adoption and execution of MBSE in an organization are methodology, standard language and tooling. SysML has emerged as the modeling language of choice for MBSE. One of the primary challenges in implementing MBSE stems from the inherent complexity of this general-purpose modeling language.

In this paper we propose a user interface (UI) to mask the complexities of SysML altogether to the average users while allowing advanced users direct access to SysML for extensibility. The user interface is built for a meticulously scoped system of interest (SoI), focusing on capturing the stakeholders' mental models of the core system architecture while ensuring simplicity, consistency, completeness, and elegance. A fundamental principle lies in bounding the system's scope and identifying a minimal set of constructs based on natural language and a structure familiar to the user. These are then mapped to a corresponding minimalist ontology of the general-purpose modeling language of SysML. Challenges are expected to arise in maintaining consistency between the user interface and SysML backend when the system model gets incrementally expanded in the backend and will need further study.

1 Introduction

Modern organizations face rapidly escalating complexity in their products, designs, technologies, processes, and organizational structures. This is compounded by the need for effective collaboration across multidisciplinary teams and the explosion of data and information. Many organizations struggle to develop the capabilities required to address this complexity at a pace that matches its growth. Systems thinking, systems engineering, and Model-Based Systems Engineering (MBSE) have emerged as key approaches for managing these challenges.

The ultimate ambition of MBSE in a product organization is to establish a system model that serves as a **single source of truth**, connecting information across domains and throughout the product lifecycle. However, product development involves dozens of engineering disciplines, each with its own domain-specific "natural languages" and "mental models." These variations often lead to communication gaps, inefficiencies, inconsistencies, and ultimately, quality issues.

To successfully implement MBSE, three critical elements must be addressed: **methodology, standard language, and tools**. Among these, methodology is arguably the most crucial. This paper focuses on the standard language, with SysML selected as the foundation for ensuring a future-proof MBSE implementation.

While SysML v1 has been widely adopted, industry experience highlights challenges, including a steep learning curve, complex constructs, and visually overwhelming system views. SysML v2 offers promising improvements, but even a more refined language cannot fully mitigate issues of accessibility and acceptance. Any standard capable of modeling systems of varying size and complexity inevitably introduces a level of inherent complexity, particularly during adoption. Users must interact with the ontology's depth and learn the syntax, creating additional barriers to implementation.

Our proposed approach seeks to **simplify this complexity** for typical users by leveraging a **custom user interface (UI)**. This UI acts as a real-time dictionary and interpreter, enabling engineers to engage with the MBSE model in their discipline-specific "natural language." SysML's own evolutionary path supports this direction, with SysML v2 introducing domain-specific customizations through implicit specializations of model library types (referencing KerML).

However, SysML's flexibility introduces another challenge: variability in modeling practices. Even users with similar expertise and domain knowledge may model the same system differently due to individual mental models.

We propose addressing these challenges by **limiting the scope of the ontology** through the UI. Success hinges on developing a robust methodology to define this scope, ensuring it meets diverse user needs while reducing complexity. The UI provides essential customization, making system models accessible across disciplines. By controlling the ontology's scope, complexity is minimized, while the UI ensures flexibility and usability.

Ultimately, the success of MBSE adoption will depend less on the tools themselves and more on the processes and methodologies underlying their implementation. Tools must support well-designed processes, enabling desired behaviors and fostering a development culture aligned with organizational goals. Simply deploying IT solutions or off-the-shelf applications is insufficient for driving meaningful change.

In our experience, prototyping and piloting processes and methods are far more effective in modeling and achieving the desired transformation. These approaches allow organizations to refine solutions iteratively, ensuring alignment with unique team structures and workflows. Just as organizations comprise distinct teams and departments, their transformation strategies must be tailored to these unique characteristics.

2 Steps to Build proposed User Interface (UI)

2.1 Define the Scope of the System Model

The system model's scope was determined by reviewing key artifacts from the documentation phase of several development projects:

Context diagrams: Captured external entities and their interactions with the primary system, typically created in Visio.

Functional models: Documented using mindmaps, Visio diagrams, Excel, and Word files, including function lists, flow diagrams, and flow descriptions. External entities acting as sources or sinks for system flows were identified as "terminal" elements.

Function-to-module allocations: Detailed in Excel, including configuration modules, performance variants, and metadata.

Interface diagrams: Documented in Visio and Word, with flow and interface descriptions in Excel and Word files.

These artifacts were managed independently, requiring constant updates to maintain consistency. The chosen scope included a) Functions and their structure, b) Functional flows and interactions (between functions and external terminals), c) Module lists with implementation variants, d) Interface descriptions at module interactions.

At its core, a system is a set of elements and their relationships. Table 1 shows the basic elements chosen to represent the system model. The system model within this scope is represented as a "graph of graphs," where entities are classified into two categories: **elements** and **relationships**. The entities shown in Table 1 are the foundational building blocks to explicitly model the system and forms the basis for the UI design.

Elements	Function	Terminal	Module	Configuration module	Variant (of module)	Item
Relationship	Membership	Flow	Allocation	Interface		

Table 1: Foundational constructs of the system model

2.2 Create Reusable Model Patterns

To simplify and standardize system modeling, the most general classification type, "element," is specialized into types such as "function," "terminal," "item," "module," and "variant." Instances inherit attributes from their types, with inheritance rules detailed in Table-2 for the specialized element type: “function”.

Relationships between elements are similarly generalized and then specialized into types like "flow," "membership," "interface," and "allocation,". These patterns form the building blocks for constructing the full system model.

Attributes in Natural Language	Description / Meaning	Mandatory field?	inherited from definition?	Inherited data mutable in the usage?
Classification type	Classification type of 'Function' as defined in 0056-8747.	Yes	Yes	No
ID#	An immutable unique identification number (typically assigned by the associated tooling)	Yes	No	No
Name	Fully descriptive name of the function.	Yes	Yes	Yes
Short name	Immutable identifier of the function.	Yes	No	

Description	Textual description that fully explains, defines or specifies the function.	Yes	Yes	Yes
Accountable organization	The organizational entity accountable for the design and implementation of the function.	No	Yes	Yes
Attribute #1, #2, ...etc	Attribute name. Full textual description of the attribute explains what the attribute is.	Yes/No	Yes/No	Yes/No

Table-2: Pattern for 'function' type of element

2.3 Develop a Taxonomy of Constructs

The identified elements and relationships are organized into a taxonomy based on SysML v2, itself grounded in the KerML standard. This taxonomy defines:

Inheritance rules: Attributes of abstract definitions are inherited by instances, with limited mutability for certain attributes.

Membership structures: Separate hierarchies for "elements" (nodes) and "relationships" (edges), visualized in Figure-1.

This taxonomy establishes reusable constructs for consistent and efficient modeling.

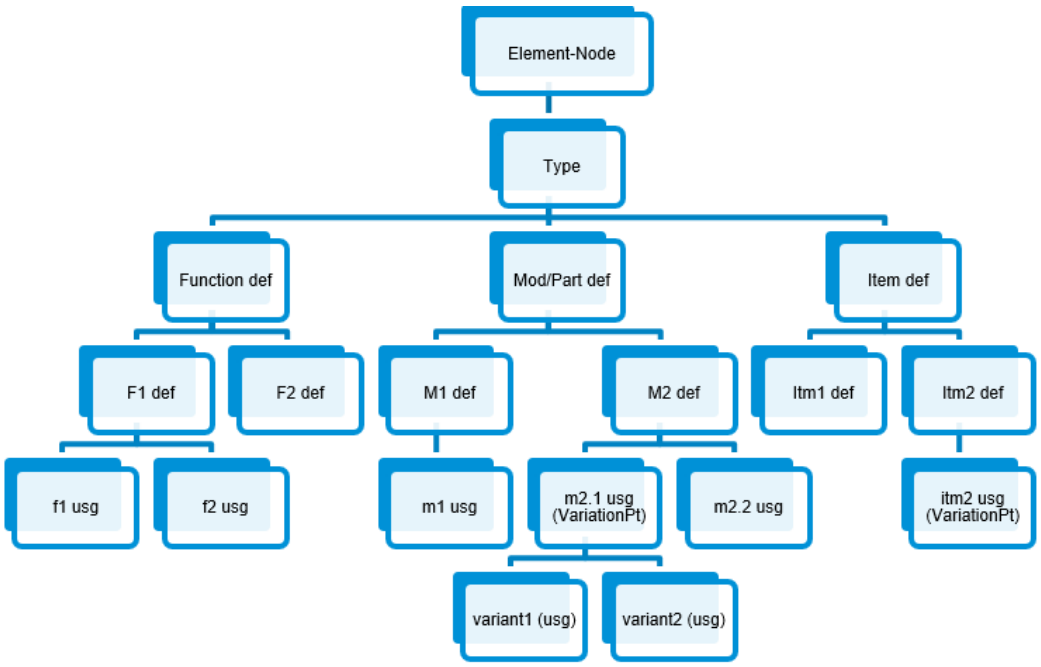

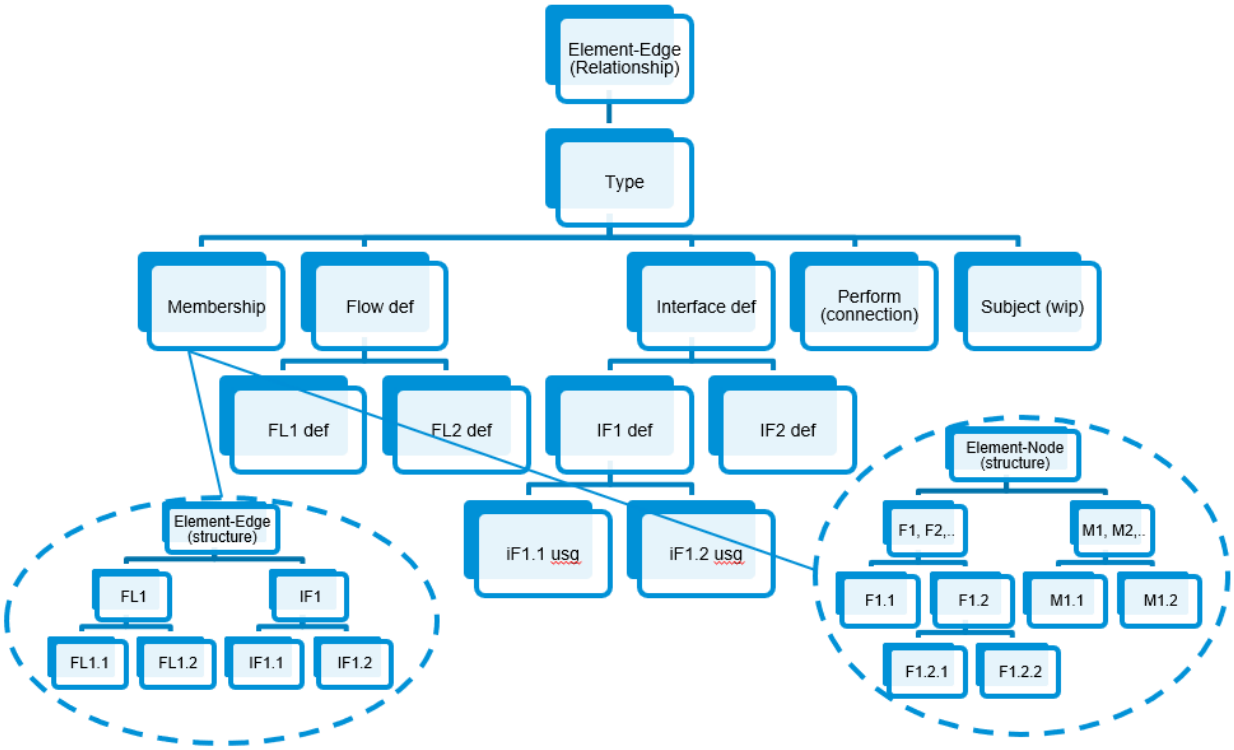

Figure 57: Taxonomy

2.4 Encode Taxonomy and Constraints in the UI

The taxonomy and associated inheritance rules, shown as an example for “function” element type in Table 2, are implemented in the UI, restricting users to predefined patterns and ensuring consistency with Vestas' internal standards. The UI stores system model data in relational tables for elements and relationships. These tables enforce taxonomy rules, inheritance, and constraints, simplifying the complexity of SysML v2 while supporting customization through the patterns.

2.5 Map Natural Language (NL) Constructs to SysML v2

The NL constructs defined earlier are mapped to SysML v2 syntax (see Table-4 for the "function" example). This mapping serves as a dictionary, enabling seamless translation of model data from NL to SysML. Customizing constructs for different design groups, illustrated by two sets of user groups interacting with the system model through two sets of UIs on the left hand side of Figure-2, ensures alignment with their terminology and mental models.

Natural Language	Description / Meaning	SysML v2 syntax
Classification type: Function	Classification type of 'Function' as defined in 0056-8747.	Action
ID#	An immutable unique identification number	Element ID

Name	Fully descriptive name with *unrestricted name standard*	'Name'
Short name	Immutable identifier of the element.	<short name==ID#>
Description	Textual description of the element that fully explains, defines or specifies the element.	Doc /* text */
Accountable organization	The organizational entity accountable for the design and implementation of the element.	Attribute with metadata annotation, and with enums
Attribute #1, #2, ...etc	Attribute name. Full textual description of the attribute explains what the attribute is.	Attribute with metadata annotation

Table-4: NL to SysML map for “function” example

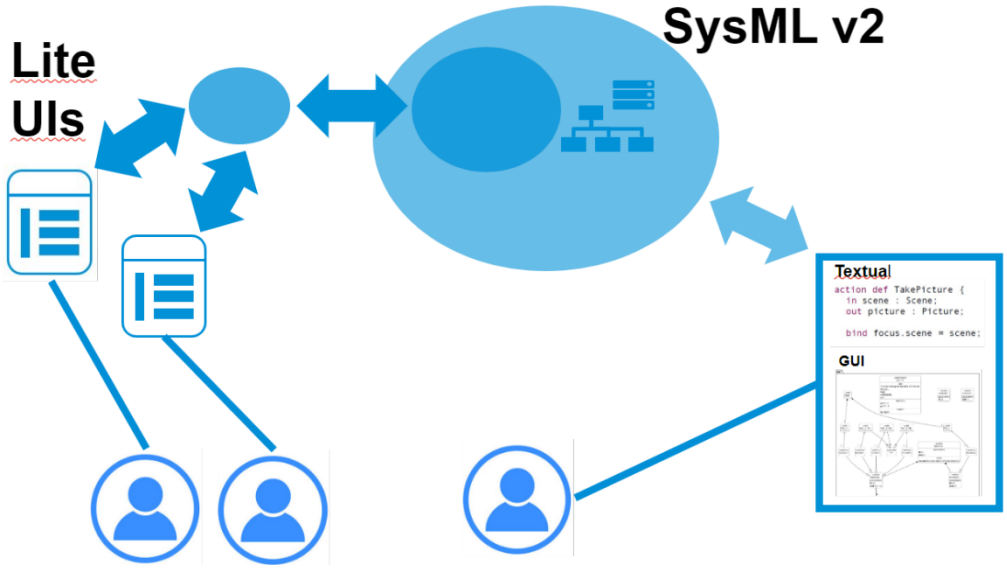

Figure 2: UI to interact with SysML model

3 Access and Views of the data

The UI provides intuitive, table-based views of model data. For instance, filtering allows users to see all "function" records as rows with attributes in columns. Custom views tailored to stakeholder needs enhance comprehension and decision-making.

Effective interaction with the model is prioritized. It is by interacting with the methods and models that the users can better comprehend the information and use it for effective and speedy decision making.

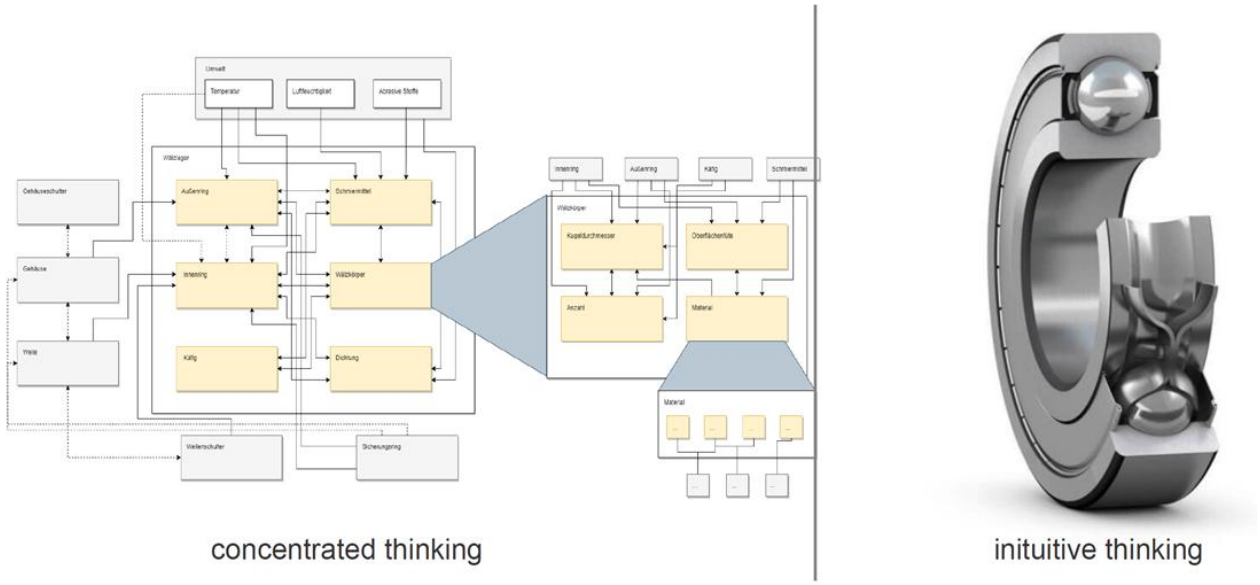

Figure 3: Trumpf example [MUS23] of a model's visual complexity

The above Figure-3 illustrates the SysML representation of a simple ball bearing written in SysML. One user may find the full SysML model to the left easy to comprehend and useful, while another may comprehend the 'real' model to the right better. Another user, for example the engineer modeling 'noise' of the bearing, may want to see its stiffness matrix! What model representation resonates with whom depends on the 'mental model' of the interacting user and can be very different in its representation. This is the power and value of custom user views of the system model for different stakeholders, and we plan to expand the UI capability to include custom views of the system model data.

4 Example application

The UI was applied to a Vestas system model developed by three design teams, coordinated by a systems engineer. Digitizing disparate artifacts using the UI revealed inconsistencies: redundant terminal and function names, as well as over two dozen flow discrepancies. The inconsistencies were resolved by integrating all data into the UI. For instance, a terminal identified differently across teams was unified under a single name. Figure-4 demonstrates the resulting functional flow view, progressing from a collapsed node to an expanded view of sub-functions. This approach ensured alignment and consistency across design teams.

5 Conclusion

This paper demonstrated the development of a custom UI for MBSE, which simplifies interactions with SysML models by tailoring them to users' natural languages and mental models. We applied the UI to existing system functional models, digitizing and unifying disparate artifacts, resolving inconsistencies, and enhancing team collaboration. The prototype revealed the importance of scoping the ontology and constraining complexity to improve accessibility and adoption.
Future work will extend the UI's application to ongoing design projects, validating its effectiveness Bin real-time system modeling and extend to the other model constructs. Additionally, we aim to

integrate SysML v2 tooling to generate graphical and textual views, further enriching the user experience while ensuring alignment with industry standards. This iterative approach prioritizes process-driven adoption, tailoring tools to organizational needs to drive successful MBSE transformations.

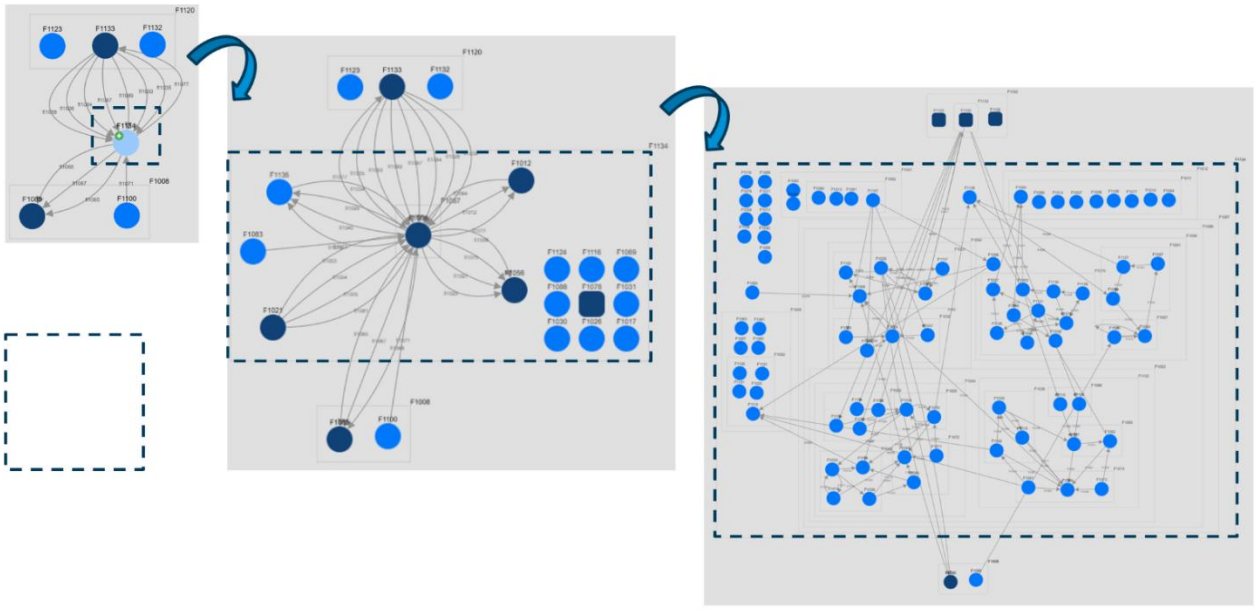

Figure 4: Functional model view

6 Bibliography

[CAM23] Piece, Michael, Cameron, Bruce: A Sheep in Wolfe's Clothing: SysML is not living up to the hype of revolutionizing product development

Technical Strategy Partners (TSP), 2023

[CED23] Cederbladh, Johan, Suryadevara, Jagadish: Light-Weight MBSE Approach for Construction Equipment Domain – An Experience Report

APSEC30 conference, 2023

[MBS25] MBSE Methodology Summary: Pattern-Based Systems Engineering (PBSE), Based On S*MBSE Models.
http://www.omgwiki.org/MBSE/doku.php?id=mbse:methodology#mbse_benchmarking_survey (14/01/2025)

[MUS23] Muschik, Sabine: An Utopia of Human-centric Systems Engineering

DSEC conference, 2023

Fluidon Cube - A SaaS development environment for technical systems

H. Baum[1]

[1]FLUIDON GmbH, Jülicher Straße 338a, 52070 Aachen

Keywords: *SaaS, scalable collaboration platform, digital twin, FMU, engineering development workflow*

Abstract: Cube is a SaaS collaboration platform that offers medium-sized companies easy access to modern CAE tools. Based on open-source toolkits, Cube provides an intuitive introduction to the simulation of complex technical systems, even for users with little experience in this field. The platform offers parameterizable workflows that automatically test system properties, allowing users to focus on interpreting the results.

In addition to technical tasks, Cube supports the integration of digital twins from different simulation tools through an FMU plug-in. Thanks to flexible combinations of the FMU plug-in and user-defined Python scripts, the platform is versatile and promotes collaborative development. Teams can collaborate internally and externally, while specialists can provide their solutions as services in the form of Cube plug-ins.

As a SaaS solution, Cube offers economic advantages such as low entry costs, scalability, intuitive user interfaces and high availability. The data is stored exclusively in European data centers, ensuring security and data protection. In addition, Cube supports common interfaces for communicating with external devices or data sources.

With these features, Cube offers medium-sized companies an efficient way to simulate the dynamic interactions of technical systems and drive innovative product development.

1 Introduction

When developing complex technical systems, the use of CAE tools [WIK25a] is already state of the art for larger companies. Only through numerical simulation, for example, can the dynamic interaction of all installed components be effectively tested and evaluated as an overall system. Buzzwords such as "model-based systems engineering" [WIK25b] , the "digital twin" [WIK25c] and "virtual commissioning" [WIK25d] are not on everyone's lips for nothing.

The situation is different with supposed standard systems, which are often produced in small batches by medium-sized companies specializing in this field. If a standard system is modified according to customer requirements or a new product generation is to be developed, simulative testing of the changes is unfortunately still too often dispensed with. This is justified by the fact that only minor modifications or scaling of existing assemblies are involved, which have already been successfully tested in practice. When designing, planners often rely exclusively on static calculations, which means that the dynamic interactions between the components or assemblies are ignored.

Experience shows that this can be risky. Even minor changes or scaling can significantly influence the dynamic behavior of the overall system. For example, changes in the size of components can shift their operating points, which can lead to non-linear changes in the behavior of the system dynamics of an assembly. Even if the same components are only spatially arranged differently in fluid power drives, other dynamic interactions already arise.

Design errors that are only now recognized in practical use sometimes have serious consequences that can lead to production downtimes and costly rework. Often, the only solution is a quickly commissioned and therefore expensive simulation by a service provider.

Many design errors could be avoided if simulation-based methods were also increasingly used in the design of supposedly “standard systems”. To achieve this goal, however, the required CAE tools must be more easily accessible and easier to use, even for users who have little experience with simulations. This can be achieved, for example, through a special development platform made for this application scenario.

2 Fluidon Cube - A flexibly scalable SaaS development platform

Fluidon Cube is a SaaS development platform specifically designed to enable experienced users to prepare pre-configured projects for the development, testing and commercialization of systems and services. Projects that focus on technical systems typically involve a workflow that either influences the properties or behavior of the technical system or provides corresponding services via it. The technical system itself is made up of various objects that represent the individual components of the system. In addition to simulation models, these objects can also include algorithms or databases. Less experienced users can use these preconfigured projects by giving them access to the cube

Users with limited simulation experience can therefore concentrate fully on the correct input and control of workflows, for example, as they are relieved of routine, simulation-related tasks. This allows them to focus entirely on their main task - interpreting the results.

The following section presents the basic structure of the Fluidon Cube SaaS development platform and outlines how to work with Cube projects. Each Cube account has a workspace in which users create their projects (**Figure 58**). These can either be new projects or templates created by the users themselves, FLUIDON or other Cube users.

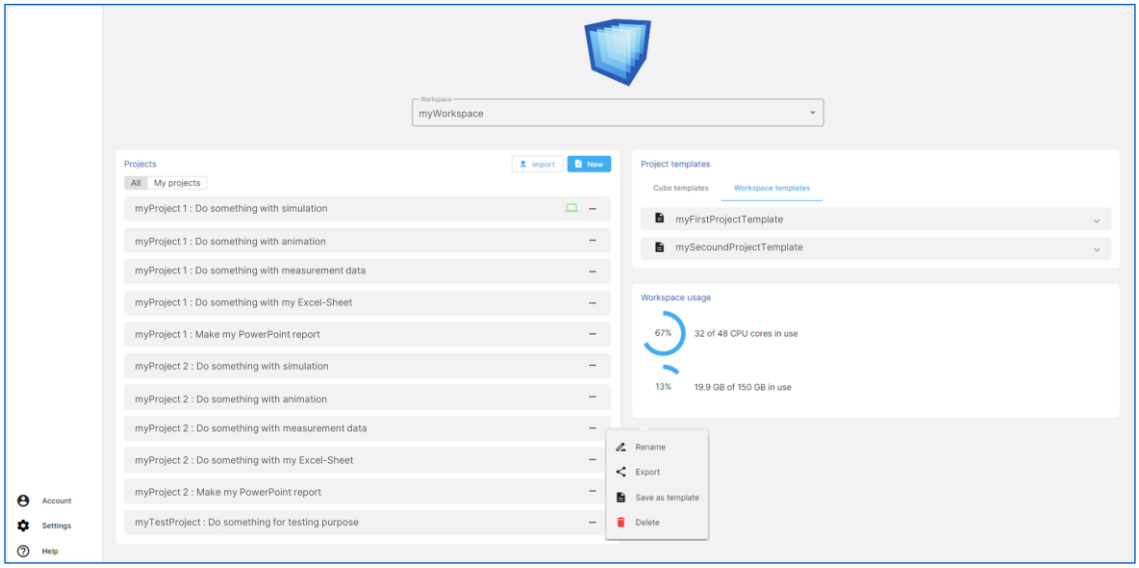

Figure 58: Fluidon Cube - Workspace view

Templates can be created directly from the Cube projects in the workspace and are then available to all members of the workspace. The templates contain all scripts, simulation models, raw and result data as well as the current configuration of the Cube project. To transfer a Cube project to another workspace, a prior export is required for data protection reasons, followed by an import into

the new workspace. All project data and the project configurations are saved in a ZIP archive, which can also be used as a backup or for archiving the Cube project.

Figure 59 presents the most important features of the Fluidon Cube workspace.

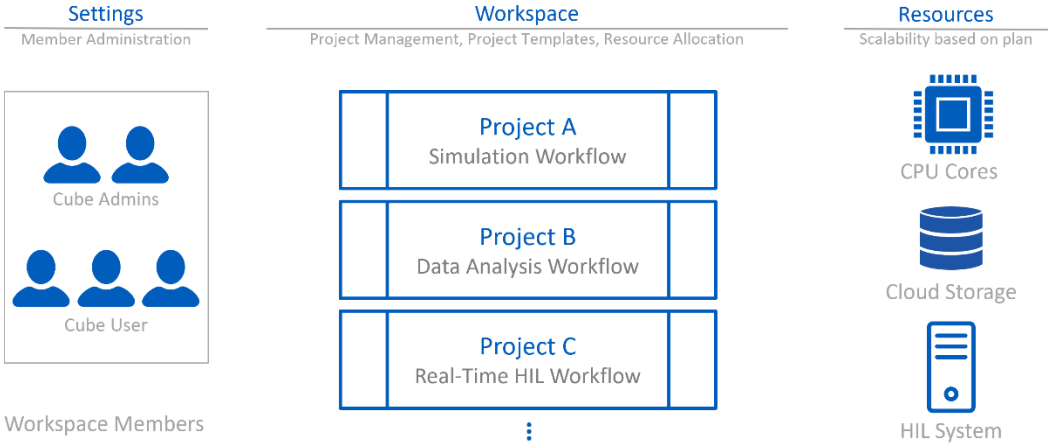

Figure 59: Fluidon Cube - Collaboration

As already mentioned in the introduction, a wide range of tasks are implemented in Cube projects. The example shown in Figure 59 focuses specifically on the presentation of workflows for the repeated execution of tasks in the area of the simulative design of drive systems. Against this background, project A could, for example, contain a workflow for simulating fluid or electric drives, project B could be a workflow for processing simulation results or measurement data from the test field and project C could be used to configure a Cube RT system needed for control system development or virtual commissioning, running a real-time digital twin.

Every Cube user who has been invited to a workspace by an administrator is a member of the workspace. Members can work on their own projects or on a joint project. The workspace area gives members an overview of the distribution of available resources. Resources are CPU cores, storage space on the cloud platform or Cube RT systems. The resources are generally located in a shared pool and can be assigned to individual projects as required.

As is usual with modern SaaS applications, a Cube account is always linked to a "plan". The plan describes the different tariffs or subscription models available to users, what additional resources or additional services cost and what other services or support options are included. The basic "Cube Free" plan, in which a workspace can be created, is free of charge.

Figure 60 summarizes the main advantages for the user of the Fluidon Cube as a SaaS application. A SaaS application is available immediately after the initial registration, which enables companies to introduce the new solution quickly. This is also supported by a lower initial investment compared to traditional software development and deployment, as companies do not need to purchase expensive computer hardware or software licenses. Instead, they pay monthly or annual subscription fees.

Thanks to the intuitive user interface typical of browser applications, users can also quickly find their way around the SaaS application without the need for extensive training.

SaaS applications are accessible via the Internet, which means that users can access their account at any time, from different locations and with different end devices.

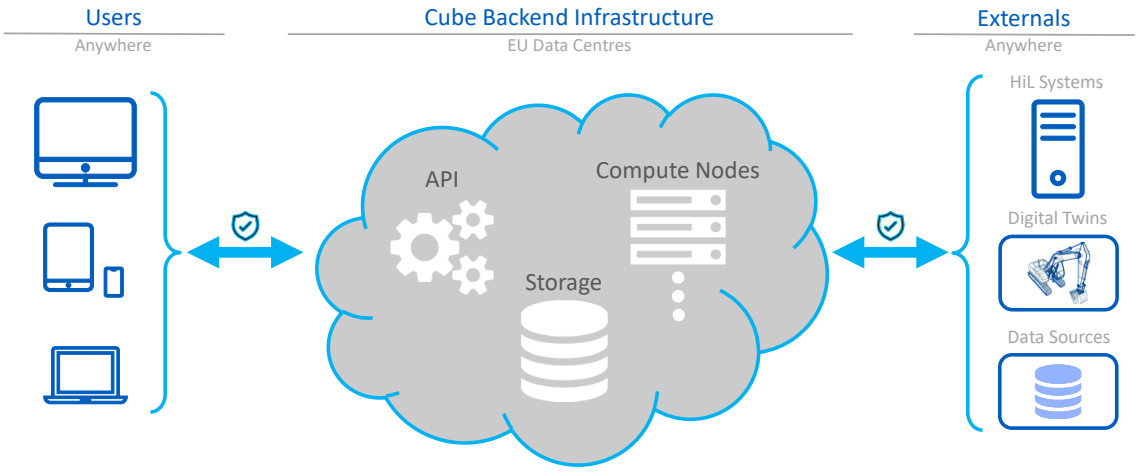

Figure 60: Fluidon Cube - Flexibility, Scalability, and Security

Scalability and high availability (middle section of Figure 60) are further advantages of SaaS applications. Storage space or computing power can be added at short notice by changing the plan and enable the user to react flexibly to increased requirements without having to carry out expensive hardware upgrades.

In addition, SaaS applications guarantee high availability, as data center operators invest in redundancy and high-availability solutions. SaaS applications are also updated automatically, which relieves users of the need to take care of maintenance and updates themselves and ensures that they always have access to the latest functions and security patches.

Another important point in favor of SaaS applications is data security. In the case of Fluidon Cube, the data is stored exclusively in European data centers. In addition to the security measures of the data centers, all areas of Fluidon Cube that can be accessed via the Internet connection are secured separately in accordance with the state of the art. This measure provides the user with a level of security that generally goes beyond what would be practical for smaller companies or organizations to implement if they had to provide it themselves.

An interesting feature of the Fluidon Cube development platform is shown on the right-hand side of Figure 60. Fluidon Cube has interfaces for accessing external devices or data sources from SaaS applications. This is used, for example, to communicate with Fluidon Cube's own RT system, access measurement data or exchange live data with other cloud applications.

Figure 61 describes the steps required to execute a workflow on Fluidon Cube. In preparation, the user has created a cube project in the workspace, set up a workflow in it, loaded any required data or simulation models and specified the CPU cores required for execution. The prepared project does not yet block any of the available computing resources. Only scripts, simulation models and data occupy cloud storage space. Only when the user creates a compute node on which the workflow is to be executed (Figure 61, top left) is the specified number of CPU cores allocated. Once the compute node is ready for use, the execution of the project or workflow is started.

Both the start of the workflow and the interaction with the ongoing workflow can be carried out using any end device, as illustrated once again in the right-hand section of Figure 61. For example, the tablet or mobile phone is used to check whether the execution has been completed. If necessary, the configuration of the workflow is updated, new data is loaded into the workflow and a new execution is started.

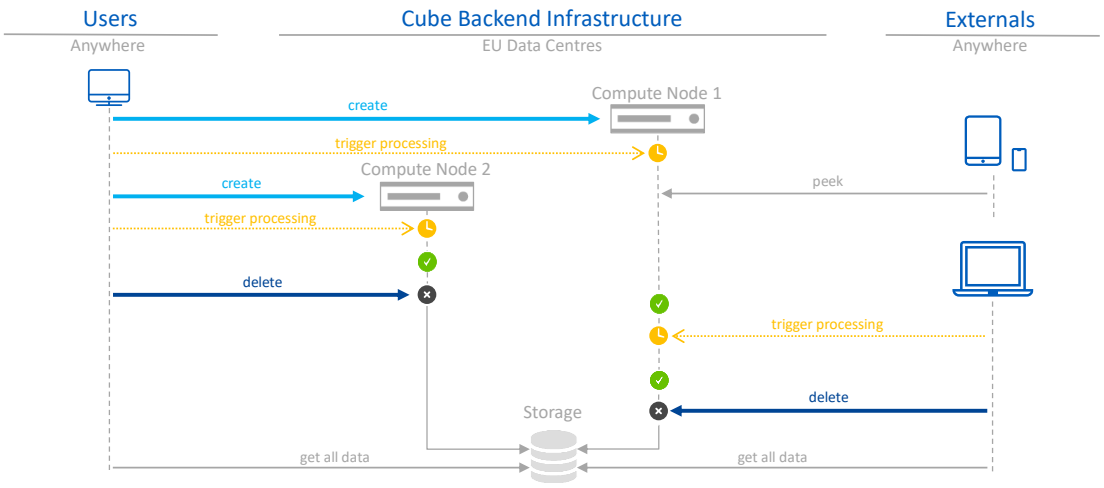

Figure 61: Fluidon Cube - Computing Power on Demand

If the results meet the requirements, the occupied computing resources are released. To do this, the user deletes the compute node and the CPU cores are available to all users again. The data generated during execution is automatically moved from the compute node to the cloud storage, where the user can continue to access it at any time.

If free computing resources are still available in the account during the execution of compute node 1, further projects can be executed simultaneously, as shown in Figure 61 using the example of compute node 2.

3 Fluidon Cube - Development as a team effort

The possibility for several users to work together on projects in the cube workspace opens up the opportunity for companies to make effective use of modern forms of collaborative development. One of these concepts, "development as a team effort" (**Figure 62**), and the resulting opportunities for companies in product development are presented in the following paragraph.

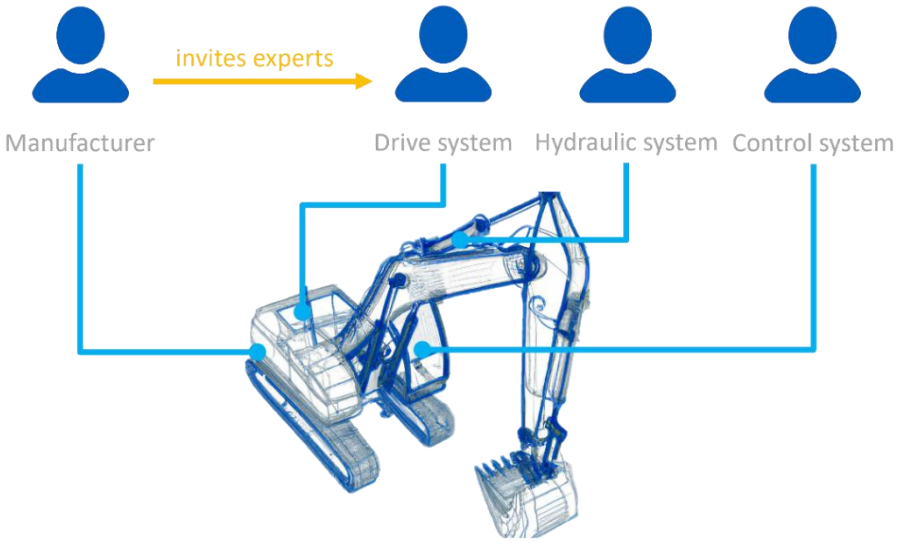

Figure 62: Fluidon Cube - Engineering as a Team Achievement

The concept of "development as a team effort" emphasizes the idea that the development of products, services or projects is most effective through the collaboration and coordinated work of a team,

rather than through individual efforts. The concept thus reflects the reality of many engineering projects and the importance of teamwork in engineering. After all, engineering projects often require experts from different disciplines to work together to solve complex problems and drive technical innovation.

The Fluidon Cube development platform promotes this approach by automatically making the company's internal experts, as members of the workspace, members of the team. If necessary, the company can also integrate external specialists into the team by inviting them to the Cube workspace.

The Fluidon Cube development platform also provides external specialists with a business model in which they can offer their solutions to several companies as service providers (**Figure 63**). For example, service providers have the opportunity to develop specific Python modules, prepare complex workflows, prepare data and make it available to the Cube platform or create Unity models for 3D visualization in Fluidon Cube.

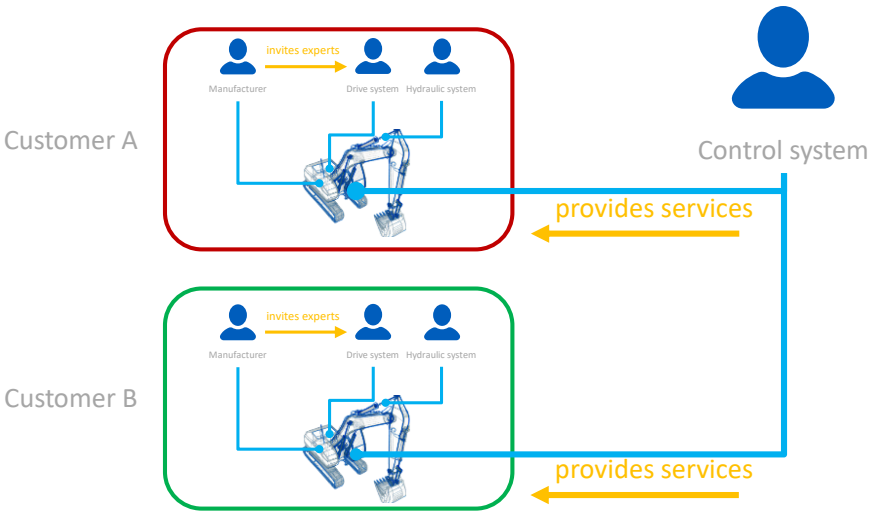

Figure 63: Fluidon Cube - Engineering as a Service

This can be done on behalf of the customer directly within an existing project or as a well-documented project template for the Cube platform. In cooperation with FLUIDON, a solution can also be designed as a Cube plug-in, which is then available to all Cube users, subject to appropriate licensing. Fluidon Cube has interfaces and methods to protect the specific know-how of the solution provider. Figure 63 illustrates the business model of providing external solutions, using the example of a service provider for control systems that offers its algorithms or simulation models to various companies.

4 Summary

The essential elements of the Fluidon Cube SaaS development platform were presented using the example of a technical task and it was described how an easy-to-use yet powerful simulation-supported workflow can be set up. However, Fluidon Cube is not limited to technical tasks, but was designed as a general development platform for solving simulation or design issues. With the FMU plugin [FMI], the digital twins required for this from various simulation tools can be integrated into the platform. Thanks to the flexible combination of workflows from predefined plug-ins and Python scripts, Fluidon Cube can be used very flexibly to solve a wide range of problems.

5 References

[FMI25] Page „fmi - Functional Mock-up Interface“.
URL: Functional Mock-up Interface
Accessed on 15. January 2025, 08:20 (UTC)

[WIK25a] Page „Computer-aided engineering (CAE)“.
In: Wikipedia – The Free Encyclopedia.
Last edited on 13 January 2025, at 05:02 (UTC).
URL: Computer-aided engineering - Wikipedia
Accessed on 15. January 2025, 07:45 (UTC)

[WIK25b] Page „Model-based systems engineering“.
In: Wikipedia – The Free Encyclopedia.
Last edited on 17 October 2024, at 09:11 (UTC).
URL: Model-based systems engineering - Wikipedia
Accessed on 15. January 2025, 07:40 (UTC)

[WIK25c] Page „Digital twin“.
In: Wikipedia – The Free Encyclopedia.
Last edited on 1 January 2025, at 18:37 (UTC).
URL: Digital twin - Wikipedia
Accessed on 15. January 2025, 07:55 (UTC)

[WIK25d] Page „Virtuelle Inbetriebnahme“.
In: Wikipedia – The Free Encyclopedia.
Last edited on 23 October 2022, at 18:39 (UTC).
URL: Virtuelle Inbetriebnahme – Wikipedia
Accessed on 15. January 2025, 07:50 (UTC)

Systems Engineering:

System Models and Model Libraries

Practical approach of system engineering to meet the challenges of agricultural machinery

Marco Ramm, Simon Drüke

CLAAS Traktor SAS, Halberstädter Str. 15-19, 33106 Paderborn

Keywords: *agricultural challenges, system engineering, multi-physical system simulation, tractor development*

Abstract: The agricultural machinery is facing huge challenges: How to maintain or even increase the productivity to feed the growing world population while implementing sustainable farming at the same time? The upcoming development steps become more difficult because it is not any more sufficient to enlarge the machines – it is now necessary to implement alternative drives and to simplify the usage of the complex machines.

Those challenges require an efficient engineering procedure specialized for the ag. machinery to avoid iterations and to ensure short time to market. Especially in the field of tractor development a specific engineering procedure is necessary that takes all relevant operations conditions, different kind of operators and all relevant implements into account. Furthermore, it is necessary to respect within the agricultural SE the relevant engineering disciplines like drivetrain, hydraulic, electronics & control and thermal management. Therefore, we have derived a procedure with different abstraction levels of system engineering (SE) to ensure a robust development of our machines.

The first level of SE is needed for a high-level concept evaluation. Here it is essential to derive performance data (e.g. efficiency, weight, cost) for the concept decision incl. the choice of the decisive modules (e.g. transmission). To do so a system model with high scope and low fidelity is utilized which enables a quick and efficient evaluations.

After choosing the main machine concept the right design criteria and targets of the modules must be defined with help of a high-scope & mid-fidelity SE model. This model is furthermore used for a product risk analysis which identify the most critical operation conditions to guide the development focus in the right direction.

With those results it is now possible to define target-oriented investigations with a high fidelity but with a low scope (e.g. NVH-sim. in drivetrains, CFD-sim. of transaxle hydraulics).

1 Introduction

The field of agricultural technology is at a pivotal crossroads, facing a myriad of formidable challenges that demand innovative solutions and strategic adaptations. As we venture further into the 21st century, extreme weather conditions, driven by climate change, have increasingly disrupted traditional farming practices, threatening crop yields and food security worldwide [RAZ24]. Concurrently, the global population continues to rise [UNA19], intensifying the pressure on agricultural systems to produce sufficient food sustainably. Compounding these issues are volatile grain prices, which reflect broader economic uncertainties and can destabilize food markets, affecting both producers and consumers [AMI24]. This confluence of challenges necessitates a reevaluation of current agricultural technologies and practices, urging the development of resilient, efficient, and sustainable solutions to ensure food security for future generations.

Beside those external influences, there is a trend of increasing farm sizes [HBS19]. This is caused by technological advancements, economies of scale, and market pressures are prompting farmers to consolidate operations. Larger farms are perceived as more capable of adopting advanced technologies and practices that enhance productivity. However, this scale of operation requires machinery that can efficiently manage larger land areas without compromising ecological integrity. As farm sizes grow, there is a pressing need for machinery that operates efficiently to minimize both environmental impact and operational costs.

From an ecological perspective, machinery must reduce emissions, and maintain soil health. Economically, the total cost of ownership (TCO) – which includes initial purchase price, maintenance, operational expenses, and depreciation – must be optimized to ensure profitability for farmers. By focusing on ecological sustainability and economic efficiency, manufacturers can provide solutions that not only meet the immediate needs of large-scale farming operations but also contribute to long-term agricultural sustainability.

Figure 64: Challenges of agriculture industry

As we have seen, the technological transformation of agricultural machinery must be comprehensive and forward-thinking, integrating cutting-edge advancements to deliver solutions that are both sustainable and highly productive. The development of eco-friendly machinery that incorporates renewable energy sources and reduces emissions is essential for minimizing agriculture's carbon footprint. The challenge lies in ensuring that these technological innovations are accessible and economically viable for farmers of all scales.

CLAAS is an agricultural machinery manufacturer which has been founded in 1913 in Harsewinkel, Germany. It is renowned for its innovative and high-quality farming equipment, including combine harvesters, tractors, forage harvesters, balers, and green harvest machinery [CLA25]. CLAAS has established itself as a leader in agricultural technology, focusing on efficiency and sustainability to meet the evolving needs of modern agriculture. With a strong global presence, the company continues to expand its product offerings and technological advancements, supporting farmers worldwide in optimizing their productivity and crop yield.

The versatility of CLAAS's offerings is evident in their lineup of machines. Each of these machines is engineered to deliver optimal performance, whether for intensive, large-scale operations or

smaller, specialized farms. For instance, CLAAS tractors come in various power ratings, from compact models (<150 hp) ideal for smaller farms to high-horsepower machines (>600 hp) designed for extensive fieldwork in large agricultural enterprises. Some equipment, like tractors and loaders, may be used year-round for a variety of tasks, while others, such as combines and forage harvesters, have more seasonal applications focused on planting and harvest times.

That is also the reason that requested change in powertrain technology looks different for a small tractor (e.g. ARION 400) which works a few hours the day in the low- to mid-power range in comparison to a big tractor (e.g. XERION) which works the whole day in full load conditions. Furthermore, the small tractors and loaders are often used on the farm and close to energy sources. The combines and big tractors are working on huge fields with often a wide distance to the next energy source. All these effects lead to the current expectation that there is a need to keep the combustion engine in place for big machines but enable the usage of alternative fuels and optimize the full powertrain. On the other hand, we have the opportunity to electrify our small power product portfolio.

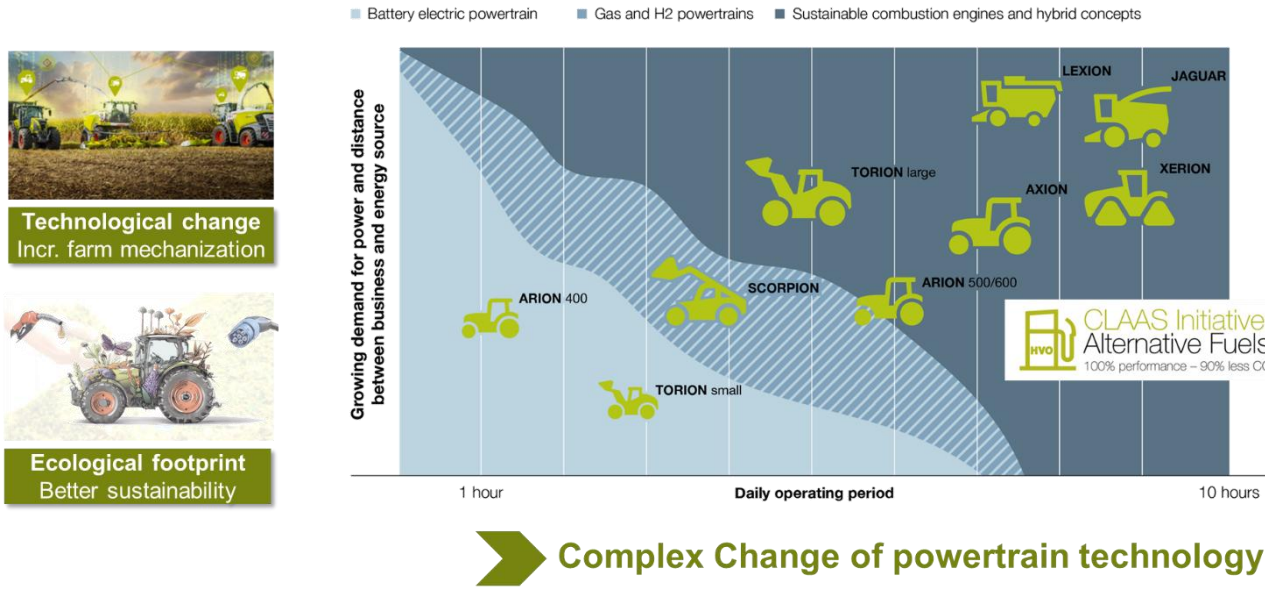

Figure 65: Different range of agricultural machines in power, daily operating period and potential distance between business and energy source

The holistic improvement of the powertrains is challenging especially in combination with the growing expectations from customers in the premium segment, as they demand advanced technologies to meet environmental standards, and to cater to a wide range of operational needs. Coordinating the diverse areas of expertise, overseen by the vehicle system engineer, presents a challenge for this kind of complex modification. Up to now, every single field of expertise has its own engineering-tool landscape and its specific mission profiles to enable the requested modifications.

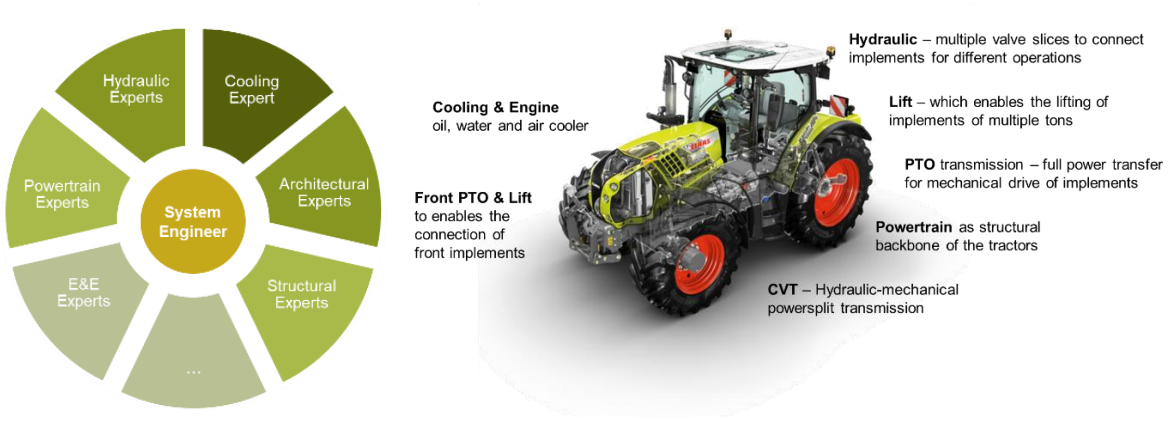

Figure 66: Different expertise which are needed to create an agricultural machine

A change of the engineering mind set towards a system engineering approach which would potentially enable the requested improvement of agricultural machines. Within this paper a practical approach of system engineering is demonstrated which enables the development of an agricultural machine like a tractor.

2 System Engineering

The development of a modern tractor is a highly intricate endeavor, characterized by complexities that surpass those found in the automotive sector. This complexity arises from the unique demands and multifaceted functionalities that tractors must fulfill, requiring advanced integration across various systems such as hydraulics, the powertrain, the onboard electronic and the structural stability in offroad conditions.

One of the primary areas where this complexity is evident is in the hydraulic system of a tractor. Unlike typical automotive hydraulic systems, which may primarily focus on braking or power steering, a tractor's hydraulics are central to its operational capabilities. They must efficiently manage multiple, simultaneous tasks such as lifting heavy implements, controlling sophisticated attachments, and providing precise motion control. This requires a robust system capable of delivering high power output while maintaining flexibility and reliability under diverse agricultural conditions.

Similarly, the powertrain of a tractor is significantly complex. Tractors need to deliver high torque at low speeds, often under varying load conditions, which necessitates a powertrain system that is both powerful and adaptable. This is compounded by the need for durability and efficiency across a wide range of terrains and tasks, from plowing fields to hauling loads. The integration of advanced transmission systems, including continuously variable transmissions (CVTs), is crucial to achieving the necessary performance and fuel efficiency.

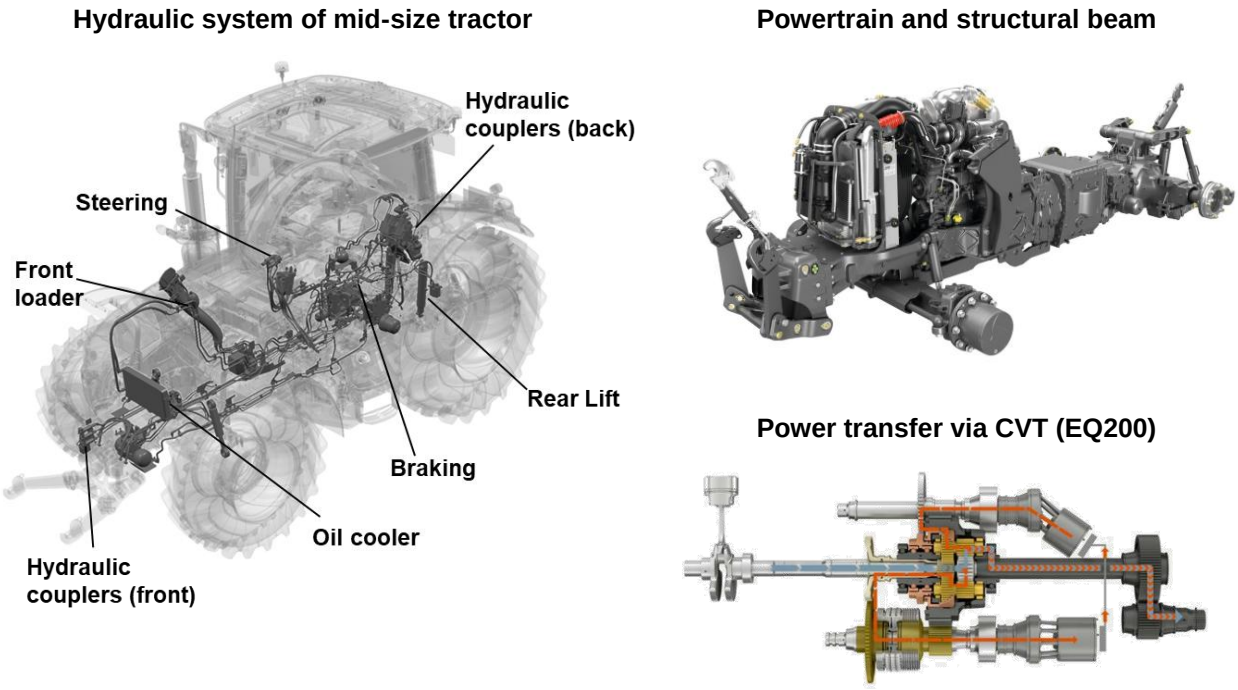

Figure 67: Hydraulic system and powertrain of a mid-size tractor

The structural design of a tractor also presents unique challenges. Unlike automobiles, tractors must endure high stress and strain due to uneven terrain and heavy loads. This requires a robust and resilient structural framework that can withstand these demands while ensuring operator safety and comfort. The structural components must be carefully engineered to balance strength and weight, optimizing the tractor's overall performance and fuel efficiency.

Given these complexities, the interdependencies between these systems cannot be overstated. Each system must be precisely coordinated with the others to ensure seamless operation and maximum efficiency. This is where the application of a comprehensive system model becomes indispensable. A system model allows engineers to simulate and analyze the interactions between different components, predict potential issues, and optimize the design before physical prototypes are built. This holistic approach is crucial for addressing the intricate dependencies and achieving a harmonious integration of all systems within the tractor.

Figure 68: System Model to develop complex tractor-implement systems (e.g. XERION with air seeder)

2.1 Concept Evaluation in Multiphysics systems

In the early stages of a development process, a system model plays a crucial role in guiding conceptual decisions. At this point, only rough information is available, making detailed modeling both impractical and time-consuming. Despite these limitations, the system model can be invaluable in concept analysis, as it allows for the consideration of key aspects such as efficiency and performance within the context of the field collective. By leveraging this initial framework, developers can make informed decisions that set the stage for more detailed work as the project progresses.

2.1.1 System Model

The system model should respect the crucial conceptual information of the powertrain, the hydraulics and other relevant fields like electronics and cooling. It should also highlight the interactions between those fields. Furthermore, the authoritative elements of each field (e.g. main hydraulic pumps, main gear stages) should be recognized in the system model. To accommodate the various physical disciplines, we have decided to use a 1D Multiphysics model, utilizing software like OpenModelica or AMESim.

In **Figure 69** you can see a system model of a battery electric powertrain concept. It respects the crucial information of the concept which are typically presented by the experts via stick-diagram, hydraulic and electronic schemes.

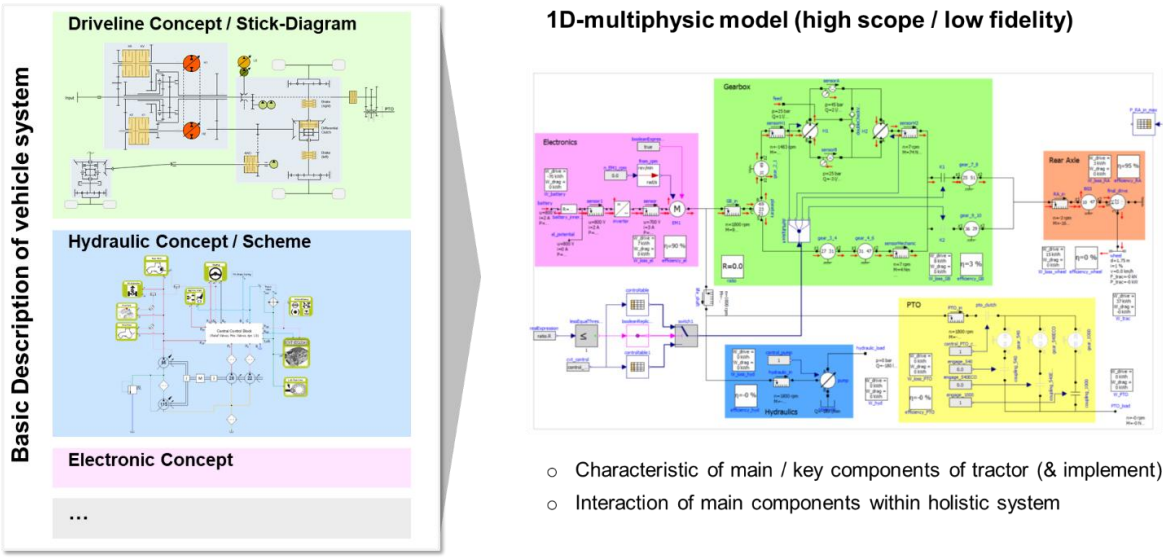

Figure 69: System Model of a battery electric tractor concept

2.1.2 Requirements & Specifications

Within the system model the main specifications of the authoritative elements are already integrated. An exchange of those (element) specifications into a separate overview allows the quick review of the main specifications (e.g. pump size, gear ratios). Additionally, it allows the transfer of the elementary information in more generic information of the tractor specification (e.g. tyre size, pulling force, gross vehicle weight) which is helpful to derive the right concept conclusions.

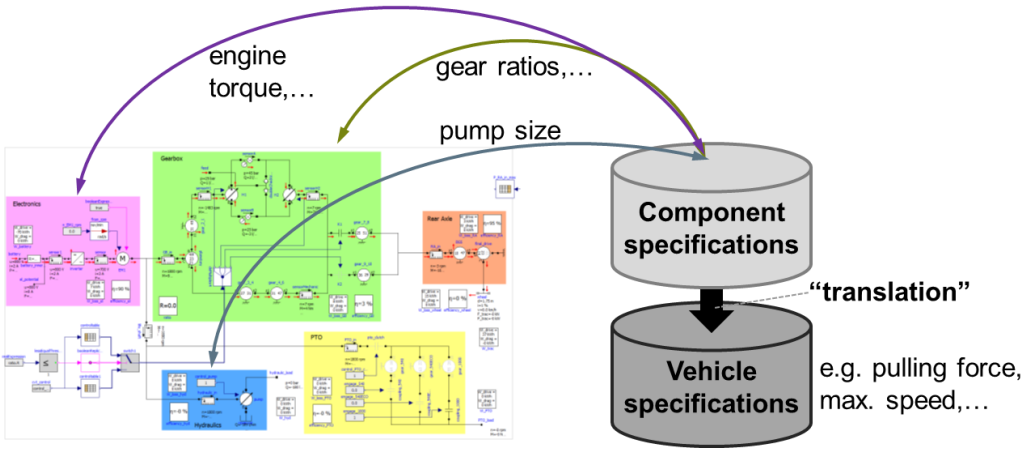

Figure 70: System Model with main characteristic and specifications of the tractor concept

2.1.3 Mission Profile

The multifaceted utility of tractors is what makes them so valuable to farmers and agricultural professionals. However, this very diversity in usage also presents a challenge when it comes to deriving a comprehensive usage or mission profile.

Tractors perform a wide range of functions. From plowing and tilling the soil to planting seeds, spraying fertilizers, and harvesting crops, tractors are integral throughout the entire agricultural cycle. Their ability to connect with various implements and attachments allows them to transform quickly from one task to another, such as mowing, baling hay, or even transporting goods (see **Figure 71**).

Figure 71: Usage or mission profile of a mid-sized tractor

The versatility of tractors is both their greatest strength and the primary reason why mapping their usage is a complex undertaking. Understanding this complexity is crucial for manufacturers aiming to optimize tractor performance, improve efficiency, and innovate future agricultural practices.

The integration of those mission profiles into the system model allows that all disciplines are aware of the later usage of the tractor. Furthermore, the model can be used to quickly investigate and identify critical operating points that may vary between different concepts, much faster than testing each scenario with sample or prototype tractors.

2.1.4 Efficiency

As already mentioned in the introduction the change of the powertrain concept of a small-sized tractor towards a battery-electric tractor is a huge step. Therefore, the shown system-model has been created to investigate different conceptional modifications. The following example demonstrates the efficiency comparison of different transmission concepts in a chosen mission profile.

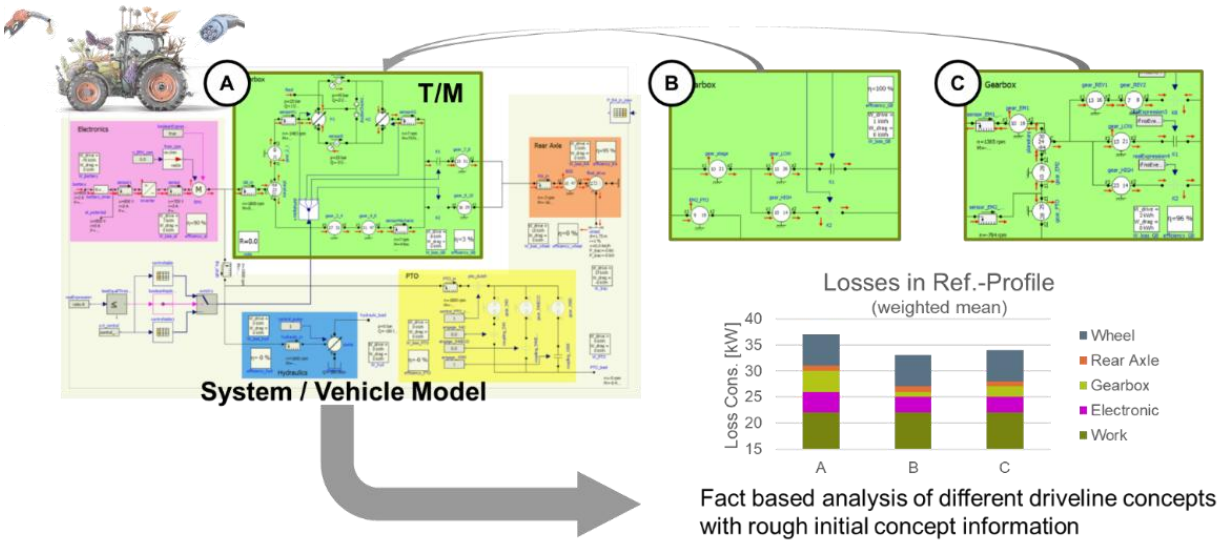

Figure 72: Efficiency comparison of different transmission concepts for a battery electric tractor

The system model on a high level (high scope, low fidelity) allows the simple exchange of the transmission concepts. In this case a hydr.-mech. powersplit transmission (A) is compared with a simple two stage transmission (B) and a more complex multi stage transmission (C). The results highlight that the transmission concepts B and C have a similar efficiency level so that further evaluation criteria can be considered to derive a concept decision (e.g. cost level & complexity).

In addition, the system model allows the detailed loss investigation of the results – which elements of the overall concept are the main contributors to the overall loss result. This is very helpful to understand the main sources of losses to derive further optimization steps.

2.1.5 Performance and risk investigation

The System Models enables the automated examination of all operational scenarios for tractor-implement combinations. By integrating and simulating the interactions of various tractor systems such as hydraulics, drivetrain, electronics, and cooling, this virtual validation process can identify critical operational situations. Once these potential issues are pinpointed, further in-depth investigations can be focused on these specific areas. This approach not only enhances the efficiency and effectiveness of the design and testing phases but also ensures that potential problems are addressed proactively, leading to improved performance and reliability of the equipment in real-world conditions. With this kind of virtual pre-investigation of the system the focus of the physical investigation can be reduced and focused on the essential operation points. Especially issues which are caused by the interaction of different systems (e.g. powertrain and hydraulic) can be investigate long before the first validation tractors are built. The increased maturity due to the virtual validation reduces the overall cost and the development time significantly.

Figure 73: Tractor in seeding operation at the headland of the field

One of those critical operation points which has been identified with help of the System Model is the seeding process with heavy implements in the front and rear lift. Especially at the headland, the engine speed is low while you have the need to lift mounted seed drill and the implement in the front and in addition having further hydraulic consumptions like steering. All of this leads to low lubrication pressures which affects the powertrain. In addition, the spontaneous drop of pulling force, due to the lifted implements at the headland, affects the temperature-based control of the cooler fan.

In conclusion, the automated investigation of tractor-implement combinations through System Modeling and Engineering represents a significant leap forward in agricultural technology. By leveraging these advanced techniques, the industry can achieve greater efficiency, adaptability, and sustainability, paving the way for a more productive future in agriculture.

3 Summary and outlook

The agricultural business is facing huge challenges due to the climate change and the need of a growing food production. This led to fundamental changes in the powertrain technology like the transformation towards a battery electric tractor in the small power range. Today's engineering methods and procedures are limited and do not cover the complexity of such significant modifications. System Engineering has emerged as a pivotal methodology to address the challenges in agricultural segment efficiently. By employing a holistic view, System Engineering facilitates the conceptual evaluation of powertrain concepts, allowing engineers to assess various design alternatives concerning their efficiency and performance outcomes. This comprehensive assessment is crucial, as it helps in identifying the most promising solutions that meet the stringent demands of modern agriculture.

One of the notable advantages of utilizing system engineering in powertrain development is its ability to identify critical operational scenarios. By simulating and analyzing these scenarios, engineers can anticipate potential issues and devise strategies to mitigate them, ensuring robustness and reliability in real-world applications. This proactive approach not only enhances the performance of the tractors but also extends their operational lifespan.

It has been highlighted that for a practical usage of system engineering the way to set up the system model is crucial. The model must effectively depict the vehicle's authoritative elements in an abstract manner. An abstraction which would be too detailed or too abstract wouldn’t allow an efficient engineering process and the efficient integration of all relevant experts would be disturbed.

In summary, the integration of system engineering into the design and modification processes of tractor powertrains represents a significant advancement in agricultural technology. It provides a structured framework that enhances decision-making, optimizes performance, and ensures that tractors can meet the evolving demands of the agricultural sector efficiently.

4 References

[RAZ24] Raza, A. et al., “Climate Change Impacts on Crop Productivity and Food Security: An Overview” In: Transforming Agricultural Management for a Sustainable Future. World Sustainability Series. Springer, 2024.

[UNA19] United Nations, “World population prospects: The 2019 revision”, New York, United Nations Population Division, 2019.

[AMI24] Agrarmarkt-Informations-GmbH, Deutscher Bauernverband e.V., „Situationsbericht 2024/25“, Berlin, 2024.

[HBS19] Heinrich Böll Stiftung, “EU/FARMS – Growing Up“, Berlin, 2019.

[CLA25] CLAAS Historie, in: https://www.claas.com/de-de/ueber-claas/historie-light, 2025.

Systems Engineering:
Virtual & Digital Twins

Digital twin concept for calculating CO_2 emissions of fluid power systems using AAS

M. Becker[1], K. Schmitz[1]

[1]RWTH Aachen University, Institute for Fluid Power Drives and Systems (ifas),

Campus-Boulevard 30, 52074 Aachen, Germany

Keywords: Asset Administration Shell, Carbon Footprint, Digital Product Pass, Industrial Internet of Things, Industrie 4.0, Fluid Power, System Engineering

Abstract: Achieving the climate goals of the European Union requires significant reductions in Carbon dioxide (CO_2) emissions within the industrial sector. A key prerequisite for this is the precise quantification of emissions across product life cycles, supported by improved emission calculation processes and robust data models. This contribution addresses the challenges associated with determining CO_2 emissions within the product life cycle of fluid power components and systems. To overcome these challenges, a digital twin concept based on the Asset Administration Shell (AAS) framework is proposed. Submodels (units of, e.g., properties that are assigned to a use case) for the AAS are developed to enable a comprehensible and consistent calculation of CO_2 emissions, these also serve as the foundation for a digital product passport for fluid power components. This contribution offers a practical and scalable framework for calculation of CO_2 emissions in terms of simulation and drive sustainability in the fluid power industry.

1 Introduction

The reduction of CO_2 emissions is essential to address the global challenges imposed by climate change effectively. A significant share of global CO_2 emissions originates from industrial processes [BUN21], presenting the industrial sector with the urgent task of reducing its carbon footprint. To achieve this, a detailed understanding of the CO_2 emissions generated by technical systems and their individual components throughout various phases of the product lifecycle is required.

Fluid power systems, known for their high power densities and long lifetimes, are employed in a wide range of industrial applications [SCH22]. Consequently, these systems contribute substantially to the industrial CO_2 emissions. Despite the critical need to mitigate these emissions, widely established systems engineering methods, for determining and attributing CO_2 emissions to specific system components, remain lacking [SPR24]. The aim of using system engineering methods is to take a holistic view of the system in terms of its emissions. Furthermore, digital twin concepts that enable consistent, transparent and accessible multi-stakeholder CO_2 monitoring have yet to be widely adopted, especially in the wake of the introduction of the digital product passport [BAR24]. Such concepts are vital for enabling efficient and comparable CO_2 monitoring across all stakeholders involved.

In this contribution, first, the fundamentals of the Industrie 4.0 and Asset Administration Shell (AAS), as well as the challenges of calculating CO_2 emissions are explained. Following up, a concept for continuous CO_2 balancing is outlined.

2 Challenges of Calculating CO_2 Emissions

The calculation of CO_2 emissions presents a significant challenge to the industry. One of the key difficulties lies in the absence of standardized methodologies [PAN11]. This issue is particularly evident in the inconsistent definition of system boundaries and functional units, as well as the varying use of data. These inconsistencies lead to substantial discrepancies in the results, making it difficult to compare components and systems based on their CO_2 emissions [SPR24]. To make CO_2 emissions, or the carbon footprint, a useful parameter for climate protection, these boundary conditions must be harmonized systemically [KLA20]. In addition, the complexity of the data landscape presents a significant hurdle. Calculating the carbon footprint requires the collaboration of numerous stakeholders across the entire value chain, as the necessary data is often distributed among various parties. Gaps in the available information frequently necessitate the usage of estimates or average values, which compromises both the accuracy and reliability of the results [SPR24]. Furthermore, certain processes or activities are difficult to quantify or are insufficiently documented.

To address these challenges, this contribution introduces a digitization framework based on the AAS. The AAS is a standardized digital data model that organizes all relevant information about physical or virtual assets in a structured and interoperable manner. This framework enables the standardized, machine-readable recording of all necessary parameters, enhancing the consistency of carbon footprint calculations and improving both the transparency and comparability of the results.

3 Digital Twin Concept of AAS

I4.0 is an initiative launched by the German government to support the fourth industrial revolution [ACA13]. The primary goal is to enhance productivity, efficiency, and flexibility through the digitization of production processes. As a result, the interoperability between people, machines, and processes is expected to improve, while also creating opportunities for new, scalable business models. Internationally, similar concepts are referred to as the Industrial Internet of Things (IIoT) [ALT19]. Within the framework of I4.0, technical systems evolve into Cyber-Physical Systems (CPS), which mirror real-world systems in the digital domain [SCH16]. One concept for realizing CPSs is the I4.0 component [PLA22b].

The I4.0 component consists of an asset and its corresponding AAS, as shown in Figure 74. Generally, assets are any objects, either physical or digital, that are under the ownership or control of an organization, and hold value for that organization [PLA22a]. The AAS serves as a digital representation of an asset, e.g. a hydraulic valve, enabling I4.0-compliant interaction. AASs contain descriptions of the asset and services related to its usage within a predefined context throughout the entire product lifecycle. [DEU16].

AASs are classified into types and instances, depending on the asset's role within the product lifecycle. Type AASs define the generic properties for all instances of a specific type, while instance AASs represent uniquely identifiable assets of a particular type [DEU16]. These instances specify attributes such as a serial number, whereas the corresponding type AAS merely defines the existence of the "serial number" property [EPP11].

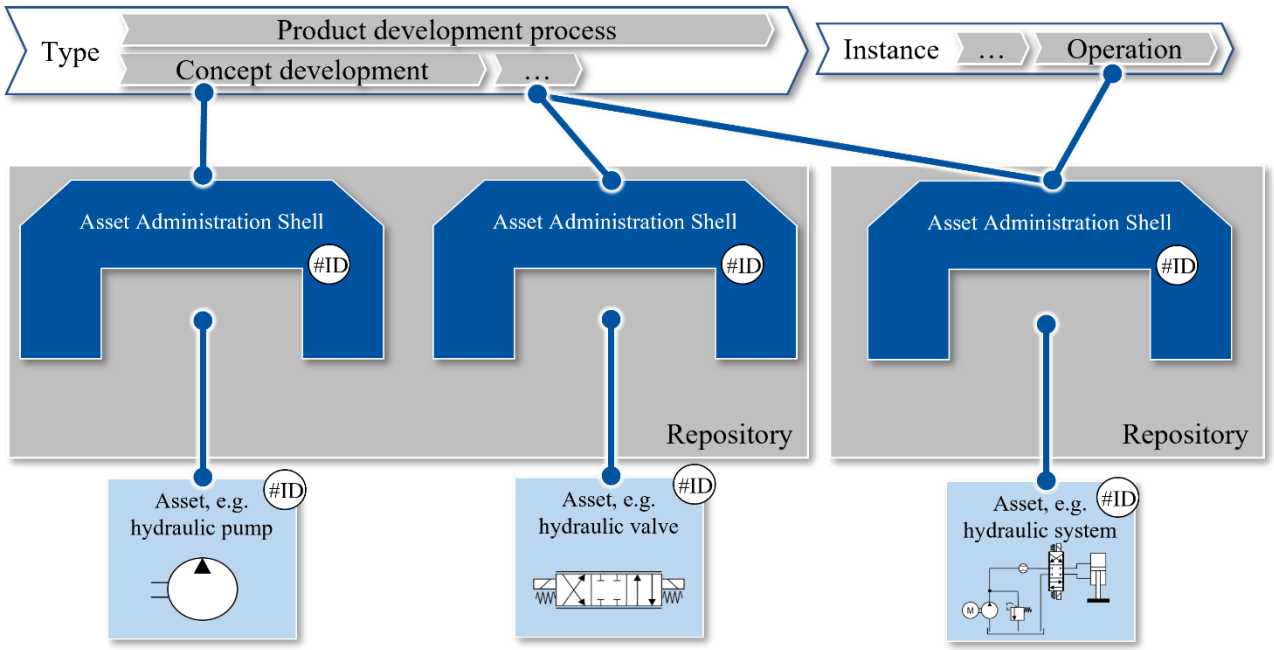

Figure 74: Industrie 4.0 components in the Product Life Cycle, consisting of AAS and Asset [DEU16]

In an AAS, the characteristics of an asset are modeled as SubmodelElements, which encapsulate various attributes, such as parameters or files. These SubmodelElements are thematically grouped into SubmodelElementCollections and Submodels. Submodels can then be standardized as templates, encompassing a set of relevant SubmodelElements, e.g. properties of physical assets, needed for specific use cases. Both Submodels and SubmodelElements can be annotated with SemanticIDs, which are unique identifiers referring to semantic descriptions in semantic dictionaries, such as eClass [ECL24] or IEC CDD [INT24]. These descriptions define the meaning of the content within the annotated element.

4 Basic Idea for an Interoperable Framework

To improve data handling within the product life cycle during CO_2 balancing, the three central stakeholder perspectives are distinguished: component manufacturers, system manufacturers, and operators (see Figure 75). Data is exchanged via an exchange framework, which is currently under development and will be partially introduced in the presentation. In addition to the various stakeholder perspectives, engineering applications such as system simulation tools are linked to the framework. This enables direct use of the data, for example, for component selection or parameterization of the system simulation.

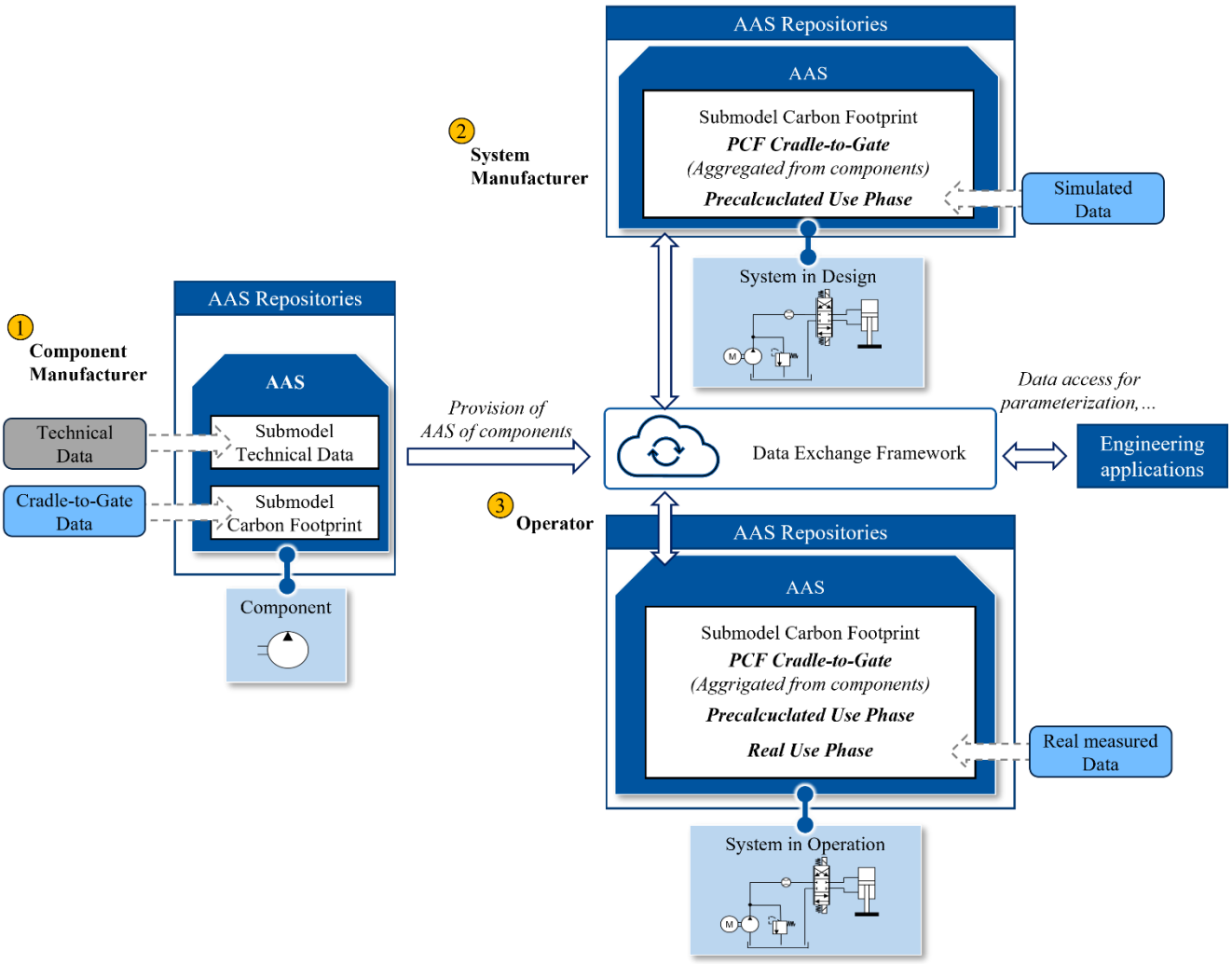

Figure 75: Basic idea of interoperable data exchange

1) The first perspective is the component manufacturer. Component manufacturers have valuable data and design files of their components, which can significantly support system manufacturers' system development processes. To facilitate interoperable data exchange between the technical disciplines, the component manufacturer provides its proprietary component data, originating from its database, via so-called AAS types. This data is embedded in semantically annotated properties. General technical data, such as the maximum volume flow of a hydraulic pump, is stored in a Submodel for technical data. In addition, CO_2-based data is stored in a Submodel for carbon footprint. The manufacturer is responsible for the initial linking of its proprietary data with the properties within the AAS. For the use case of CO_2 balancing, the component manufacturer must provide CO_2 data from the cradle-to-gate phase. This includes the carbon footprint created during the component's

manufacturing. For example, the Eclipse Tractus-X Framework[1] can provide such data in the context of Industrie 4.0. The AASs are stored in the component manufacturer's own AAS repositories.

2) The second perspective is the system manufacturer. The system manufacturer has an AAS of his system, aggregated from the existing components' AAS. This AAS comprises the Carbon Footprint Submodel and contains pre-calculated CO_2 and energy values. In addition, the cradle-to-gate (Product Carbon Footprint) PCF values of the individual components are aggregated in this Submodel. This pre-calculation can be carried out by system simulation. A simulation framework for integration into an AAS has already been presented in previous work, e.g., in [BEC23].

3) The third perspective is that of the operator, who has received the developed system from the system manufacturer. The AAS records the real measured values, which can serve as the basis for decisions regarding the machine's operation. Furthermore, the AAS is stored in the operator's database and linked to the real machine. In summary, the framework connects all these stakeholders and ensures consistent data management.

5 Data Models

In the context of the AAS, data models are required as semantically organized Submodels. These describe a data model that is as complete as possible for the use cases on which the Submodel is based. In this contribution, a Submodel for technical data and one for the carbon footprint are considered (see Figure 2).

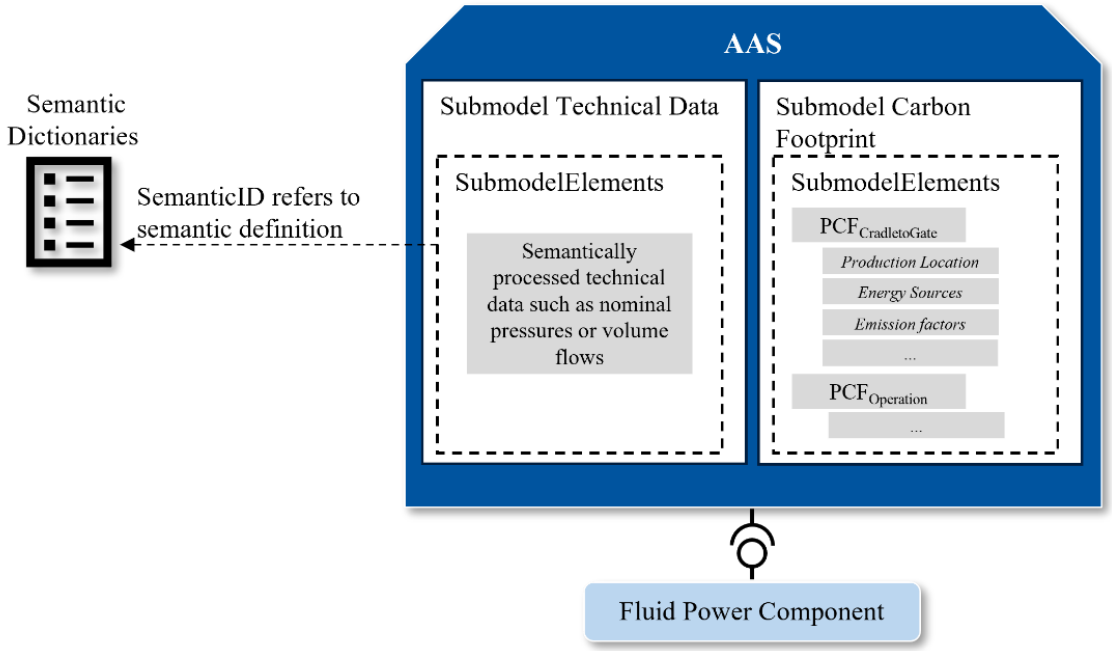

Figure 76: Section of required Submodels

The current state of the art already considers Submodels that address the carbon footprint use case at a very general level, for example [IDT23]. However, the current state of the art does not consider the characteristics of fluid power components and systems, particularly in the operating phase. Therefore, an extract of a proposal for a Submodel for carbon footprint, especially related to

[1] https://eclipse-tractusx.github.io/docs-kits/kits/PCF%20Exchange%20Kit/Adoption%20View/

the context of fluid power, is presented. This Submodel encompasses various cumulated energy forms, such as hydraulic, electrical, and pneumatic energy, as well as PCF values and boundary conditions for the respective life cycle phases (e.g., cradle-to-gate, use phase). It also includes corresponding emission factors, such as those related to the production site and the energy source. To ensure clarity and comparability, predefined properties are assigned to each energy form as boundary conditions, including parameters like accuracy and the unit of measurement.

To enable component selection or parameterization workflows during the development process, an additional already standardized Submodel for generic technical data is used. The standardized Submodel Generic Frame for Technical Data for Industrial Equipment in Manufacturing (Submodel Technical Data) [IDT22] serves this purpose by defining both the component class and its relevant technical parameters. This data facilitates the search for components based on defined specifications, supports automated design processes, and enables the parameterization of simulation models.

6 Summary & Outlook

This contribution first presents the basics of I4.0 and the challenges in CO_2 balancing. Based on these challenges, a concept was presented that is intended to significantly improve data exchange between component manufacturers, system manufacturers, and operators. To implement this concept, two fundamental aspects must be examined below. Firstly, it is necessary to establish fluid power-related semantic data models. Secondly, the data exchange framework must be implemented, considering stakeholder-specific interfaces for data exchange, integration, and security.

7 Acknowledgements

The project on which this contribution is based, with the funding code 13IK039K, is financed by the European Union (NextGenerationEU) and supported by the Federal Ministry for Economic Affairs and Climate Protection based on a resolution of the German Bundestag. Responsibility for the content of this contribution lies with the author.

Funded by the European Union
NextGenerationEU

Supported by:

Federal Ministry for Economic Affairs and Climate Action

on the basis of a decision by the German Bundestag

8 References

[ACA13] Acatech: *Recommendations for implementing the strategic initiative INDUSTRIE 4.0 -Final report of the Industrie 4.0 Working Group*, 2013.

[ALT19] Alt, R., Schmitz, K. *Basic requirements for Plug-and-Produce of 14.0 fluid power systems,* The 8th International Conference on Fluid Power and Mechatronics, 2019.

[BAR24] Barwasser, A., Schuseil, F. et al. *Der Digitale Produktpass*, https://publica-rest.fraunhofer.de/server/api/core/bitstreams/771a840f-dea6-4457-8c51-f52005c881bf/content, 2024.

[BEC23] Becker, M., Heppner, S. et al. *Improving Fluid Power System Simulation Through an AAS-Based Simulation Framework,* Proceedings of ASME/BATH 2023 Symposium on Fluid Power and Motion Control (FPMC2023), 2023. DOI: 10.1115/FPMC2023-109807.

[BUN21] Bundesministerium für Umwelt, Naturschutz, nukleare Sicherheit und Verbraucherschutz: *Novelle des Klimaschutzgesetzes beschreibt verbindlichen Pfad zur Klimaneutralität 2045,* 2021.

[DEU16] Deutsches Institut für Normung: *Reference Architecture Model - Industrie 4.0 (RAMI4.0),* Beuth Verlag, 2016, Berlin, Germany, 2016.

[ECL24] EClass e.V. *eClass standard*, https://eclass.eu/, 2024.

[EPP11] Epple, U. *Merkmale als Grundlage der Interoperabilität technischer Systeme,* Automatisierungstechnik, Vol. 59, Nr. 7, S. 440–450, 2011. DOI: 10.1524/auto.2011.0939.

[HEP23] Heppner, S., Miny, T. et al. *Asset Administration Shells as Data Layer for Enabling Automated Simulation-based Engineering,* in 2023 IEEE 28th International Conference on Emerging Technologies and Factory Automation (ETFA), S. 1–7, 2023. DOI: 10.1109/ETFA54631.2023.10275474.

[IDT22] IDTA: *IDTA 02003-1-2 Generic Frame for Technical Data for Industrial Equipment in Manufacturing,* 2022.

[IDT23] IDTA: *IDTA 02023-0-9 Carbon Footprint*, https://industrialdigitaltwin.org/en/wp-content/uploads/sites/2/2024/01/IDTA-2023-0-9-_Submodel_CarbonFootprint.pdf, 2023.

[INT24] International Electrotechnical Commission: *IEC 61360-4 - IEC/SC 3D - Common Data Dictionary*, https://cdd.iec.ch/cdd/iec61360/iec61360.nsf/TreeFrameset?OpenFrameSet, 233.2024.

[KLA20] Klaaßen, L., Stoll, C. *Harmonizing corporate carbon footprints,* Nature Communications, Vol. 12, 2020. DOI: 10.1038/s41467-021-26349-x.

[PAN11] Pandey, D., Agrawal, M., Pandey, J. *Carbon footprint: current methods of estimation,* Environmental Monitoring and Assessment, Vol. 178, S. 135–160, 2011. DOI: 10.1007/s10661-010-1678-y.

[PLA22a] Plattform Industrie 4.0: *Details of the Asset Administration Shell - Part 1 - The exchange of information between partners in the value chain of Industrie 4.0 (Version 3.0RC02)*, 2022a.

[PLA22b] Plattform Industrie 4.0: *Industrie 4.0 Glossar*, http://www.plattformi40.de/I40/Navigation/DE/Service/Glossar/glossar.html, 2022b.

[SCH22] Schmitz, K. *Fluidtechnik - Systeme und Komponenten,* Shaker Verlag, 2022.

[SHC16] Schroeder, G. N., Steinmetz, C., et al. Digital Twin Data Modeling with AutomationML and a Communication Methodology for Data Exchange. IFAC-PapersOnLine, Vol. 49, Nr. 30, S. 12–17, 2016. DOI: 10.1016/j.ifacol.2016.11.115.

[SPR24] Sprink, J., Schmitz, K. Product Carbon Footprint of Hydraulic and Pneumatic Components - Challenges in Accounting and Comparability. Proceeding 14th International Fluid Power Conference, 2024

Digital twins of wind turbines' gear transmissions for decision making

Maite García[1], Iñaki Mugarza[1], Xabier Olamendi[1], Mikel Escalero[1]

[1]Ikerlan, Basque Research and Technology Alliance, J. M. Arizmendiarreta, 2, Arrasate-Mondragón 20500, Spain

Keywords: *digital twin, gear, transmission, decision making*

Abstract: Lately, various needs have been identified in relation to the operation of wind turbines, such as, life extension, repowering or predictive maintenance. All those needs involve making complicated decisions that account for the structural health of critical systems. Among all the critical systems, this work focuses on gear-based transmissions such as the pitch system or the gearbox. Here a parametric digital twin of gear pairs is developed for evaluation of fatigue damage, and is applied to two examples. The first example consists of the pitch gear system, which is analyzed for different blade loads (for pristine and progressively degraded blades) and different maintenance strategies. The results show that, thanks to the digital twin, the decision for life extension can be safely taken, almost doubling the original lifetime of the pitch gear. The second example consists of the intermediate gear stage of a gearbox. Through the study of the shear stresses that produce the tooth flank fracture and the combination of manufacturing and operation effects, the potential of this gear set is quantified for undergoing larger loads coming from a repowering action. Overall, the digital twin is found to be a powerful asset to know the real structural health of gear transmissions of wind turbines, allowing to make informed decisions that ultimately lead to an optimal operation of the wind turbines.

1 Introduction

Wind energy is one of the most promising renewable energy sources, as shown by the important investments performed by the European Union [EUR25]. Yet, the operation of the wind turbines for the generation of electricity is hard and poses the need for making difficult decisions [BOR24]. For example, decisions related to the following aspects:

- Life extension: to operate wind turbines beyond their initial design life.
- Repowering: to perform minor or major modifications to wind turbines to increase the output power.
- Predictive maintenance: to assess the current health and future behavior of wind turbine's components to take optimal repair actions.
- Operation under unpredicted loads: to operate wind turbines under wind speeds higher than those considered during design.

Of course, the referred decision making must be conducted by adequately considering the structural health of the critical subsystems, so that economic profitability and safety are preserved. Among the critical subsystems many can be mentioned, such as, blades, hub, pitch and yaw bearings, main axis and main bearing, the gearbox and the generator. In particular, this work focuses on the gear transmissions that are present in the gearbox or the pitch and yaw mechanisms.

For the mechanical fatigue assessment of the geared transmissions, various well-known computer programs exist (KissSoft, Romax). They allow detailed calculations following the most popular

standards (for example, ISO 6336 [INT19]), while considering gears' corrected microgeometry, the influence of axis and joint deflections, load spectra, etc. However, these powerful tools are oriented to the design of transmissions, rather than for the "on-line" evaluation considering realistic operating conditions.

Thus, the present work has two objectives: 1) to develop a parametric digital twin of geared transmissions for on-line structural health assessment, and 2) to exploit the digital twin for making decisions related to transmissions of wind turbines.

2 Digital twin developed

A parametric digital twin is developed, noting that "parametric" means that it can be particularized to any gear pair (spur or helical, internal or external), regardless of geometry, material and loads.

2.1 Digital twin's workflow

The digital twin follows the workflow shown in Figure 77.

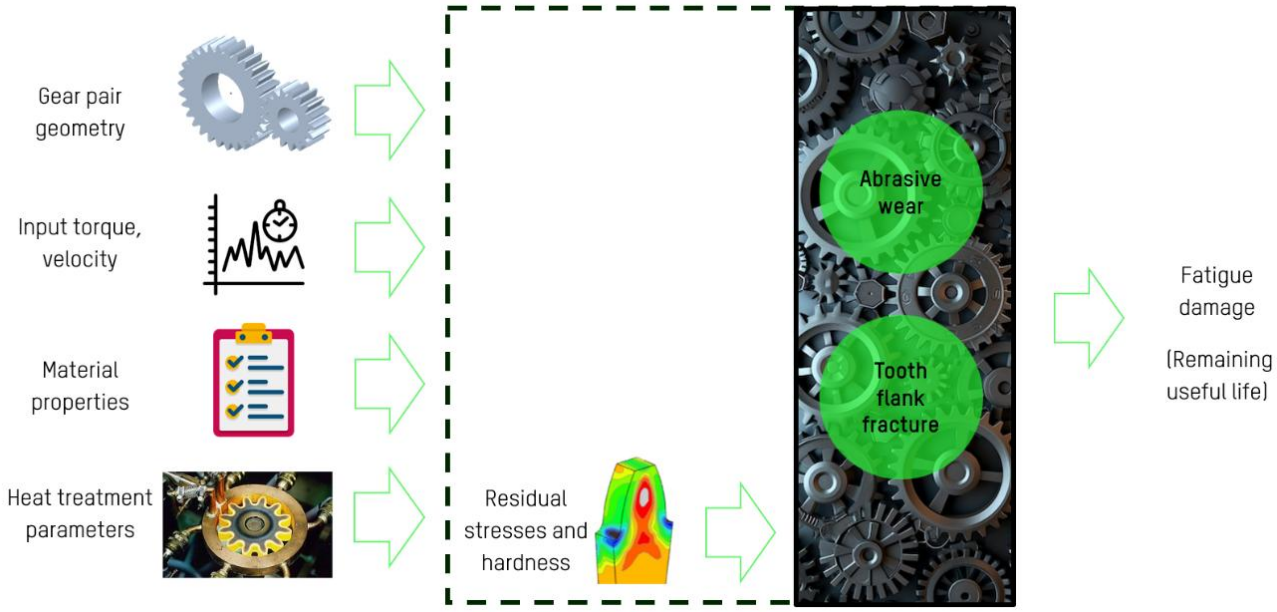

Figure 77: Digital twin's workflow.

The main inputs are:

- The gear pair geometry, specified by the module, number of teeth, pressure angle, helix angle, and profile shifting coefficients.
- The input torque and velocity, specified by time series (values vs. time).
- Material properties: depending on the failure mechanism, these properties may include the coefficients of frictions and wear, the endurance limit for normal and shear fatigue, or hardness and residual stress profiles in depth.
- Induction hardening parameters: for induction hardened gears, the digital twin has a module to simulate hardness or residual stresses based on process parameters (voltage, intensity, scanning velocity, etc.). → This module is not used in this paper.

The main output of the digital twin is the evolution of the fatigue damage resulting from the operation, which can be converted to remaining useful life under postulated future operating conditions.

For the time being, the digital twin contemplates two failure mechanisms that may produce the mechanical failure of the gears:

- Abrasive wear, which changes the involute shape of the contacting flanks.
- Tooth flank fracture (TFF), which is the generation of a subsuperficial crack that starts in the interface between the hardened layer and the core, leading to a tooth breakage.

2.2 Fatigue methodologies

The assessment of the failure mechanisms is based on physically based fatigue methodologies that are briefly explained below:

Methodology for abrasive wear

This methodology, presented by García et al. [GAR25], consists of the following steps:

- Static equilibrium: loads transmitted by the single or double contact pairs are determined by the load sharing equations of AGMA 925-03 or by a Finite Element (FE) model.
- Contact normal conditions: the pressure distributions of the contacts are obtained by Hertz theory.
- Global kinematics and tangential conditions: the frictional stress is calculated by Coulomb theory, assuming full sliding. The sliding distance is determined by the multiplication of the relative velocity (given by the compatibility of motion) and the time step between two moments.
- Energy dissipation: the wear depth increment is quantified by the multiplication of the frictional stress, the sliding distance, and the coefficient of wear. Wear is accumulated in all calculated tooth flank positions.

The fatigue damage due to wear is defined as the ratio between the worn material depth and the case-hardened depth. Gear failure is expected when that ratio reaches a value of 1.

Methodology for tooth flank fracture

The currently implemented methodology for the evaluation of TFF is based on ISO 6336-4 procedure, as described below. Note that this methodology is not applicable to time series of operating conditions but to equivalent cases (continuous rotation under characteristic load):

- The effective shear stress is estimated accounting for the stress contributions coming from the contact load and the residual stresses of the heat treatment. The equations for the different stress components are found in the standard.
- The permissible shear stress is estimated from the hardness distribution in depth, following equations from the standard.
- The material exposure is estimated based on the comparison of the effective and the permissible shear stresses.

Thus, the material exposure is used as the indicator of TFF damage.

3 Exploitation of the digital twin for decision making

The parametric digital twin is adapted to represent two gear transmissions of wind turbines, and then it is used for decision making.

3.1 Use case 1: Pitch gear

3.1.1 Case description

The pitch gear (Figure 78) is the transmission that rotates the blade with respect to its axis, and therefore allows to regulate the power extracted from the wind. It consists of an internal spur gear pair that is constituted by 1) the driving pinion attached to the motor and 2) the bearing ring with internal teeth.

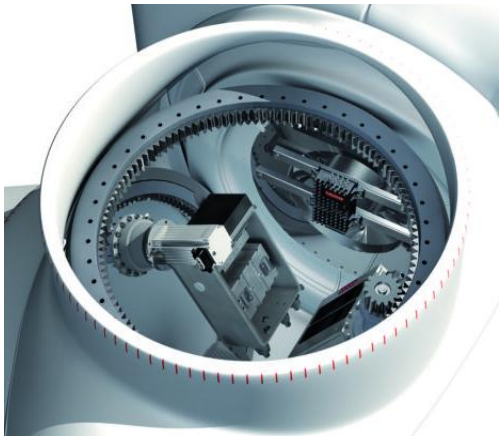

Figure 78: Representation of a pitch gear.

For the example of an NREL-5 MW wind turbine, the module is 16 mm and the numbers of teeth are 15 and 198, yielding a gear ratio of 13.2. The pinion is commonly made of 18CrNiMo7 and case-carburized up to a hardness of 60 HRC, whereas the ring is made of 42CrMo4 subject to mass-quenching and tempering (50 HRC).

Regarding the loads, the distribution of wind events (with mean velocity and recurrence) can be known for specific locations, while the blade-root loads and pitch gear's torque can be calculated by aerodynamic simulations. For all the wind events, 30 minute long time series are available to feed the digital twin.

Overall, four different scenarios are calculated:

- Scenario 1: pristine blade, no maintenance actions.
- Scenario 2: progressively degraded blade (decreasing loads), no maintenance actions.
- Scenario 3: pristine blade, pinion repositioning every 10 years (180º shift).
- Scenario 4: progressively degraded blade (decreasing loads), pinion repositioning every 10 years (180º shift).

The pitch gear is assumed to fail due to abrasive wear.

3.1.2 Wear damage in a representative tooth

Figure 79 (left) displays the worn profile of a representative tooth of the pinion after the lifetime of 20 years, according to the simulation performed by the digital twin. Both left and right flanks are found to wear out in a similar way, following an uneven pattern through the contact flank.

In fact, Figure 79 (right) displays the wear distribution of the right flank in quantitative terms. It is observed that the single contact region (B-D) is the most degraded zone, with higher wear close to D (the transition from single to double contact). That observation can be explained by the operating conditions of this case, characterized by a high transmitted torque and a relatively low velocity. Close to the pitch (C), the wear decreases locally, which can be attributed to the rolling motion that happens at that characteristic point. In the double contact regions (A-B and D-E) the digital twin simulates a decreasing wear towards the entry (A) and the exit (E), reaching the minimum at the entry.

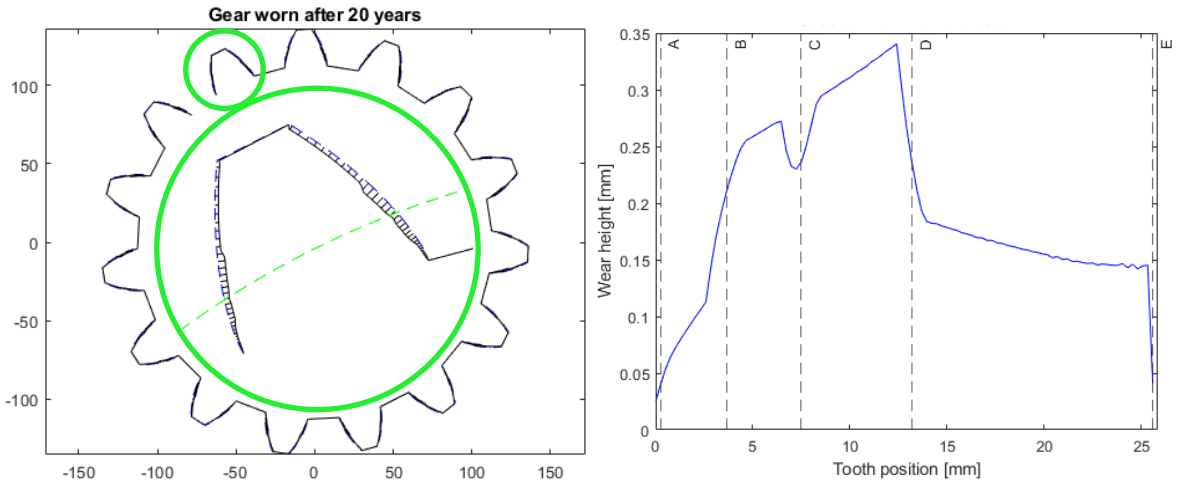

Figure 79: Worn tooth (left) and distribution of wear depth (right).

3.1.3 Decision making: life extension and maintenance actions

Figure 80 displays the evolution of the pinion's capacity (1-worn depth ratio) estimated by the digital twin for the four scenarios.

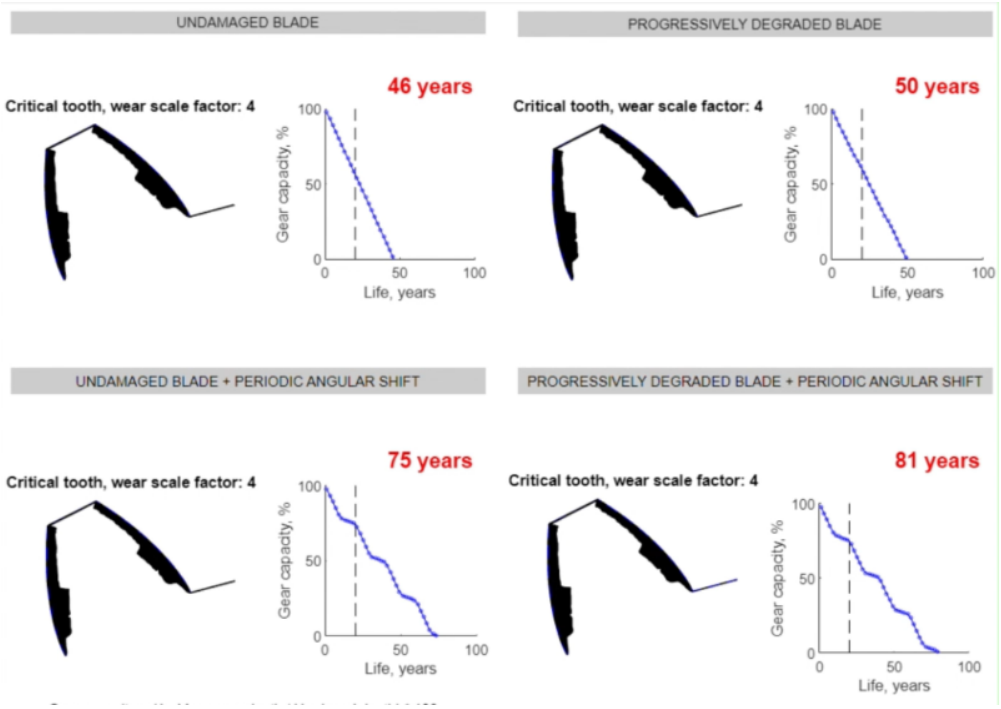

Figure 80: Gear capacity (1-hworn/CHD) evolution for different scenarios.

In Scenario 1, a linear decrease of the capacity is estimated, with a value higher than 0.5 for the design life of 20 years. Beyond that time of operation, the wind turbine can be operated, and the pinion is predicted to be operable up to 46 years (over double the design life).

In Scenario 2, the input torque applied to the pitch gear is progressively lower because the degraded blades suffer lower tilting moments. In this scenario, the decrease of the capacity is slightly non-linear, with a descending slope slightly smaller than in Scenario 1. In fact, the digital twin predicts that the lifetime can be extended over the initial 20 years, up to 50 years.

In Scenario 3, the decrease of the capacity is highly non-linear and the slope is drastically reduced every time the pinion is shifted 180º. The repositioning action is so beneficial that the digital twin shows that life can be extended up to 75 years.

Finally, in Scenario 4, where the decrease of blade loads and beneficial maintenance actions are combined, the pinion's capacity decreases slowly, reaching a lifetime of 81 years, quadrupling the design life.

3.2 Use case 2: Gearbox

3.2.1 Case description

The gearbox (Figure 81) allows the multiplication of the slow rotational velocity of the rotor (order of 15-20 rpm) to the high rotational velocity of the axis connected to the generator (around 1500 rpm). Such velocity multiplication is commonly achieved in three stages: planetary or low-speed stage, intermediate-speed stage, and high-speed stage.

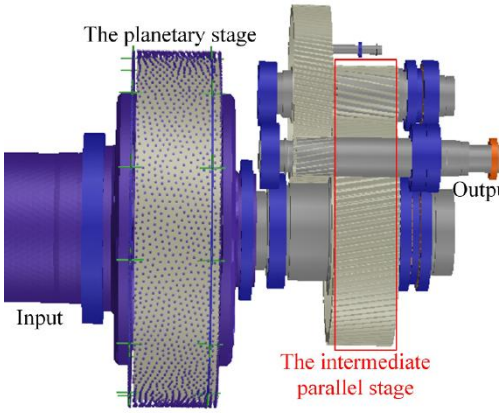

Figure 81: Schematic representation of a gearbox.

Here, the 2 MW design from [ZHO22] is considered, focusing on the intermediate-speed stage due to its higher criticality. This stage consists of two helical gears with respectively 121 and 24 teeth and a module of 11 mm, yielding a transmission ratio of 0.198. The gears have a helix angle of 20º and are made of 18CrNiMo7, case-hardened up to 2.3 mm.

Regarding the operating conditions, the gear pair is subject to a continuous rotation at 77 rpm under a nominal 282.8 kNm torque (Scenario 1). Additionally, this work considers other two scenarios with loads that increase the pitch point's pressure contact in 10% and 20% (Scenarios 2 and 3).

In this use case, the tooth flank fracture is known to be the dominant failure mode [ZHO22], so this mechanism is assumed to drive the failure.

3.2.2 Shear stresses in a representative tooth

Figure 82 displays, for the three scenarios, the distribution of the effective (applied) and permissible shear stresses under the pitch point (point C).

For all of them, the effective shear stress is found to be variable in depth: close to the surface the value is high because of the contact stresses, and then the value decreases until the case-core interface. At that point, the effective shear stress increases suddenly because the favorable effect of residual stresses vanishes, and beyond that point the value consistently decreases due to a lower influence of the contact. As the applied load increases, the effective shear stress distribution increases, and in all scenarios the maximum is found slightly below the case-core interface: 92 MPa, 110 MPa, 129 MPa respectively.

In relation to the permissible shear stress, the values are independent of load (as expected), and two clearly differentiated regions are observed. In the hardened case a plateau is found with a value around 300 MPa, whereas in the core a plateau is also found but with approximately the half value.

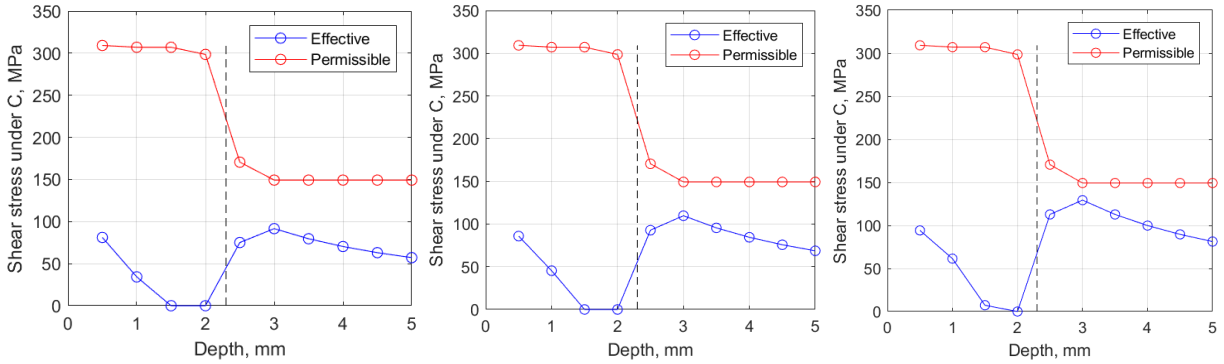

Figure 82: Effective and permissible shear stresses under pitch point for Scenario 1 (left), 2 (middle) and 3 (right).

3.2.3 Decision making: repowering

Figure 83 displays the distribution of the material exposure. Overall, the core region is subject to higher material exposures, especially for higher loads. The maximum peak is identified slightly below the case-core interface (3 mm deep), exactly where the effective shear stress is maximum and the permissible shear stress is virtually lowest. Therefore, the highest damage is predicted at a point, but failure is only predicted for Scenario 3, where the maximum material exposure exceeds the admissible limit suggested by the ISO 6336-4 standard (0.8).

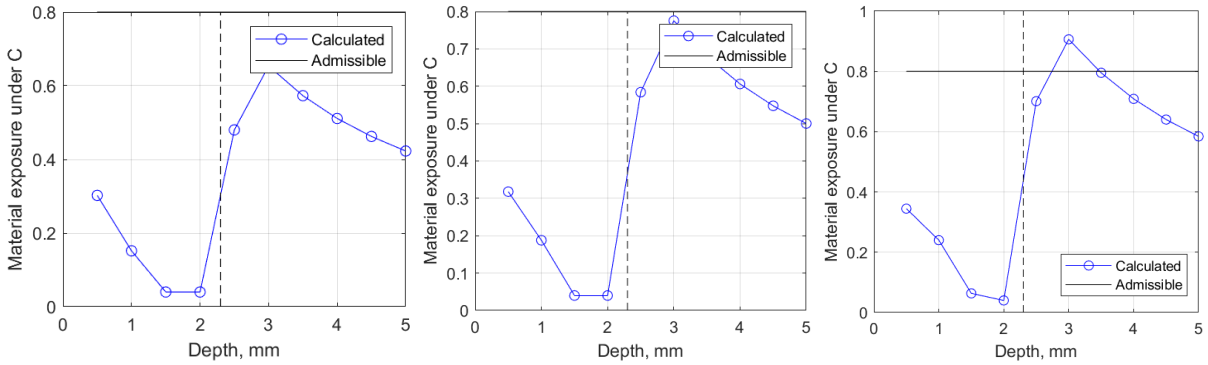

Figure 83: Material exposure under pitch point.

Thus, the results of the digital twin indicate that the load applied can be increased while avoiding failure up to a point where the contact pressure is 10% higher than in the base scenario, making it possible to undertake repowering actions.

4 Conclusions

In this work a parametric digital twin for the on-line evaluation of the structural health of gear transmissions is presented. Additionally, it has been proved that it can be used for making practical decisions.

In the analyzed pitch gear of a 5 MW wind turbine:

- Life can be safely extended up to 50 years.
- Life can be safely extended up to ~80 years if the pinion is repositioned every 10 years.

In the analyzed critical stage of a gearbox of a 2 MW wind turbine:

- Repowering actions can be taken up to torques that produce a 10% increase in the contact pressure.

5 Bibliography

[BOR24] Borissova, Daniela: Decision-Making in Design, Maintenance, Planning, and Investment of Wind Energy.

Springer, 2024

[EUR25] European Commission: EU Wind Energy.

https://energy.ec.europa.eu/topics/renewable-energy/eu-wind-energy_en

(20/02/2025)

[GAR25] García, Maite et al.: Metodología de simulación del proceso de desgaste en engranajes de dientes rectos considerando series temporales de operación.

Elsevier, under review.

[INT19] International Organization for Standardization: Calculation of load capacity of spur and helical gears.

ISO, Switzerland, 2019

[ZHO22] Zhou, Ye et al.: Analytical study of tooth flank fracture in case-hardened gears considering non-metallic inclusion.

Elsevier, 2022

Systems Engineering:

Artificial Intelligence and SysML v2

Postersession

Functional Screening Methods for Performance Assessment of Transmission Components

G. Patzer[1], P. Beau[2]

[1]Optimol Instruments Prüftechnik GmbH, Flößergasse 3, 81369 Munich, Germany

[2]Beau Engineering Services, Hinter der Wiese 3, 38162 Cremlingen, Germany

Keywords: *gears, tribology, seizure, fatigue*

Abstract: The increasing complexity of powertrain systems, coupled with growing performance demands and tighter development timelines, has amplified the need for efficient and reliable testing methods for transmission components. This paper introduces advanced tribological screening techniques designed to assess critical functional properties, such as load-carrying capacity, friction reduction, wear resistance, and material compatibility. These properties are essential to optimizing gear performance under varying operational and environmental conditions. The proposed methods leverage model tests to evaluate the performance of materials, coatings, lubricants, and individual components with high statistical reliability. By correlating laboratory findings with real-world performance, this study provides a robust framework for improving transmission efficiency, durability, and sustainability. Key innovations include the development of a refined testing protocol for low-viscosity fluids and new approaches to assess micro-pitting and pitting resistance using non-circular test disks. These advancements offer gearbox engineers practical tools to meet the challenges of modern transmission design and maintenance.

1 Introduction: the importance of tribological optimization in gear performance

The performance of gears is critical in a wide array of mechanical systems, ranging from automotive applications to industrial machinery. Gears are subject to intense mechanical and thermal stresses, making tribological optimization essential to ensure their durability, efficiency, and overall reliability. This discussion highlights the significance of tribological optimization concerning four key aspects: seizure resistance (load carrying capacity), friction reduction, surface coatings, and fatigue.

Enhancing seizure resistance (load carrying capacity):

Seizure, a common form of surface damage in gears, occurs when high contact stresses lead to the formation of small local welding on the gear surface (seizure). Tribological optimization plays a crucial role in enhancing seizure resistance by improving material properties, surface hardness, and lubrication effectiveness.

Reducing friction:

Friction is a key contributor to energy loss in gear systems, manifesting as heat generation and wear. Tribological optimization aims to reduce friction by refining surface roughness, employing advanced lubrication strategies, and utilizing materials with low friction coefficients. By minimizing friction, gears not only achieve higher efficiency but also operate at lower temperatures, which reduces thermal stress and the likelihood of premature failure. This improvement is particularly critical in high-speed and high-load applications, where even minor reductions in friction can lead to significant energy savings and performance gains.

Advancing surface coatings:

Surface coatings are indispensable in modern gear technology, providing an additional layer of protection against wear, corrosion, and thermal degradation. Tribological optimization focuses on developing coatings with superior adhesion, hardness, and resistance to environmental factors.

Mitigating fatigue:

Fatigue failure, resulting from cyclic loading over extended periods, is a critical concern in gear systems. Tribological optimization addresses this issue by improving material toughness, optimizing surface textures, and ensuring effective lubrication. Proper lubrication regimes prevent the formation of cracks and other defects that could propagate under repeated stress.

Conclusion:

Tribological optimization is a cornerstone of modern gear design and maintenance. By focusing on seizure resistance, friction reduction, advanced coatings, and fatigue mitigation, engineers can significantly enhance the performance, reliability, and efficiency of gear systems. These advancements not only ensure longer gear life but also contribute to energy efficiency and sustainability, making tribological research an indispensable aspect of mechanical engineering.

2 Load carrying capacity of gear fluids – status quo

Since 2012, several studies have shown that the load carrying capacity of gear fluids can be tested with simple model tests in reversing oscillating tribometer tests (SRV®). For these tests, a crowned cylinder (diameter 6 mm x length 8 mm with initial contact length 4 mm) made of 100C6 bearing steel is pressed horizontally with an inclination of 10° against the direction of movement onto a test disc made of 100Cr6 with a lapped surface and a hardness of 60 to 62 HRC and oscillated at a frequency of 50 Hz at 4 mm stroke (Figure 1). The test temperature on the surface of the test disc is maintained at 90°C.

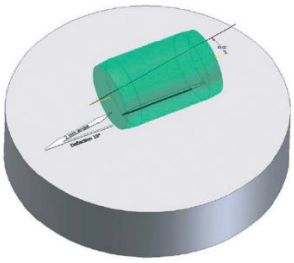

Figure 84: Specimen geometries for SRV® tests according to DIN 51834-4 [PAT16]

The normal force is applied in stages according to the load levels from Figure 2, each with a step duration of 217 s. The step duration of 217 s is based on FZG test method A/8.3/90 by converting the number of revolutions per load stage into a corresponding holding period for the SRV® test. The load levels were calculated in such a way that the mean surface pressures of the tooth contact of the aforementioned FZG method were transferred via the Hertzian contact surface in the geometry and material combination described above. This results in the load levels according to Figure 2.

Since then, several international round robin tests have already been carried out under a DIN method in the draft stage as part standard 7 of the DIN 51834 series, which confirmed good repeatability and comparability of this test method. The correlation of the results with the results of the FZG method A/8.3/90 was also demonstrated in several individual projects. As an example, the

results of Massochi et al. [MAS22] can be mentioned, which were able to confirm the transferability for various gear oil types of different viscosity classes (Figure 3).

ISO 14635-1 (FZG, A/8,3/90)		**DIN 51834-7 SRV®** Roller-on-disk, 10°
Oil temperature: **90°C**		Temperature on disk: **98°C**
Hertzian contact stress P_{0max} [MPa]	FZG load stage	Normal force (load) [N]
146	1	7
295	2	28
474	3	73
621	4	126
773	5	195
929	6	282
1080	7	381
1223	8	489
1386	9	628
1539	10	774
1691	11	934
1841	**12**	1107
1994	(13)	1299
2147	(14)	1507
2290	(15)	1713
2443	(16)	1950
2596	(17)	2202

Figure 85: Calculation of the normal forces for SRV® tests according to DIN draft 51834-7 [PAT16]

Oil Name	Oil Type	ISO VG	SRV Failure Stage	FZG Failure Stage
GT15	Gas turbine	15	11	12
GT32	Gas turbine	32	11	12
GT46	Gas turbine	46	12	12
TO46	Turbine	46	8	9
GO320	Gear	320	>12	>12
GO460	Gear	460	>12	>12
CO68A	Circulating	68	>12	>12
CO68B	Circulating	68	N.D.	12
CO68C	Circulating	68	>12	N.A.
CO68D	Circulating	68	>12	>12

Figure 86: Correlation results for 10 different fluids between SRV DIN E 51834-7 draft and FZG Test Method A/8,3/90 [MAS22]

2.1 Recent findings

With raising the number of samples and users of this method, it showed up that there is still potential for improvement in terms of robustness of the method as well as in the aspect of transferability of the results to the real field performance of gear and transmission fluids. The robustness of the method in view of reproducibility and influences like the amount of present fluid, specimen orientation and cutoff criteria has been reviewed by the authors since 2023. The outcome of this review was that the amount of available fluid as well as specimen orientation as well as application of cutoff criteria and parameters of the oscillation drive (standard vs. component mode) had a too strong influence and that the ranking of the results did not meet the expectations from the field.

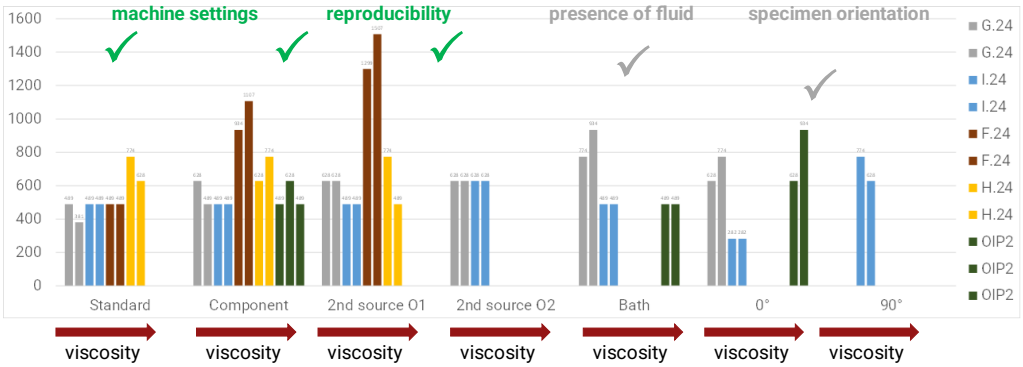

Figure 87: Outcome of the parameter study at Optimol 2024 for gear performance testing in variations of DIN 51834-4

Nevertheless, Schmidt and Breitsprecher [SCH24], could recently demonstrate that in case of testing super low viscosity fluids, the frictional heat in the contact zone is increasing by several decades of K during the step load tests according to DIN 51834-4, so that the fluid will fail due to overheating instead of mechanical shearing of the tribofilm. Consequently, the repeatability and transferability of the results got worse. Thus, the use of a fluid bath with fluid circulation at 25 mL/min flow rate was introduced (Figure 5).

With this modification, the temperature can be controlled more reliably as the generated heat is absorbed by the flowing and circulated fluid. By this modification, the precision of the results of not only the load carrying capacity (± 1 load stage) but also the coefficient of friction (CoF, ±0,01) could be improved significantly. Also, the load carrying capacity determined in this way was much nearer to the expected results. Figure 6 shows the exemplary results for one conventional automatic transmission fluid. The kinematic viscosity of this fluid is 4,1 mm²/s at 100°C and 18,1 mm²/s at 40°C. [SCH24]

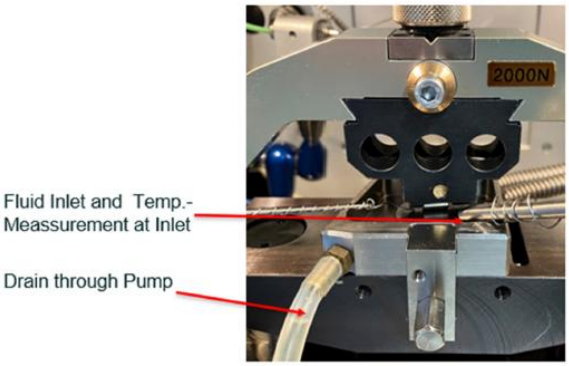

Figure 88: Test setup developed at Mercedes for low viscosity fluid SRV® tests in an extended DIN 51834-4 test [SCH24]

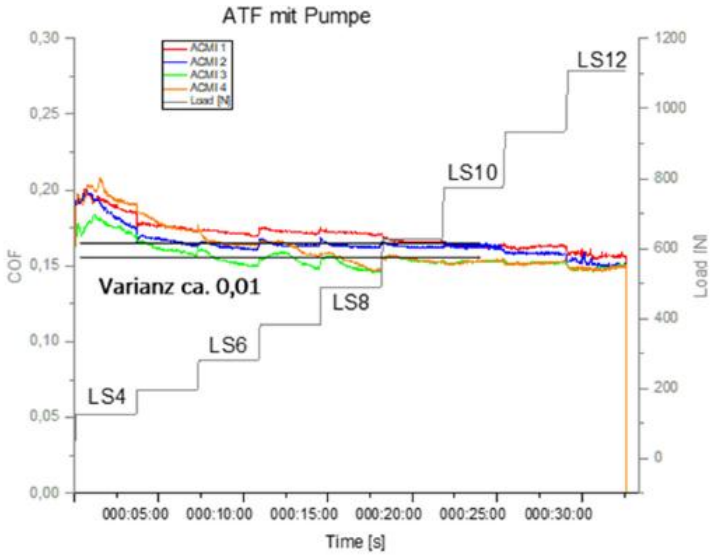

Figure 89: Repeatability study at Mercedes for a low viscosity ATF in an extended DIN 51834-4 test [SCH24]

2.2 Newest approach

With the experience of the aforementioned studies, the authors of this paper conclude that a new approach should be undertaken to develop a more robust and easier to apply gear fluid performance screening (GPS) which enables tribologists to quickly and efficiently rate gear fluids in terms of load carrying capacity with high security of exactly predicting the performance in the real application.

For this purpose, four well described reference fluids with known field performance were selected. These reference gear fluids are described in table 1.

Fluid name	Performance level	Viscosity @ 40°C mm²/s	FZG A/8.3/90 failure stage
RL219/6	low	50,9	6
RL237/4	good	46,0	11,5
L23-0415	high	25,0	15

Table 6: Reference fluids used in this study

After extended parameter studies, it was found that a setup with a diameter 10 mm ball (material 100Cr6, hardened) and a test disk of the same material and hardness with lapped surfaces, diameter 24 mm and 6,9 mm height as lower specimen was the most promising. The lower specimen is placed in a fluid bath and dipped in 1 mL of fluid. The test parameters are:

- Stroke length 2,0 mm
- Temperature 60°C
- Frequency 60 Hz (V8-mod) and 30 Hz (V10-mod)
- Test force: 50 N for 30 s, 100 N for 4,5 min, then 50 N steps each with 1 min duration

As for the failure criteria, fluctuations in stroke as well as in CoF are supervised. Either a deviation of stroke by more than 10% of the setpoint or an increase of CoF to a value higher than 0,2 indicates failure and determines the test.

One can see that for both frequencies, the resulting ranking of the load carrying capacity of all fluids corresponds to the expected performance. Nevertheless, the lower frequency leads to higher sensitivity and thus, earlier failures of the samples which improves the differentiability (figure 7).

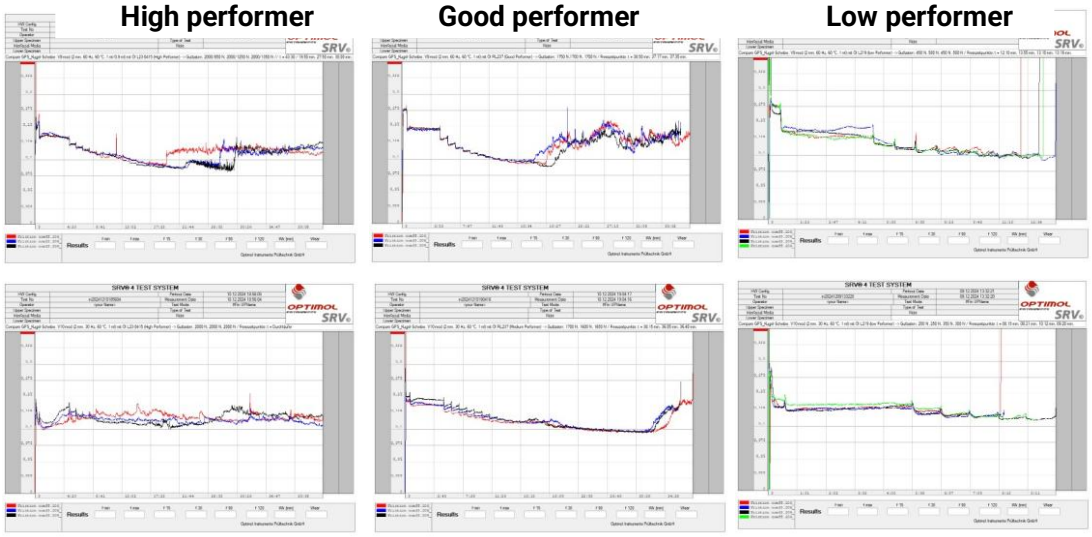

Figure 90: Results of the newest parameter study at Optimol Instruments with ball on disk geometry at 2 mm stroke, 60°C test temperature and 60 Hz (upper row) and 30 Hz (lower row). Note: the time axis is not equally scaled for all charts.

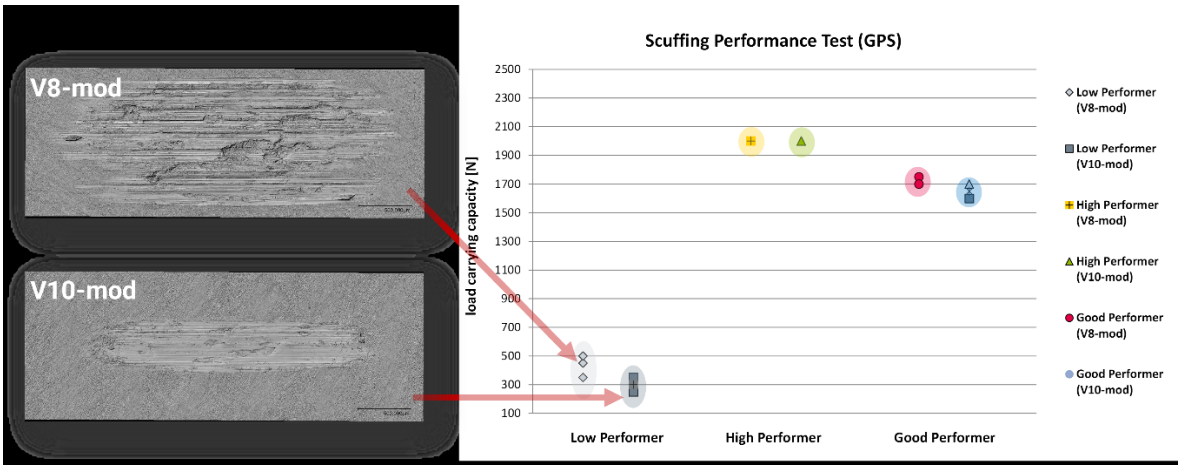

Figure 91: Microscopic images of the wear marks of the low performer sample at 60 Hz (V8-mod) and 30 Hz (V10-mod). In both test variants, the failure stage is in very good consistency. During the 60 Hz tests, the wear damages seem to be significantly harsher than after the 30 Hz tests.

Microscopic analyses of the worn surfaces of the samples after the test clearly visualize the existence of scuffing before the test was automatically stopped. But, due to the higher dissipated energy with 60 Hz movement frequency, the surface damage is more severe than with 30 Hz frequency (figure 8). In conclusion, the first recommendation of the authors will be to conduct these performance tests at a frequency of 30 Hz.

In further method development, Optimol Instruments will conduct international round robin tests with different fluids to verify the robustness and precision of this newly developed test method.

3 Optimization of gear coatings

One other aspect of gear optimization and improving gear performance is the possibility to reduce friction and wear of gear components to improve efficiency and prolong the lifetime of the gearbox. Emanuel Tack and Theresa Huben recently presented a method for model tests on the SRV®-(Schwing-Reib-Verschleiß-) tribometer, where a sample disk is coated in the real gear coating process so that the coating characteristic on the test disk exactly corresponds to that one found in the real gear. With this method, they were able to develop a gear optimized coating which reduces as well as friction by roughly 20% as well as wear by more than 80%. [TAC24]

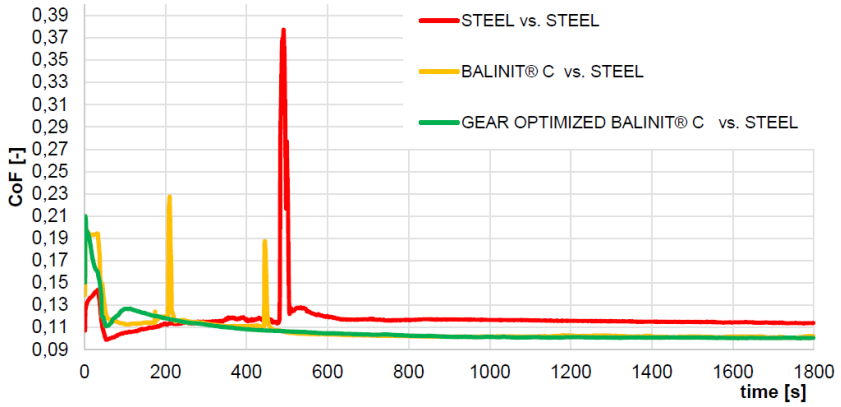

Figure 92: Gear coating optimization by SRV® tests: comparison of the evolution of the CoF for uncoated, standard coated and gear optimized coated 16MnCr5 steel [TAC24]

4 Outlook: rating of anti-fatigue performance of gear fluids

In regards of longevity of gearboxes, protection against fatigue damages is of great importance for gear fluids and gear materials. State of the art techniques for the rating of anti-fatigue protection in terms of micro-pitting and pitting are either rig tests using real gears, which are cost intensive and not flexible in terms of material selection and surface modifications, or two- or three- disk test benches, which generally don't reflect the real dynamic slip-roll conditions occurring in the real gear. Thus, Optimol Instruments – together with the Ruhr University Bochum is developing a test rig for non-circular test disks (figure 10), which are cost efficient in production as well as provide high flexibility in material selection and surface modifications. [RUL24]

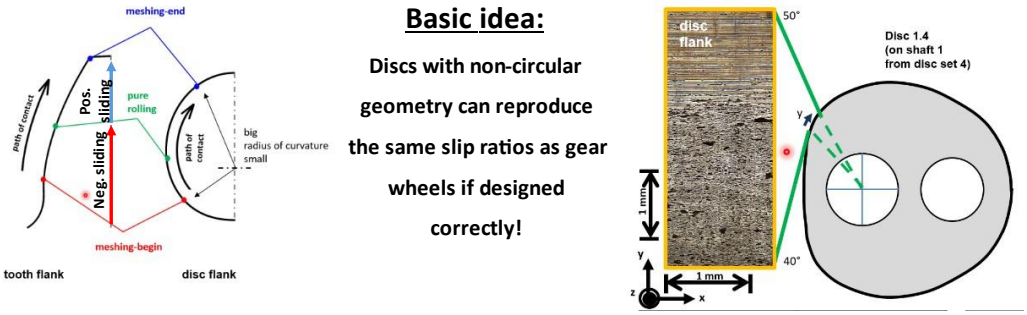

Figure 93: Basic idea of the test rig for non-circular test disks enabling a quick and efficient rating of micro-pitting and pitting characteristics of gear fluids and materials [RUL24]

5 Bibliography

[PAT16] Patzer, Gregor, Ebrecht, Johannes: Vorstellung eines Prüfkonzepts als Screeningmethode für Getriebeöle auf dem translatorischen Oszillationstribometer (SRV®) In: Tribologie + Schmierungstechnik 63. Jahrgang, 2/2016, pp 58 – 64, expert Verlag, Tübingen, 2016

[MAS22] Massocchi, D.; Lattuada, M.; Chatterton, S.; Pennacchi, P.: SRV Method: Lubricating Oil Screening Test for FZG. Machines 2022, 10, 621. https://doi.org/10.3390/machines10080621

[SCH24] Schmidt, Timo, Breitsprecher, Frank: Application of DIN 51834-4 - SRV test- for low-viscosity fluids In: Proc. of the 65. Tribologie-Fachtagung, pp. 18/1 – 18/10, Gesellschaft für Tribologie e.V., Göttingen, 2024

[TAC24] Tack, Emanuel, Huben, Theresa: Steigerung der tribologischen Leistungsfähigkeit von Diamantartigen Kohlenstoffschichten (DLC) auf Zahnrädern für Reduktionsgetriebe in Elektrofahrzeugen In: Proc. of the 65. Tribologie-Fachtagung, pp. 10/1 – 10/7, Gesellschaft für Tribologie e.V., Göttingen, 2024

[RUL24] Ruland, Michael, Patzer, Gregor.: Konzeptstudie eines neuartigen Tribometers zur Nachstellung der Verschleißmechanismen Pitting und Micropitting im Stirnradeingriff unter Zuhilfenahme unrunder Scheiben In: Proc. of the 65. Tribologie-Fachtagung, pp. 43/1 – 43/4, Gesellschaft für Tribologie e.V., Göttingen, 2024

Unleashing the Potential of Hydrodynamic Plain Bearings: Powering the Future of Drive Trains

P. Bergmann[1], K. Stadlmayr[1]

[1]Miba Gleitlager Austria GmbH, Dr.-Mitterbauer-Str. 3, 4663 Laakirchen, Austria

Keywords: Slide bearings, hydrodynamic plain bearings, high power density, gear box, hydrodynamic bearings

Abstract: This contribution discusses the potential of Hydrodynamic Plain Bearings (HPB) in enhancing the performance and efficiency of high-power density drive trains, particularly in planetary gearboxes. These gearboxes are favored for their compact size, high power density, and efficiency but face limitations when equipped with Roller Element Bearings (REB) under high demands. HPB, with their high load-carrying capabilities, compact design, and longevity, present a superior alternative for such requirements. Miba, an Austrian technology company with nearly 100 years of expertise in design and production of HPB, has been a leading supplier for high-performance internal combustion engines and industrial applications. The paper explores the challenges faced by drive train systems and how Miba's HPB solutions can address these issues. The advantages of HPB include increased life expectancy, reduced total cost of ownership, low noise, good damping characteristics, and compatibility with impact loads. The paper also highlights the application of HPB in wind turbine main gearboxes, where increasing power requirements demand durable and efficient solutions. Miba's customer-focused profile ensures tailored, high-performance bearing solutions that meet evolving customer needs.

1 Introduction

Enhancing power density is essential for improving the total cost of ownership of drive train systems. This can be achieved by reducing design space and increasing loads, speeds, or temperatures. Planetary gearboxes are ideal for high power drive trains due to their compact size, high power density, efficiency, and flexibility. However, such systems, usually equipped with Roller Element Bearings (REB) face limits in durability, design space, speed, and torque under high demands. Due to the high load carrying capabilities, small design space, high endurance and longevity Hydrodynamic Plain Bearings (HPB) are an excellent solution targeting the high requirements of high-power drive trains. Miba, an Austrian technology company grounded in engineering excellence and material competence, has been a leading supplier of HPB for high-performance internal combustion engines and demanding industrial applications such as compressors, gearboxes, and pumps for nearly a century. The unwavering commitment to innovation has empowered Miba to deliver top-tier products, consistently meeting the evolving needs of Miba’s customers. This contribution explores the current challenges faced by drive train systems and how Miba's expertise and technology can help overcome these challenges through the integration of HPB solutions.

2 Description of Hydrodynamic Plain Bearings (HPB)

In HPB, a lubricating gap separates the two surfaces of the bearing partners shaft and housing or gear wheel, see Figure 91. The hydrodynamic pressure is dependent on speed, load and lubricant characteristics, especially viscosity. The supply can be designed in a way that already available low-pressure pumps can be utilized which allows an easy-to-handle introduction of HPB. HPB in high-power drive train systems usually consists of bearing shells or bushings that meet compact design requirements.

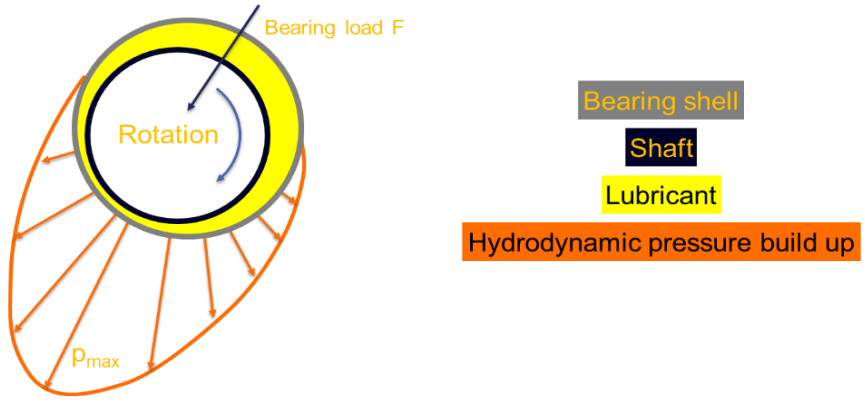

Figure 94: Principle of an HPB: A hydrodynamic pressure in the lubrication gap counteracts the acting bearing load F and separates the two bearing partners.

Together with the hydrodynamic function principle, the technology of HPB provides advantages such as increased life expectancy, reduced total cost of ownership, low noise, good damping characteristics and outstanding compatibility with impact loads. The requirements for HPB are versatile and include additional aspects beyond those described. Figure 96 shows the most important performance criteria and a qualitative comparison of the widely spread REB technology compared to conventional and Miba's hydrodynamic plain bearing technology. To fulfill the versatile requirements, Miba relies on a multilayered bearing structure, see Figure 92. Each of the layers and their interplay ensure that the bearings provide the desired performance, which differentiates them from conventional HPB technology.

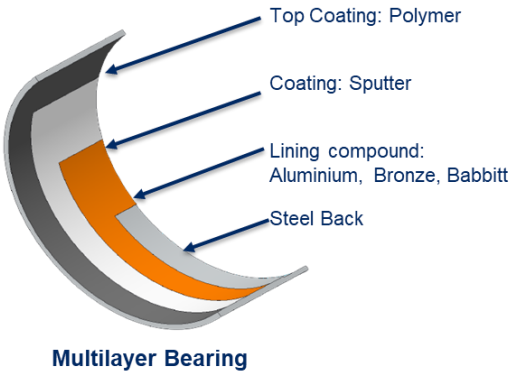

Figure 95: Miba's multilayer bearing technology.

	Life expectancy	Maintenance effort	Total cost of ownership	Overall efficiency	Noise emission	Lubrication system	Required oil quality	Positioning accuracy	Tolerance to misalignment	Impact loads
Roller Element Bearings										
Conventional HPB										
Miba HPB										

Figure 96: Qualitative comparison of bearing characteristics based on literature and Miba experience.

3 Role Model: Wind Turbine Main Gear Box

A representative show case of such a drive train subjected to increasing demands on high power requirements is the wind turbine drive train. Recent trends show increasing power class and turbine

size, resulting in higher input torque. To stay competitive in terms of Levelized Cost of Energy (LCoE), future turbines will continue this trend. Consequently, this increased input torque is split among an increased number of planets to ensure sufficient load-carrying capability of the gear wheels and meshing, which reduces the design space within a planetary stage as well as within the gear wheels. In addition, demanding operating conditions like idling, start/stop and single blade installation lead to intense mixed lubrication. Due to the small design space, the high load-carrying capability and the multilayered bearing structure, Miba's products ensure a technically and economically durable solution.

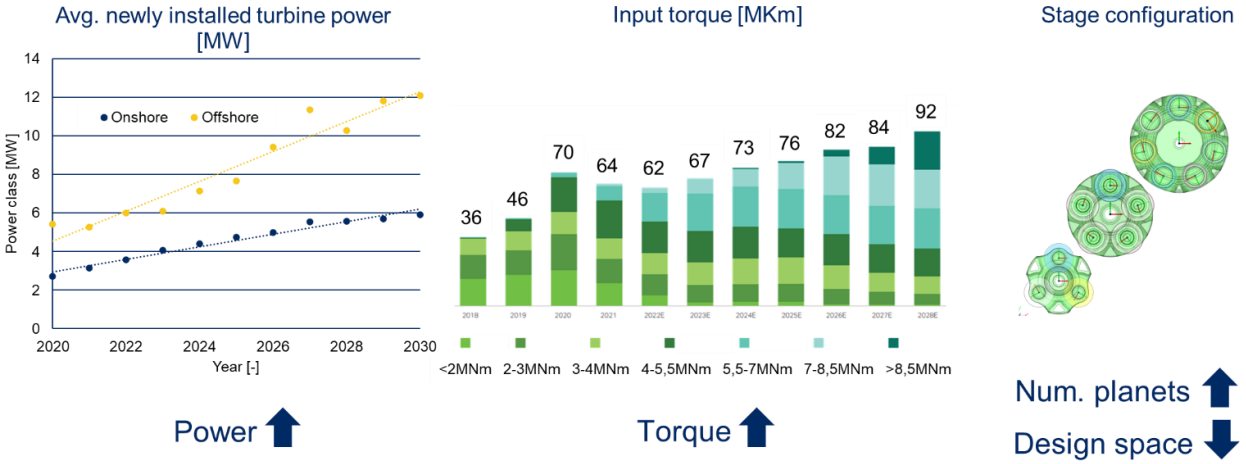

Figure 97: Visualization of impact of application drivers on planetary gear set: The increase in power class (left) can mainly be realized by increase of rotor input torque (center) which finally leads to increased number of planets and reduced design space (right) [1] [2]

4 Successful Innovation References

To push the performance of planetary gear box systems, Miba provides HPB solutions in many shapes and forms. Dependent on customer needs and application requirements, solutions are in form of bushings or direct coatings, see Figure 98. An integration is possible on the stationary or moving part as well as on the pin or in the gear wheel.

Figure 98: Support of planetary gear wheels by versatile HPB solutions. 1) Bushing with tribologically active material on the outer diameter, mounted on pin. 2) Bushing with tribologically active material on the inner diameter, mounted in gear wheel. 3) Direct coating of gear wheel. 4) Direct coating of pin.

5 Miba Profile Accelerates Your Business

Based on nearly 100 years of plain bearing technology knowledge, Miba by now has several decades of experience in providing HPB technology for high power density drive trains, especially for planetary gear stages. Leveraging the application knowledge, material expertise, and production

capabilities, Miba delivers high-performance bearing solutions that excel beyond conventional options.

Customer-Focused Development

Everything at Miba starts with understanding the customers. Miba supports the technological advancements of the customers' system developments and validations using the V-model. This approach, based on system engineering methods, allows for the derivation of component requirements starting from the voice of the customers. By using basic and advanced calculation methods like elastohydrodynamic (EHD) calculations necessary requirements for target-oriented product development and validation are derived. The high vertical manufacturing integration paired with material expertise ensures a target-oriented product with the right balance of performance and cost fulfilling the customers' requirements.

Miba supports validation through principal testing, component testing, and system tests. The high level of manufacturing integration and continuous bearing evaluation ensures ongoing improvements and optimal product performance. This process fosters continuous learning about our methods and products, ensuring Miba provides the best possible product version before it reaches the customers.

Figure 99: Miba's profile to accelerate Miba's customers' business.

6 Summary / Conclusion

Based on 100 years of hydrodynamic plain bearing technology and its proven track record, Miba is a worldwide leading partner in increasing the performance of high-power density drive trains. Close interaction with customers, engineering excellence and product competence were key factors in the past to introduce the technology of hydrodynamic plain bearings in high power density drive trains and is Miba's offer to future customers to improve their systems.

7 Bibliography of sources

[1] Wood Mackenzie – Global Wind Supply Chain Trends Series - Article 4; Dec.2022

[2] GWEC Global Wind Report 2022